Postural control in larval zebrafish : vestibular behavior repertoire and a new method to study it

Natalia Beiza Canelo

SORBONNE UNIVERSITÉ

LABORATOIRE Jean Perrin

THÈSE DE DOCTORAT

de Sorbonne Université

Spécialité : Physique

École doctorale nº564: Physique en Île-de-France

réalisée

au Laboratoire Jean Perrin

sous la direction de Volker BORMUTH

présentée par

Natalia Belén BEIZA CANELO

Sujet de la thèse :

Postural control in larval zebrafish: vestibular behavior repertoire and a new method to study it

soutenue le 31 mai 2022

devant le jury composé de :

M.	Beraneck Mathieu,	Rapporteur
M.	Portuguese Ruben,	Rapporteur
M.	Del Bene Filippo,	Examinateur
Mme	Hong Elim,	Invitée
Mme	Wyart Claire,	Invitée
M.	Bormuth Volker,	Directeur de thèse

Version Wednesday 22nd June, 2022, 14:47

A man walking is never in balance,
but always correcting for imbalance.

Gregory Bateson

Abstract

The vestibular system in the inner ear plays a central role in sensorimotor control by informing the brain about the orientation and linear acceleration of the head. In the present work, we studied the zebrafish larva response to different vestibular stimulus, to characterize the vestibulospinal reflexes and the underlying neural substrates. In the first part of the thesis, we described the tail movements elicited by vestibular stimulation, finding that larvae use their tail to compensate imbalance. Next, we characterized different neural populations that are active during sinusoidal-roll stimulation. Despite the fact that vestibular cues are central for locomotion and postural control, most neurophysiological experiments are performed using head-fixed configurations depriving animals of vestibular inputs. To overcome this limitation, we decorated the utricular otolith of the vestibular system with paramagnetic nanoparticles. This procedure effectively endowed the animal with magneto-sensitive capacities: applied magnetic field gradients induced forces on the otoliths resulting in robust behavioral responses comparable to that evoked by rotating the animal by up to 20°. We recorded the whole-brain neuronal response to this fictive vestibular stimulation using light-sheet functional imaging. Experiments performed in unilaterally injected fish revealed the activation of a commissural inhibition between the brain hemispheres. This magnetic-based stimulation technique opens new perspectives to functionally dissect the neural circuits underlying vestibular processing and to develop multisensory virtual environments including vestibular feedback.

Keywords : Zebrafish · vestibular system · postural control · vestibulo-spinal reflex · behavior · calcium imaging · ferrofluid

Résumé

Pour se déplacer, les animaux doivent constamment garder leur équilibre et compenser les écarts à leur orientation corporelle préférée, causés par des perturbations externes et leurs mouvements propres. Le contrôle de la posture, ou contrôle postural, fait référence aux mécanismes du système nerveux (SN) qui sont impliqués dans le maintien d'une posture contrôlée, verticale (dans le cas des animaux bipèdes) ou dos vers le haut (pour les quadrupèdes et les animaux aquatiques), en produisant des réponses motrices adéquates, selon les entrées sensorielles provenant à la fois du corps lui-même et de l'environnement. Les systèmes visuel, vestibulaire et proprioceptif (somatosensoriel) sont les principaux systèmes sensoriels participant au contrôle postural.

Le maintien de la configuration corporelle de base chez les animaux est une fonction motrice vitale, car les organismes en dépendent pour adopter différents comportements nécessaires à leur survie (déplacement, capture de proies, fuite, etc.). Le contrôle postural est une activité involontaire qui se produit au niveau subconscient et repose sur des mécanismes neuronaux innés mis en place au cours du développement. Les substrats neuronaux du contrôle postural sont situés dans le cerveau antérieur, le cerveau moyen, le tronc cérébral et la moelle épinière, ce qui en fait l'un des systèmes moteurs les plus complexes et les plus étendus chez les vertébrés.

Nous pouvons définir le contrôle postural comme une interaction complexe de différentes boucles de rétroaction, qui combinent des éléments de multiples modalités de perception, de traitement cérébral et de réponses motrices à travers une série de voies neuronales. Le processus par lequel les informations sensorielles provenant de canaux multiples (somatosensoriels/proprioceptifs, vestibulaires et visuels) sont intégrées dans une réponse motrice est appelé intégration sensorimotrice et est au cœur du contrôle postural. L'intégration sensorielle signifie que les différentes modalités sensorielles ne sont pas traitées comme des unités indépendantes, mais plutôt assimilées ensemble pour fournir une interprétation cohérente de la position et de l'orientation du corps. Ces informations sont ensuite utilisées pour générer les commandes motrices adaptées qui permettront de maintenir la posture souhaitée.

Le système vestibulaire dans l'oreille interne joue un rôle central dans le contrôle

sensorimoteur en informant le cerveau de l'orientation et de l'accélération linéaire de la tête. Pour cette thèse, nous avons étudié la réponse des larves de poisson zèbre à différents stimuli vestibulaires, afin de caractériser les réflexes vestibulospinaux et les substrats neuronaux sous-jacents.

Dans la première partie de ma thèse, j'ai étudié les comportements déclenchés par la stimulation vestibulaire de larves âgées de 5 à 9 jours. Ce chapitre ne traite pas des réflexes vestibulo-oculaires (VOR) mais se concentre sur l'étude des réflexes vestibulospinaux (VSR). Le réflexe vestibulospinal entraîne des mouvements compensatoires du cou, du corps et des membres pour stabiliser la posture du corps lorsque les animaux sont inclinés ou roulés par rapport à leur position normale. Comparé au VOR, ce réflexe a été moins étudié et les mécanismes impliqués ne sont pas encore totalement compris. Ainsi, le premier objectif de ma thèse (Chapitre 2) était de caractériser les mouvements corporels compensatoires provoqués par le roulement des larves de poisson (rotation le long de l'axe tête-queue).

Cette stimulation déclenche de manière répétable un mouvement de pivot de la queue, qui semble être principalement provoqué par une entrée vestibulaire unilatérale et qui est dirigé vers le côté opposé à la stimulation (contraversif). Nous émettons l'hypothèse que ce mouvement de pivot de la queue est impliqué dans le contrôle postural.

J'ai observé qu'un poisson qui roule vers la droite (oreille droite vers le bas) fait pivoter sa queue vers le côté gauche contraversif. Il pourrait s'agir d'un mécanisme permettant de contrebalancer une déstabilisation du corps en repositionnant le centre de masse de la larve de sorte que le poisson roule à nouveau vers sa position dos vers le haut. Cela serait comparable au fait que les humains lèvent leur bras gauche pour rétablir l'équilibre lorsqu'ils sont déséquilibrés vers la droite.

Lorsque les larves ont été roulées à des angles plus importants, elles ont commencé à nager. Nous proposons que les accès de nage observés ont le même rôle que les déviations de la queue : ils servent à ramener le poisson à sa position naturelle lorsqu'il est poussé hors d'équilibre, mais d'une manière plus rapide et plus efficace. Cela pourrait être comparable aux humains qui doivent faire un pas pour stabiliser leur posture lorsqu'ils sont poussés trop fortement hors de leur position d'équilibre. Ehrlich et al.[1] ont montré qu'un mouvement vers l'avant d'une larve de poisson zèbre peut stabiliser la posture autour de l'axe de tangage. Un mécanisme similaire

pourrait permettre de stabiliser l'orientation du corps autour de l'axe de roulis.

En 2017, Favre-Bulle et al.[2] ont montré que le fait de tirer sur l'otolithe de l'oreille droite avec des pinces optiques vers le côté latéral du poisson provoquait une déviation de la queue vers la gauche, dans la direction opposée au stimulus. Ils ont également observé que des forces plus importantes sur l'otolithe provoquaient des déviations plus importantes de la queue et augmentaient également la probabilité d'observer des tentatives de nage. Ces résultats sont comparables à ceux que nous avons obtenus : nous avons observé le même mouvement de pivotement de la queue, provoqué par une stimulation vestibulaire non fictive (naturelle).

De plus, j'ai enlevé l'utricule d'une seule oreille, afin d'étudier la contribution de chaque oreille également sous stimulation vestibulaire naturelle. Nous avons observé la réponse de la queue pivotante uniquement lorsque l'oreille intacte était tournée vers le bas, ce qui induisait un mouvement latéral de l'otolithe. Ce résultat est cohérent avec l'expérience des pinces optiques et confirme que la stimulation utriculaire unilatérale, même dans des conditions naturelles, est suffisante pour entraîner cette réponse compensatoire de la queue [2]. Enfin, l'ablation de l'utricule dans les deux oreilles a démontré que l'utricule est nécessaire pour ce comportement, puisque les poissons avec ablation bilatérale de l'utricule ne présentaient pas du tout cette réponse de la queue lorsqu'ils étaient roulés.

Le second objectif de ma thèse (Chapitre 3) était de décrire l'activité cérébrale globale provoquée par la stimulation vestibulaire et de la relier au comportement observé dans le premier chapitre. Nous avons mis à profit des rapporteurs calciques génétiquement encodés dans le poisson zèbre larvaire, et nous avons utilisé différentes lignées qui marquent les régions du cerveau connues pour être impliquées dans la réponse vestibulaire. Nous avons généré une petite bibliothèque de neurones et de régions du cerveau qui sont actifs pendant la stimulation vestibulaire sinusoïdale.

Dans ce chapitre, nous avons profité de la vaste bibliothèque de lignées transgéniques qui a été développée chez le poisson zèbre pour examiner plus en détail les substrats neuronaux qui sous-tendent les réponses vestibulaires. Et même si les résultats présentés ici sont préliminaires, et que l'analyse des corrélations neuronales est encore manquante, nous avons décrit la réponse étendue du cerveau et de la moelle épinière au stimulus vestibulaire.

Pour ce faire, nous avons utilisé la configuration et le protocole décrits par Migault et al. [3]. Nous avons prouvé que le nMLF (voir liste des abréviations), les neurones oculomoteurs, les neurones trochléaires, les sous-populations des neurones réticulospinaux et les motoneurones primaires de la moelle épinière sont actifs lors du roulement controlatéral. Au contraire, le noyau tangentiel, les neurones vestibulo-spinaux, les motoneurones de la région MON et des abducteurs des nageoires pectorales sont actifs pendant le roulis ipsilatéral. De plus, nous avons prouvé, par des moyens mécaniques et une mesure directe de l'activité des cellules ciliées, que les canaux semi-circulaires ne sont pas encore fonctionnels entre 5 et 7 jours post-fertilization. L'idée que les canaux semi-circulaires ne sont pas fonctionnels avant 34 jours est basée sur leur morphologie et l'absence de VOR horizontal. Ici, nous mesurons l'activité du crista postérieur pendant le roulement sinusoïdal, montrant qu'aucune activité n'est générée. Enfin, nous avons montré qu'un seul utricule est suffisant pour générer une réponse complète, au moyen d'une désinhibition commissurale des neurones vestibulaires de second ordre controlatéraux.

La description fine de la façon dont les mouvements de la queue sont contrôlés par le signal de l'utricule restent inconnus et des questions restent ouvertes. Par exemple, quels sont les neurones vestibulaires de deuxième et troisième ordres qui participent à ce comportement ? Quels sont les neurones moteurs responsables des déviations de la queue ? L'inhibition du nMLF altère ce comportement lors d'une stimulation vestibulaire ? Quel est le rôle des voies vestibulospinales dans la production de réflexes en réponse à toute une série de stimuli vestibulaires ?

Pour disséquer et déchiffrer les circuits neuronaux, l'un des paradigmes actuels en neurosciences concernant le modèle du poisson zèbre consiste à manipuler, à l'aide d'outils optogénétiques, des régions cérébrales spécifiques, pour voir si elles déclenchent ou inhibent un certain comportement. Jusqu'à présent, ces études ont permis de relier les neurones au comportement, mais elles n'ont pas pris en compte le système vestibulaire dans l'équation, en raison de la complexité du couplage d'une configuration avec la stimulation vestibulaire. Pour stimuler le système vestibulaire, la tête de l'animal doit être tournée ou déplacée dans l'espace, ce qui est incompatible avec les installations qui nécessitent des animaux dont la tête est fixée.

Pour résoudre ce problème, nous avons développé une méthode permettant de

réaliser une stimulation vestibulaire fictive par des forces magnétiques chez des larves dont la tête est fixée. Le troisième objectif de ma thèse (chapitre 4) porte sur le développement et la preuve de principe de cette nouvelle méthode.

Notre travail démontre que l'injection d'une solution de ferrofluide dans l'oreille interne de larves de poisson zèbre permet d'appliquer ensuite des forces contrôlées à l'otolithe utriculaire *in vivo*, imitant ainsi les stimuli vestibulaires naturels chez les animaux immobilisés.

Un petit aimant permanent permet une stimulation vestibulaire fictive de roulis et de tangage qui suscite des réponses motrices semblables à qu'on observe pendant la stimulation du mouvement naturel. La diaphonie entre les deux directions de stimulation était négligeable, à condition que l'aimant soit bien centré sous le poisson.

Cette méthode de stimulation vestibulaire est compatible avec l'imagerie fonctionnelle simultanée de l'ensemble du cerveau au moyen de la microscopie à nappe laser. En réponse au stimulus vestibulaire fictif, nous avons observé une activité neuronale cohérente dans le noyau vestibulaire et dans les noyaux en aval dans tout le cerveau.

La carte des réponses neuronales provoquées chez les poissons ayant reçu une injection bilatérale était comparable à celle obtenue lors d'une stimulation vestibulaire réelle à l'aide d'un microscope rotatif à feuille lumineuse. Cela confirme que la force magnétique agit sans délai sur l'otolithe de la même manière que les forces gravitationnelles lorsque l'animal est, par exemple, roulé le long de son axe corporel longitudinal.

Les cartes de déphasages enregistrées pendant la stimulation unilatérale suggèrent la présence d'une inhibition commissurale prononcée entre les deux noyaux vestibulaires, typiquement conservée chez tous les vertébrés. Les résultats sont joints dans un format d'article scientifique, cet article a été soumis pour être publié dans un journal à comité de lecture.

Mots-clés : Poisson-zèbre · système vestibulaire · maintien de l'équilibre · réflexe vestibulo-spinal · comportement · imagerie calcique · ferrofluide

Acknowledgements

First, thanks to Volker Bormuth, who directed this work and who, in many occasions, believed in me more than I did. Thanks to all the members of the Laboratoire Jean Perrin, specially the fish team. Thanks to the people who read this thesis: Darka, Guillaume, Marcus, and Leonardo. Thanks to the people who participated in the article, specially Thomas Panier for developing the instrumental part. Thanks to Geoffrey for all the scientific input and for being a support in the group. Thanks to the Lab Managers, Malika and Anissa. Thanks to the fish facility of the IBPS.

También quiero agradecer a mi familia y amigos, los que me han apoyado incondicionalmente en los altos y bajos que han ocurrido en los últimos años. Gracias a mi Tata Oscar, por su apoyo. Gracias a mi mamá, papá, hermana y hermano. Gracias a Kaleb y a Norita por ser amor y luz en mi vida. Gracias a Camila, Pollo, Fabi y las Biologas. Gracias a mi familia parisina: Diego Contreras, Alex, Seba, Estefi, Diego Candia, Cata, Jorge y Marce, también a los clisonianos: Giulia, Flavia, Ila y Giacomo. Y finalmente, gracias a leoncito, por todo su apoyo emocional y por ser mi hogar.

Contents

List of abbreviations

CoM centre of mass

dpf days post fertilization

GCaMP green fluorescent protein - calmodulin- M-13 peptide.

GECI geneticaly encoded calcium indicator

GFP green fluorescent protein

hpf hours post fertilization

hpi hours post injection

MiV middle ventral

MON medial octavolateralis nucleus

nIII oculomotor nucleus

nIV trochlear nucleus

nMLF nucleus of the medial longitudinal fasciculus

NS nervous system

OKR optokinetic reflex

OMR optomotor reflex

RLS Rotating Light-sheet microscope

RoM rostal medial

RS reticulospinal

SPIM single-plane imaging microscopy

TN tangential nucleus

VOR vestibulo-ocular reflex

VS vestibulospinal

VSR vestibulo-spinal reflex

Introduction

Je n'ai fait cette lettre-ci plus longue
que parce que je n'ai pas eu le loisir de la faire plus courte.

Blaise Pascal

1.1 Postural control and sensory-motor integration

1.1.1 What does postural control mean?

Postural control refers to the mechanisms in the nervous system (NS) that are involved in maintaining a controlled, upright (in the case of bipedal animals) or dorsal-up (for quadrupeds and aquatic animals) posture [4] by producing adequate motor outputs in response to sensory inputs that come from both the self and the environment. The visual, vestibular, and proprioceptive (somatosensory) systems are the primary sensory systems participating in postural control. Maintenance of the basic body configuration in animals is a vital motor function, since organisms rely on it to perform different behaviors that are necessary for survival (moving, prey capture, escaping, etc.) [5].

Postural control is an involuntary activity that happens at the subconscious level and is based on innate neural mechanisms circuited during development [6, 7]. The neural substrates of postural control are located in the forebrain, midbrain [8], brain stem [9] and spinal cord [10, 9], making it one of the most complex and wide motor systems across vertebrates. The main role of postural control is the maintenance of equilibrium. Most animals learn to control their orientation in relation to gravity when they are perturbed from their natural position, engaging movements that

correct and maintain posture while standing, but that are also required during locomotor behavior [11]. Thus, maintaining appropriate equilibrium involves the coordination of sensory-motor mechanisms to balance the body's center of mass (CoM) during postural perturbations generated by both voluntary movements and external factors [12]. A postural perturbation can be defined as a sudden change in conditions that displaces the body posture away from equilibrium. Depending on the nature of the perturbation, mechanisms of postural control can be divided in two modes:

- The feed-forward mode, when perturbations are expected. Thus, the postural response is targeted to counterbalance the destabilizing effects of voluntary movements. This mode is based on open-loops neural mechanisms [13, 4].
- The feed-back mode, when perturbations are unexpected. These deviations are perceived by the visual, vestibular and proprioceptive/somatosensory system. The output of these signals is a corrective movement that returns the body to the initial position [13, 4]. This mode is based on closed-loops neural mechanisms or "reflexes" [14] that either complement or cancel each other [15, 16].

Regarding how postural control operates in vertebrates, the most accepted model was first proposed by Erich von Holst in the mid 30s [17]. He suggested that understanding balance as a set of separated simple spinal reflexes was an over-simplification of this behavior, and that balance should be considered rather as a feedback system that integrates different inputs at a central level. Later, other works showed that posture stabilization involves supra-spinal control from the brain stem, the cerebellum and the motor cortex (in mammals), which receive visual, vestibular and somatosensory inputs, generating motor outputs in the spinal cord via descending pathways (e.g., vestibulospinal and reticulospinal tracts) [5].

1.1.2 Sensory systems involved in postural control: sensorimotor integration

We can define postural control as a complex interaction of different feed-back loops (described in the previous section, (see Figure 1.1B), which combine elements

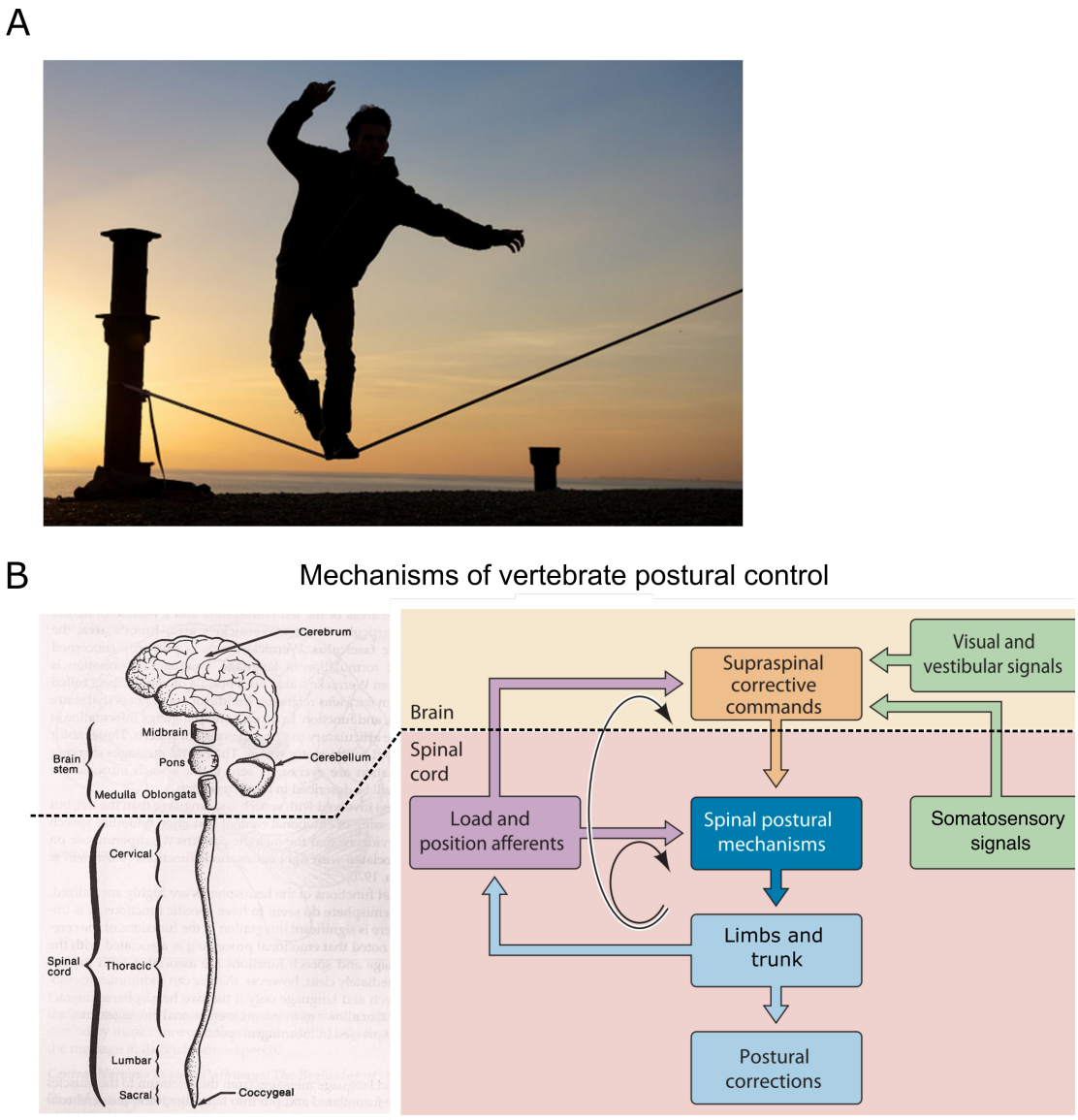

Figure 1.1 Postural control mechanisms in vertebrates. (A) A picture that illustrates a condition in which postural control is highly challenged. The person on the tightrope needs to balance constantly their center of mass, so limbs and trunk movements will be involuntarily evoked in order to not fall (photo from http://www.greenbookblog.org). **(B)** Figure adapted from Deliagina et al. [5]. Schematic of the basic mechanisms of postural control in quadrupeds. The brain integrates visual, vestibular and somatosensory signals to coordinate descending postural control. The changes in muscle load and position produced by the corrective movements give the necessary feedback for this mechanism. There are two levels in which feedback process occurs: brain and spinal cord (left panel, figure from Snell, 2010 [18]).

of multiple perception modalities, brain processing and motor outputs through a series of neural pathways [19]. This process in which sensory information from multiple channels (somatosensory/proprioceptive, vestibular and visual) is integrated in a motor response is called *sensorimotor integration* and is central to postural control. Sensory integration means that the different sensory modalities are resolved not as independent units, but rather assimilated together to provide a coherent interpretation of the body's position and orientation. The integration of this information generates adapted motor commands that will maintain the desired posture [13].

On the one hand, the fact of having high redundancy on the system makes it quite robust. Therefore, balance can be maintained in the absence of one of the sensory modalities, and animals with impaired vestibular apparatus learn to compensate and recover postural control by using visual and proprioceptive inputs [20, 21].

On the other hand, the fact that the sensory receptors are part of the body itself makes interpretation of the afferent information, with respect to the surrounding world, not singular but ambiguous. Thus, the postural control system uses multiple inputs in order to resolve ambiguities about the body's position and motion. For example, the movement of an image across the retina (retinal slip) inform us that there is a relative motion between our head and the surrounding visual environment. But the visual system alone cannot determine what has moved: ourselves or the world. To resolve this kind of ambiguity the brain uses sensory-integration, e.g., proprioceptive neurons in the neck can report if the head was rotated relative to the body, or the vestibular system can detect body accelerations. Studying how different sensory modalities integrate to converge postural control is not an easy task, and studies often consider only one system. In addition, performing visual stimulation is easier compared to vestibular (given the easier access compared to the vestibular apparatus). Therefore, studying the role of vestibular input and developing techniques that help such studies are crucial to dissect postural control.

The present research work focuses on the righting reflexes (closed-loop feed-back) elicited by vestibular input and in tool development for vestibular research.

1.1.3 Postural control in different animal models

There are three principal ways of locomotion that are environment-dependent: walking, flying and swimming. But despite the fact that all vertebrates move in different ways, the mechanisms underlying postural control are highly conserved among this group. In particular, the role of the vestibular system in balance, documented for the first time by Pierre Flourens in 1825 [22]. Over the past two hundred years, systematic investigations of inner ear end organs (otoliths and labyrinth) in several vertebrate models, such as fish [23, 24], frogs [25], pigeons [22] and mammals [26], have brought to light many details of the function and anatomy of this sensory system and established that it is remarkably conserved across vertebrate phylogeny [27, 28].

So far, these comparative studies have established that the neuroanatomy and physiological properties underlying vestibular signal processing are evolutionary inherent, evidencing the general principles of vestibular processing [29]. Thus, using different animal models can improve our understanding of the role and function of the vestibular system in balance and postural control. In addition, given the highly conserved neurophysiology of this system, cross-species studies can be crucial in the understanding of human vestibular diseases.

One big advantage of the highly conserved function and anatomy of the vestibular system (Figure 1.4) is that it allows to use simpler organisms to address questions that are difficult to study in more complex organisms. For example, the use of lampreys as a model has allowed to perform detailed analysis of the neural circuits involved in righting reflexes and gaze stabilization [24, 30, 31]. In this study, we will use the zebrafish model to decipher neural substrates of postural control. The characteristics and advantages of this model are described in the next section.

1.2 The zebrafish in neuroscience

The zebrafish (*Danio rerio*) is a ray-finned fish (*Actinopterygii*) originally found in India. It lives in fresh water and has been a common aquarium fish for decades. About fifty years ago, George Streisinger introduced the zebrafish as a model organism. He found in this animal three important qualities: 1) production of numerous

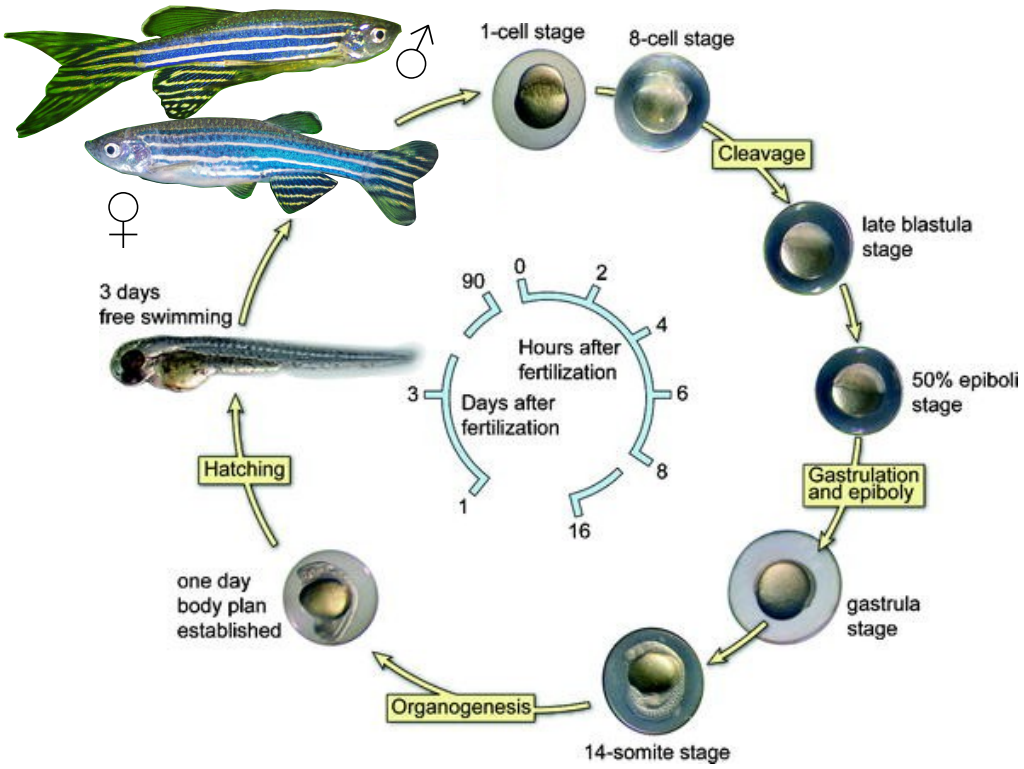

Figure 1.2 Schematic of the zebrafish life cycle. Figure adapted from Willemsen et al. [35] .

eggs, 2) optical transparency of the developing embryos, and 3) a diploid genome, allowing genetic manipulations and studies of gene function.

In the early 1980s, the publication in *Nature* by Streisinger et al. [32] drew the attention of other scientists studying vertebrate development to this organism, and the zebrafish rapidly became a model animal in developmental biology and genetics [33]. The development of zebrafish is impressively fast for a vertebrate, hatching between 48 and 72 hours post fertilization (hpf) and swim onset already at 5 days post fertilization (dpf) [34] (Figure 1.2). The larva stage is from hatching (2-3 dpf) until 30 dpf, when they are considered juvenile. During this period, the larva continuously grows and develops. At 3 months (90 dpf) they reach sexual maturity and are considered adults (Figure 1.2).

It was just in the last two decades that this organism gained popularity in the neuroscience field and emerged as a new important species for studying mechanisms of brain function and behavior [36, 37, 38]. Zebrafish larvae possess a rich behavioral

repertoire. Around 5 dpf they inflate their swim bladder and are able to swim in the water column (Figure 1.3A-B). At this stage they begin to show stereotypical behavioral responses such as: optomotor reflex (OMR), optokinetic reflex (OKR), vestibulo-ocular reflex (VOR), postural control, startling response and prey capture [39]. Some of these behaviors are also present in higher vertebrates, in particular all the vestibular reflexes, enhancing the interest to study this model in behavior and brain sciences.

Since it was introduced into the laboratory, the zebrafish has been a robust model for genome editing, supporting the development of several genetic tools that gave origin to different lines of transgenic [43] and mutant animals. These genetically modified organisms (GMOs) have many applications, and proved to be useful also in the context of *in vivo* brain imaging. For example, an interesting mutant is the *Nacre* mutant (Figure 1.3C), which has a mutation on the *mitfa* gene that impairs melanocytes production [44], originating a larva that is more transparent than the wild type, giving unique optical access to image deeper in the brain (Figure 1.3C).

In 2001, Nakai et al. [45] developed the GCaMP probe, which is a high-affinity Ca^{2+} probe composed of GFP that becomes more fluorescent when it is bound to Ca^{2+}. This probe can be inserted in the genome of the fish by transgenesis and expressed widely in the brain (Figure 1.3D) or in specific regions only. This method together with whole-brain/single-cell resolution functional light-sheet imaging allowed recording of neuronal activity in thousands of neurons simultaneously for the first time in a vertebrate brain (Figure 1.3E) [42, 46].

Thus, the rich behavior repertoire, the genetic accessibility plus the vast toolkit for brain imaging and manipulation make the zebrafish larva an extremely powerful model to study the neuronal circuits underlying complex behaviors. In addition, the fact that their brain shares many anatomical and functional features with mammalian organisms [36] together with their low cost and high throughput, have made the zebrafish larva a suitable model for biomedical research, with emphasis in drug screening and neural and psychiatric diseases [47].

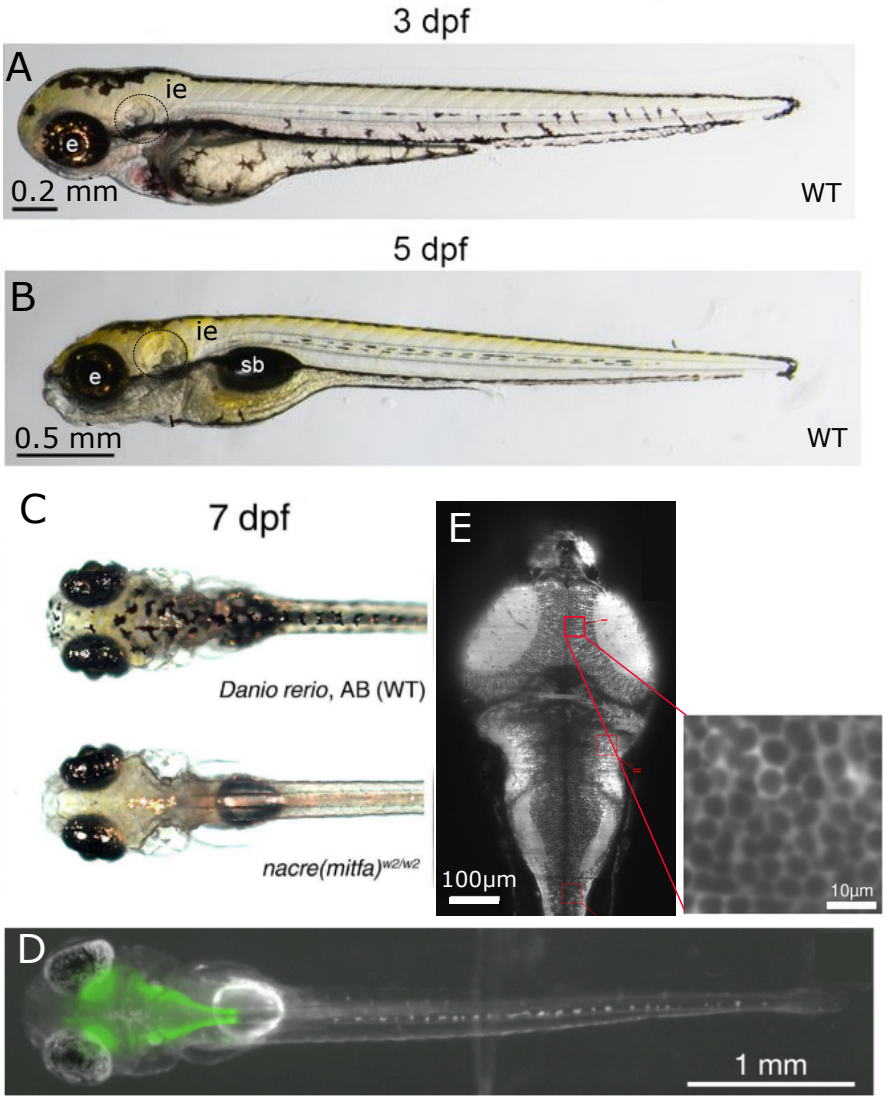

Figure 1.3 Wild-type, nacre mutant and transgenic GCaMP zebrafish larva. **(A-B)** Wild-type zebrafish larva to show the swim bladder (sb) inflation and the eye (e) and inner ear (ie) development between 3 dpf and 5 dpf. Panels adapted from Watt et al. [40]. **(C)** 7 dpf larva to show the differences between wild-type phenotype and nacre mutant. The mutant lacks melanophores and only posses iridophores (iridescent pigments). Panel adapted from Antinucci and Hindges [41]. **(D-E)** *Tg(elavl3:GCaMP3)* nacre larva expresses GCaMP3 under the control of the pan-neuronal promoter *elavl3* in the neurons' cytoplasm, and is optically accessible. **(E)** Section from a brain volume. Inset shows single neurons optical resolution. Panels adapted from Panier et al. [42].

1.3 The vestibular system

1.3.1 Origin and evolution

The vestibular system is the main organ responsible for the sense of balance. But among the classical five senses: vision, taste, smell, touch and hearing, our sense of balance is rarely mentioned. We only notice its existence under extraordinary conditions, such as when we get sick on a boat or a car, or when we experience vertigo. This system was discovered late compared to the other sensory systems, and the first descriptions that we know come from the studies done by the Italian anatomist Antonio Scarpa in 1789 [48], not much over two centuries ago.

Evolutionarily speaking, the vestibular system appears for the first time in the *Craniata* clade (Figure 1.4). This basal ear (a simple torus as in hagfish) evolved into two separated semicircular canals in lampreys (Figure 1.4). A third canal, the horizontal semicircular canal, evolved in jawed vertebrates [49]. The emergence of the vestibular system provided a sensor for rapid head movements. The evolution of this system resulted in a complex organ: the labyrinth, composed of two parts: 1) semicircular canals to sense angular acceleration, and 2) otolithic organs for linear acceleration and gravity perception in the horizontal and vertical planes [50].

The evolution of the vestibular apparatus (labyrinth) goes hand in hand with the evolution of the neuronal and motor substrates that support gaze and postural stabilization. The stabilization of retinal image motion (retinal slip) during head rotation or translation, is performed by directing compensatory eye movements: the vestibulo-ocular reflex (VOR). This reflex appeared together with the eye muscles and the neurons that connect them to the vestibular system (Figure 1.4). Vestibulo-spinal reflexes (VSR) mediate postural control, which evolved together with the vestibular system. Such mechanisms include afferent vestibular neurons, processing of the vestibular information in the brain (vestibular nuclei) and activity of the vestibular descending tracts [51] (not shown in the figure).

Being part of the jawed vertebrates, the adult zebrafish inner ear presents three orthogonal semicircular canals: anterior, posterior and horizontal or lateral (Figure 1.4); and three otolithic organs: the utricle, saccule and lagena (Figure 1.5G). Each semicircular canal terminates in a widening of the canal called *ampula*, which

contains a sensory patch of hair cells called *crista*, perpendicular to the canal axis. The otolithic organs consist of an ear stone attached to a hair cell sensory patch called *macula* [52].

The semicircular canals and the utricle constitute the vestibular system of the fish ear, which is implicated in balance via acceleration and gravity-sensing. The saccule and lagena instead, have the principal function of hearing [23, 53]. Despite the fact that fish have no outer or middle ear, and that they lack a specific hearing organ such as the cochlea in mammals, the organs of balance and gravity-sensing, i.e., the semicircular canals and otoliths and the related neuronal pathways remain functionally comparable in all vertebrate groups [54, 28] (Figure 1.4).

1.3.2 Development and physiology of the zebrafish inner ear

During zebrafish development, the structure that will form the inner ear –the otic placode– is morphologically evident from 16 hpf, when it is beginning to form an elongated cavity, which becomes later the otic vesicle [52] (Figure 1.5A-D). Two early patterning events in the otic placode are the determination of the prosensory and proneural domains [55], which will give rise to sensory hair cells and sensory neurons, respectively (Figure 1.5G).

The two first otoliths, the utricle and saccule, appear at 19 hpf [56]. By 24 hours, the first hair cells are visible, grouped in two separate patches, one beneath each otolith, reaching by 7 dpf a number of 80 hair cells per macula [57] (Figure 1.5F). The third otolith: the lagena, appears by day 14 dpf [58] (Figure 1.5G).

In parallel, the development of the semicircular canals starts around 45 hpf [56]. The hair cells that will form the cristae start appearing around 60 hpf (Figure 1.5D), and by 5 dpf all the components of the adult structure are present and innervated by the vestibular sensory neurons [59] (Figure 1.5E). However, the semicircular canals become functional only after 35 dpf, when the canal's lumen reaches an optimal size [60, 61] (Figure 1.5H). Regarding the otoliths, the saccule and lagena have essentially a hearing role [62, 53], meaning that the utricle is the main organ involved in vestibular perception, and it becomes functional by 72 hpf [63].

The utricle, as well as the other otolithic organs, is composed by an otolith (ear stone, from the greek: *oto*-ear and *lithos*-stone), a calcium carbonate structure,

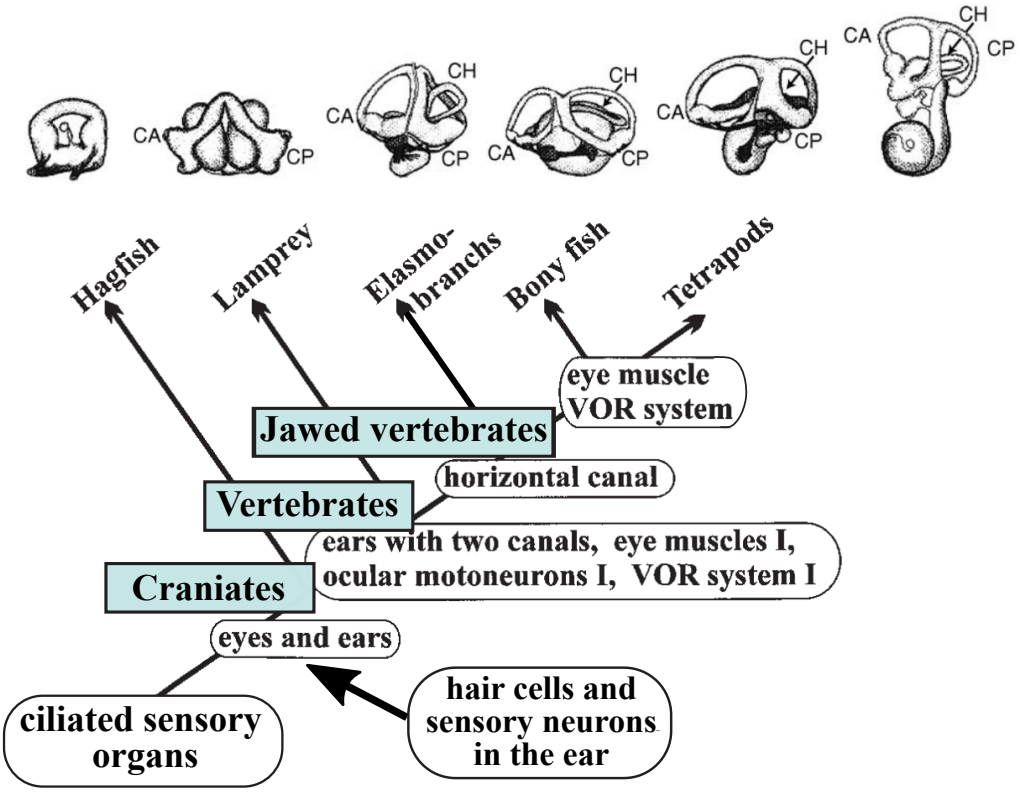

Figure 1.4 Evolution of the vertebrate inner ear and the VOR circuit. Top: the morphological evolution of the labyrinth, from hagfish to mice. Figure adapted from Graf et al. [27]. Bottom: Hagfish are the most basal organisms in the *Craniata* branch, in which eyes and ears appeared but eye muscles were absent. Extraocular muscles evolved with the ancestors of lampreys and appeared for the first time in the Vertebrate group. Together with this set of eye muscles (I), the associated VOR system (I) evolved, with only two vertical semicircular canals (CA: anterior canal; CP: posterior canal). The horizontal semicircular canals appeared in the ancestor of all jawed vertebrates (*Gnathostomata*; i.e., bony fish, amphibians, birds, and mammals), making the system sensitive to horizontal head translation. Figure adapted from Fritzsch [50].

suspended on top of the macula, buffered by a gelatinous matrix (Figure 1.5D). Due to their higher density, otoliths have an inertia relative to the rest of the fish body. During linear accelerations, when the animal's head rotates or translates, the otolith glides relative to the hair cells, deflecting the hair bundles. This deflection triggers an influx of ions into the hair cell (mechanotransduction), releasing glutamate onto vestibular afferents of the eighth cranial nerve that relay this initial signal to the vestibular centers of the brain [52, 64] (Figure 1.5G). These centers encode head movements in different directions and project directly to motor centers, such as the oculomotor nucleus and the spinal cord [64].

1.3.3 Vestibular circuits involved in postural control in the zebrafish larva

Vestibular circuits refer to the neural substrates that sense instability and translate it into corrective motor output. These corrections must be fast, since animal survival depends on the rapidity of the adequate motor responses that stabilize both posture and gaze. In order to produce rapid sensory-motor transformations for both responses, the nervous system relies primarily on reflex arcs [67, 68]. Reflex arcs are simplified models rather than real functional units of the nervous system (as discussed in the first section). They are only useful in the case of two-neuron reflex arcs [69], in which a sensory neuron (afferent) contacts directly a motor-neuron (efferent). But in general, most of the connections between afferents and efferents in the nervous system are mediated by one or more intermediate components: the interneurons, forming a three-neuron reflex arc or even more complex reflex mechanisms [69]. These reflex arcs are surprisingly conserved in the vestibular system [28], adding in favor to the idea that findings in the zebrafish larva can be generalized and extrapolated to higher vertebrates, with the advantage of a simpler model.

One advantage of the zebrafish larva is that, at this stage, the only functional vestibular organ is the utricle [70]. The utricle detects translational and gravitational accelerations, thus providing signals related to the position of the head in space that will induce vestibular reflexes.

There are two vestibular reflexes that are evident in the larval zebrafish:

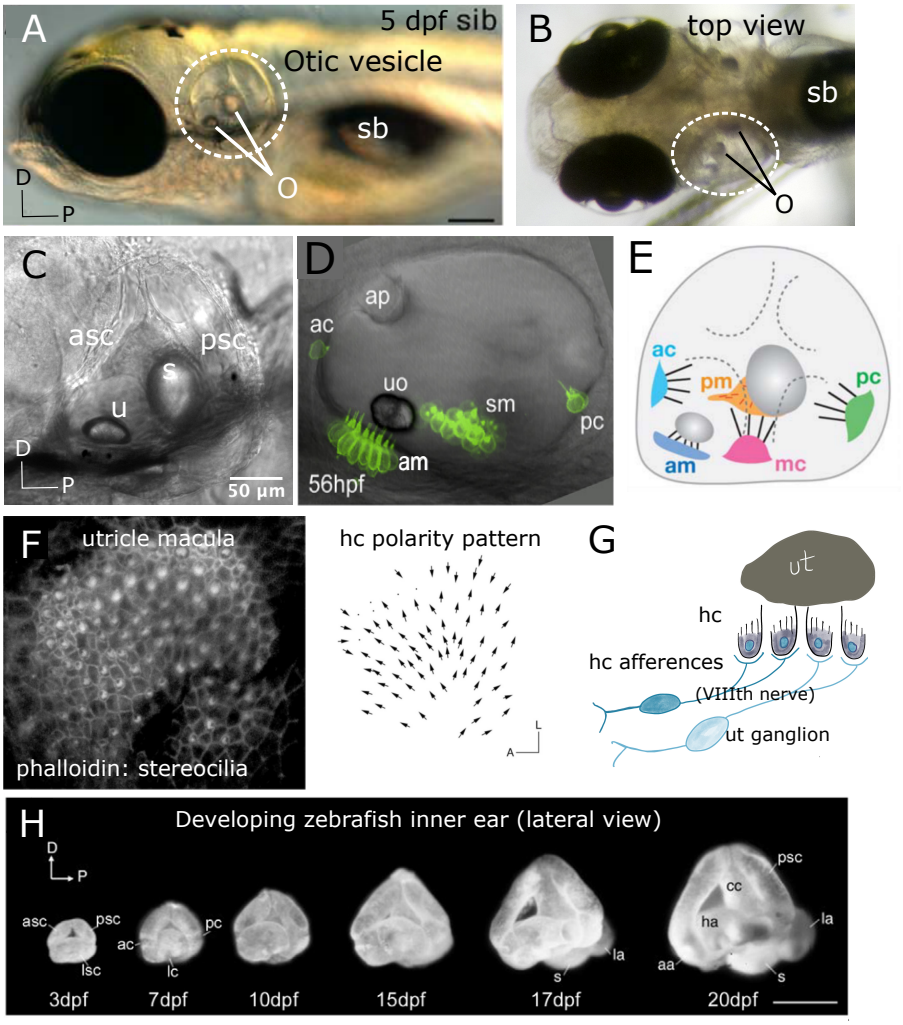

Figure 1.5 Zebrafish larva inner ear. (A-B) Lateral and top view from a 5 dpf larva. The otic vesicle and otololiths (o) are enclosed within a segmented line. **(C-D)** Otic vesicle close-up in lateral view showing the utricle (u), saccule (s), the developing anterior and posterior semicircular canal (asc, psc), the anterior and sacular macula (am,sm) and the emerging anterior and posterior cristae (ac,pc). The hair cells (hc) are shown in green underneath the utricular ear stone (u). **(E)** Schematic of the 5dpf larva's inner ear; mc: medial crista, pm: posterior macula (saccular macula).**(F)** Phalloidin staining of the utricle macula (anterior macula) showing the hair bundles and kinocillia orientation revealing hc polarity. Figure adapted from Haddon et al. [65] (caption continues in next page).

Figure 1.5 Continued caption. **(G)** Schematic of the utricle, which is the only gravity-sensing system in the larva inner ear. The hc (gray) in the utricular macula are innervated by the hc afferents (blue) from the VIIIth nerve. The cell bodies of these neurons form the utricular ganglion and project to brainstem neurons (not shown) involved in posture and oculomotor reflexes. **(H)** Morphology of the developing zebrafish inner ear. Lateral view of paint-filled ears from 3 to 20 dpf; aa: anterior ampulla; ac: anterior cupula; cc: crus commune; lc: lateral cupula; la: lagena; pc: posterior cupula; s: saccule. Scale bar = 250 mm. Figure from Bever et al. [66].

a) *The vestibulo-ocular reflex (VOR)*

The vestibular-ocular reflex (VOR) is the circuit that connects eyes to ears in order to stabilize retinal image motion (retinal slip) during head rotation or translation, by directing compensatory eye movements [68] (Figure 1.6D-E). The first vestibular-induced eye movements appear at 3 dpf [63] and become more robust over time, reaching a plateau by 10 dpf [71]. In this gaze-stabilizing utricle-specific VOR circuit, the inter-neurons involved are the neurons from the tangential nucleus [72, 71]. In non-mammalian vertebrates, the tangential nucleus represents a discrete neuronal cluster within rhombomere 5 [73] that receives a dense utricular input [74]. Tangential vestibular neurons receive dendritic inputs from utricular afferents and project contralaterally to oculomotor nuclei completing the three-neuron arc mediating the VOR in zebrafish larva, where the semicircular canals are not yet functional [59] (Figure 1.6D-E).Thus, 3-10 dpf larva show VOR evoked by utricular stimulation mostly in two axis: pitch (Figure 1.6D) and roll (Figure 1.6E).

b) *The vestibulo-spinal reflexes (VSR)*

Vestibulo-spinal reflexes are sensory-motor mechanisms to maintain body stable or prevent animals from falling despite postural perturbations (i.e. roll or pitch, Figure 1.6A) [75]. The examination of the VSR is more complex than that of the VOR, because the behavioral response may involve several body arrangements, engaging sets of various muscles, whose changes will interact with the vestibular system in a closed loop [76, 16]. As a consequence, there are much less studies that

describe the VSR compared to those that describe the VOR.

In aquatic animals, perturbations to posture result from hydrostatic and hydrodynamic forces. Hydrostatic instabilities are intrinsic to the fish's body and arise from the discrepancy between the centers of mass (CoM) and of buoyancy, and create perturbations in roll, yaw, and pitch axes (Figure 1.6A-B) [77]. Due to this discrepancy, the zebrafish larva tends to tilt along its rostro-caudal and left-right axes: paralyzed or anesthetized larvae fall nose-down or roll over onto their dorsal or lateral side [70, 1] (Figure 1.6A-C). To move, the larva swims in discrete bouts, followed by pauses. During this pause, the larva slowly glides nose-down but swimming movements place the larva upwards [1]. Thus, unbalance triggers swimming but the neural circuits underlying this response remains unclear.

Another interesting vestibular behavior arises from the fact that before swim bladder inflation (around 5 dpf), larvae usually lie on their side when static. Locomotion then always starts with a righting movement that places the animal in the characteristic dorsal-up orientation [78] (Figure 1.6F).

In 2014, Bagnall et al. [64] characterized the motor activity underlying this righting behavior by using calcium imaging to quantify the activity in motor neurons innervating dorsal and ventral trunk muscles, in both sides of the fish. To do so, they evoked swim bouts in 4-5 dpf larvae mounted in agarose by applying a short electrical pulse in the tail and recorded the Ca^{2+} transients in the spinal cord. Their results showed a larger Ca^{2+} transient in ventral-projecting than in dorsal-projecting motor-neurons on the ear-up side, and an inversion of this pattern on the ear-down side, demonstrating an asymmetric activation of trunk musculature (Figure 1.6F). If this connectivity relies on direct synapses between descending tracts and primary motor neurons or indirect synapses via spinal pre-motor populations remains unclear [79].

Another study by Favre-Bulle et al., [2] showed that fictive utricular stimulation elicited contraversive tail movements and swimming, establishing that movements of the utricular otoliths alone are sufficient to drive compensatory responses. Based on the results of Thiele et al. [80], in which optogenetic stimulation of the nucleus of the medial longitudinal fasciculus (nMLF) elicited ipsilateral tail deflections, they suggest a circuit that could underlie this behavior. They theorize that afferences from the utricle relay the information to the contralateral nMLF via the tangential

nucleus [71]. So far, there are no publications that show or quantify this reflex using non-fictive vestibular stimulation in larval zebrafish.

1.4 Studying and understanding vestibular circuits

How brain produces motor responses and generates complex behaviors, still remains one of the most challenging questions in neuroscience. As discussed previously, the highly conserved mechanisms and anatomy together with the possibility of wide-brain imaging, make the zebrafish larva an excellent model organism to study vertebrate sensory encoding and behavior [37].

In the last decade, the development of three main fields: molecular biology, microscopy and computational neurosciences, have expanded the way to study and interrogate neuronal circuits. These techniques include: 1) molecular methods to label, identify and manipulate precise types of neurons in the nervous system, 2) functional calcium imaging to visualize activity patterns across large numbers of neurons with single-neuron resolution and a temporal resolution of one hundred milliseconds and 3) advances in quantitative methodologies to characterize behavior and to analyze large-scale neuronal population recordings [38].

In this section I will review these methods and how they have been useful to scrutinize the neural circuits underlying fish behavior, and specifically the vestibular behaviors involved in gaze and postural control. I will also report the latest findings that concern the neural mechanism underlying postural control, focusing on vestibulo-spinal reflexes.

1.4.1 Functional calcium imaging and other tools

The development of calcium imaging over the past 30 years, has allowed to obtain signals with a high degree of temporal and spatial resolution. And it has become a powerful tool for *in vivo* imaging of cellular activity in living animals. Imaging Ca^{2+} signals in ensembles of cells within the brain enables recording activity patterns in local circuits. The calcium signal is a proxy to measure neuronal activity and development of miniaturized head-mounted two-photon microscopes have allowed to make functional imaging of the brain activity in behaving ani-

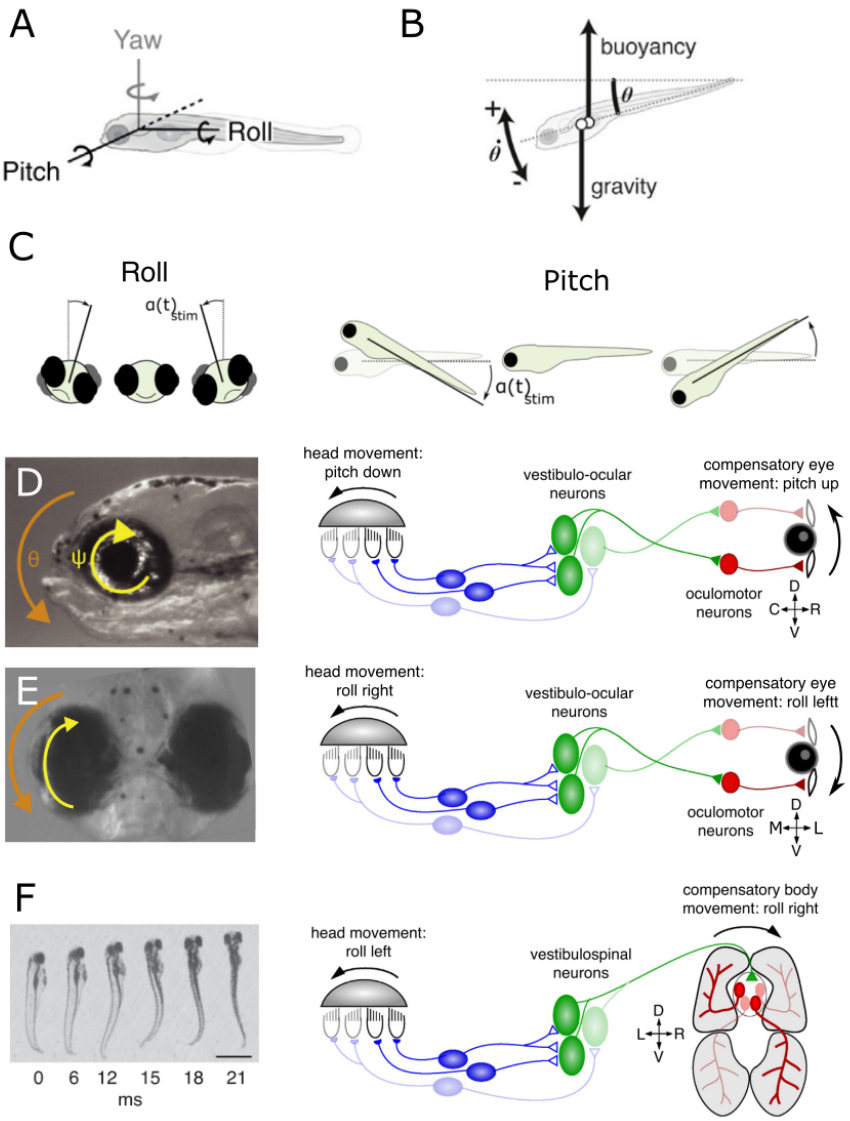

Figure 1.6 Vestibular reflexes from larval zebrafish. **(A)** Schematic of the three axes of rotation: roll, pitch (nose-up/nose-down) and yaw (left/right turns) that fish can undergo while swimming. **(B)** The larva's center of gravity is situated anterior to the center of buoyancy, causing a nose-down torque that rotates inactive fish nose-down. Adapted from Bagnall and Schoppik [79]. **(C)** Schematic of roll and pitch, α indicates the rotation angle. **(D-F)** Schematic of the vestibular circuits underlying gaze and posture stabilization. **(D-E)** Vestibular-driven gaze stabilization mediated by the vestibulo-ocular reflex (caption continues in next page).

Figure 1.6 (Continued) **(D)** When fish pitches nose-down, the utricular otolith glides depolarizing some hair cells (black) and hyperpolarizing others (gray), depending on the kynocillium orientation. The brainstem vestibular nuclei connect to oculomotor neurons, driving eye rotation up-wards (active pathway, dark green). **(E)** Equivalent circuit for a rightward roll producing a compensatory leftward eye roll. **(F)** When larva are rolled to their side, the ear-down utricular otolith slides lateral relative to the hair cells. This vestibular drive sets up asymmetric activation of trunk muscles, ventral muscle on the right and dorsal muscle on the left (shaded regions) producing a self-righting torque through vestibulospinal neurons.

mals, including mammals [81, 82]. Moreover, fast scanning technologies, such as light-sheet microscopy, have been developed for ultrafast time-resolved imaging of large regions of tissue comprised of many cells in 3D space [83]. This technique is advantageous to study neural circuits, and despite the loss of temporal resolution compared to electrophysiology, it is a good trade-off to image large regions or even the whole brain of a vertebrate [42, 46, 81].

Another set of tools comes from the combination of optics with genetically encoded light-gated ion channel (e.g., channel-rhodopsins). These channels are ion-specific and undergo conformational change when excited by light, changing from a closed to an open state, thus increasing the membrane conductance to the specific ion. Cation-conducting channels will be excitatory and anion-conducting channels will be inhibitory. These genetic tools for manipulating neuronal activity with light are called *optogenetics*. The development of different optical techniques to stimulate light-gated ion channels expressing neurons in single cells or large neuronal circuits [84, 85], together with Ca^{2+} imaging techniques, enabled monitoring whole-brain dynamics and describe neural circuits underlying behavior by manipulating neural activity *in vivo* [84, 80, 86, 87].

1.4.2 State-of-the-art

The study of the vestibular system in the larval zebrafish started quite late compared to other model organisms, including mammals and other fish. The first

characterization of a vestibular evoked response corresponds to the work by Easter and Nicola in 1997 [88] and, in 2010, Mo et al. [63] made the first quantification of vestibular evoked eye movements. Regarding postural control, the first work that described the role of the utricle in larva's balance corresponds to Whitfield et al. in 1996 [89]. They described a variety of mutants with impaired otolith development showing a defective balance phenotype. These mutants were named *circling mutants* [90].

The delay on the study of the neural substrates of vestibular-driven responses is due to the fact that implementing a protocol of "natural" vestibular stimulation is not straightforward: the head of the animal needs to be rotated or translated in space, making simultaneous neuronal recording difficult. Various studies have taken different approaches to tackle this problem. In the next paragraphs I will discuss those that I found of particular interest for my thesis.

In 2014, Thiele et al. [80] (mentioned previously in section 1.3.3) showed that optogenetic stimulation of nMLF neurons, a small group of reticulospinal neurons in the zebrafish midbrain (Figure 1.7), activated the posterior hypaxial muscle, producing an ipsilateral tail deflection. Moreover, ablation of this population lead to biased contralateral swimming when fish performed OMR. This results indicated that neurons of the nMLF provide control of tail orientation and thus steer the direction of swimming.

Two recent studies [91, 92] used a practical approach to make electrophysiology recordings from vestibulospinal (VS) neurons. The experimental set-up is composed by a stage that can translate horizontally in order to stimulate the larva's utricles. The electrodes for recordings, once placed, move together with the fish on this stage. Using this set-up, Liu et al. [92] established that VS neurons receive excitatory inputs from ipsilateral utricles (Figure 1.7) and that they are recruited during both rolling and pitching. Although, they are tuned for ipsilateral tilt in the roll axis, they show more heterogeneous responses in the pitch axis, including tuning for rostral or caudal acceleration. Hamling et al. [91] showed that ablation of this neuronal population disrupts regulation of body posture in the pitch axis (nose-up, nose-down) [1] compared to control sibling, but did not affect swimming dynamics (bout speed, bout duration or bout frequency) nor the preferred posture (dorsal-up). In this study, they did not asses the behavior on the rolling axis, but the fact

that VS ablation does not disrupt the dorsal-up preferred position may imply that these neurons do not have a main function in maintaining fish dorsal-up. Together, these two studies show an important role for the VS neurons in coordinating postural control in the pitch axis, but the pathways underlying this behavior remain unclear. Also, the role of tangential nucleus and other reticulo-spinal neurons are disregarded.

In the next paragraphs I will present two works that used Ca^{2+} imaging to describe whole-brain dynamics during vestibular stimulation.

In the first work, Migault et al. [3] used a rotating light sheet microscope (see subsection 3.2b), Figure 3.1) to stimulate the vestibular system while imaging the whole brain. The larvae rotates together with the microscope, in order to maintain the sample always in the same focal plane relative to the microscope. To image the fluorescence they used a lightsheet unit for fast scanning, achieving an acquisition rate of 2.5 brain stacks per second. They were able to observe the activity of all neurons in response to sinusoidal vestibular stimulation in the roll axis. Their results showed that neurons in the tangential nucleus (TN) and VS neurons are activated ipsilaterally in the ear-down side but the activity in the nucleus of the medial longitudinal fasciculus (nMLF), oculomotor nucleus (nIII), trochlear nucleus (nIV) and inferior olive was mostly contralateral to the ear-down side. Large populations of active neurons were also found in the cerebellum and the hindbrain. The phase maps were spatially organized, with an evident separation between the two hemispheres with antisymmetric activity.

In the second one, from Favre-Bulle et al. [93], they used an optical-tweezers set-up previously developed by them [2] to trap the utricle of stationary larvae, generating a fictive vestibular stimulation during whole-brain Ca^{2+} imaging with SPIM microscopy. One advantage of this method is that they could exert separate control over the left and right utricles, allowing to study the laterality of brain-wide vestibular processing by distinguishing between neurons with unilateral and bilateral vestibular sensitivity. In addition, this method allowed to perform conflicting signals from both ears showing that they mutually cancel. Their results showed vestibular responses in specific regions of the larval zebrafish brain, similar to those shown by Migault et al. [3]. Whereas for unilateral utricle trapping the response was lateralized, showing excitation in the medial octavolateralis nucleus (MON)

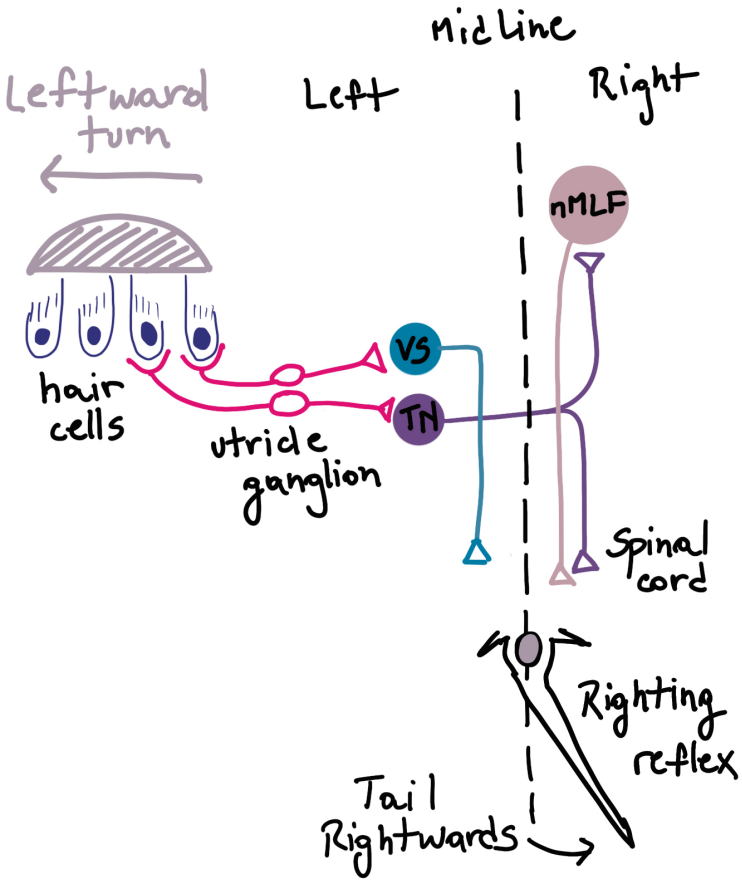

Figure 1.7 Schematic circuit of descending tracts in postural control. The vestibular afferents innervate the utricle hair cells. During a leftward turn, they relay information to both vestibulospinal neurons (VS) and the tangential nucleus (TN). The VS neurons axons descend ipsilaterally, whereas in the tangential nucleus neurons with ascending/descending axons cross the midline and contact contralaterally both the nucleus of the medial longitudinal fasciculus (nMLF) and the spinal cord, producing a rightward tail deflection.

ipsilateral to the stimulus. This result was expected, since these neurons are the first to receive input from the sensory ganglia. A less expected result was the excitation, at lower levels, in the MON contralateral to the trapped utricle. They suggested this activation most likely results from inter-hemisphere communication between the two MON, possibly through the commissural tangential neurons described by Bianco et al. [71]. These particular neurons innervate the contralateral octavolateral neuropil [71]. These commissural neurons in the vestibular system were described previously in cats for both semicircular canals [94] and otoliths [95]. They are inhibitory and facilitate bilateral integration of vestibular signals from the two ears providing increased sensitivity to horizontal linear acceleration and lateral tilt of the head by a convergence of facilitation and disinhibition, or by disfacilitation and inhibition [95].

As in the work of Migault et al.[3], Favre-Bulle et al. also found contralateral activation (and to a lesser degree, ipsilateral inhibition) of the nMLF. Most likely, the nMLF is activated via the tangential nucleus input [71] (Figure 1.7) and causes postural adjustments in the tail [80] which bends contralaterally from the fictive stimulus [2]. This work showed the importance of fictive stimulus in understanding the individual contribution of each utricle, to dissect the circuits underlying postural control.

1.5 Aim of this work

Maintaining the correct posture while animals move is a complex task that involves different sensory cues such as visual, vestibular and proprioception. Most of the postural control is done unconsciously via the tectospinal and the vestibulospinal pathways, which are among the most ancients neural pathways for motor control in vertebrates.

The tectospinal circuit makes adapted orientation movements guided by visual cues. The vestibulospinal circuits exert tonic postural control. My thesis deals with the latter and I do not discuss the former.

The vestibulospinal tracts are responsible for carrying out the vestibulospinal reflexes. A *vestibulospinal reflex* is one that uses inputs from organs of the vestibular system (otoliths and semicircular canals) and recruits skeletal muscles in order to

maintain balance and posture. And even though the vestibulospinal reflexes consist basically in few processing steps of neuronal relays, the understanding of several details of the underlying neuronal circuits is still missing. The main reason for the lack of information is that the studies have been performed mostly in mammals and the vestibular system is not fully accessible. This makes both stimulation and neural recordings difficult. Moreover, most of the studies done in vestibular system consist in electrophysiological recordings of small numbers of neurons, that cannot access the neuronal activity on the full circuit and population level.

The zebrafish larva is the only vertebrate model that allows whole-brain functional calcium imaging, making it a good model for systems neuroscience. Moreover, the vestibular system is highly conserved among vertebrates, so we consider that using this model organism to study vestibular sensory-motor integration can shed light about the mechanisms underlying postural control that can be extrapolated to other vertebrates.

In the first part of my thesis we studied the behaviors evoked by vestibular stimulation of 5-9 dpf zebrafish. This chapter does not deal with vestibulo-ocular reflexes (VOR) but concentrates in the study of vestibulospinal reflexes (VSR). The vestibulospinal reflex drives compensatory neck, body, and limbs movements to stabilize body posture when animals pitched or rolled out from their normal position. Compared to VOR, this reflex has been less studied and the mechanisms involved are not yet fully understood. Thus, the first aim of my thesis (Chapter 2) was to characterize the compensatory body movements elicited by rolling the fish larva on their long axis (Figure 1.6A-C). Using different vestibular stimulation protocols, we investigated different strategies larvae use to compensate when forced out of their preferred posture. Finally, we described the set of tail responses evoked by roll stimulus, to depict the vestibulo-spinal behaviors of larval zebrafish.

The second aim of my thesis (Chapter 3) was to describe the whole brain activity elicited by vestibular stimulation and relate it to the behavior observed in the first chapter. We took advantage of the calcium indicators genetically encoded in the larval zebrafish, and we used different lines that label regions in the brain that are involved in the vestibular response. We generated a small library of neurons and brain regions that are active during sinusoidal vestibular stimulation.

The third aim of my thesis (Chapter 4) was to develop a new method to com-

bine whole-brain imaging with tools of neural manipulation during vestibular stimulation. Recording the brain activity and performing optogenetic stimulation or inhibition during vestibular stimulation is a difficult task, since the animal's head needs to be rotated to stimulate the vestibular system. To solve this problem, we developed a protocol to accomplish fictive vestibular stimulation via magnetic forces. The last chapter deals with the development and proof of principle of this new method.

The vestibulospinal reflex and vestibular behavioral repertoire

2.1 Introduction

In addition to detecting vibrations and acoustic cues, the inner ear plays a central role in maintaining balance by continuously informing the brain about body orientation within the gravitational field and about the head acceleration profile. In zebrafish larva, the utricle is the only organ responsible for sensing gravity [62, 71, 59], and thanks to utricular cues, wild type larvae maintain a dorsal-up orientation when stationary. They also show near perfect upright stability while engaged in fast locomotor activity such as escape response. This stability is severely impaired in fish without utricles [70, 96], confirming that this otolith is central to postural control in the larval stage. In addition, this balance does not only rely on passive support from the swim bladder or fish morphology, but rather is actively maintained [1, 97]. For example, anesthetized or paralyzed larvae roll over onto their dorsal or lateral surfaces, and they float upside-down or vertically [70]. Thus, the interaction between the vestibular system and the body muscles (vestibulospinal) is necessary to maintain a correct balance. Despite this fundamental role of vestibular-spinal behaviors in postural control, most vestibular studies in larval zebrafish focused on the vestibulo-ocular reflex (VOR) [88, 98, 59, 63, 71, 99], only few studies investigated vestibulo-spinal or righting reflexes [64, 1].

In this chapter, I characterize the behavioral response repertoire of larval zebrafish to controlled postural destabilization. With a system called *Balançoire*, I rolled head-restrained larval zebrafish along their rostro-caudal body axis at differ-

ent angular speeds and amplitudes and characterized the evoked tail responses. I will first present the method and the experimental protocol, then I will describe my results and I will finish with a discussion of how the observed behavioral responses can help larval zebrafish to maintain balance.

2.2 Methods

2.2.1 Experimental methods

a) Fish husbandry

All experiments in this chapter were performed using 5-7 days post fertilization (dpf) wild type zebrafish larvae. Adult fish were maintained at 28°C in system water in the fish facility of the Institut de Biologie Paris-Seine. Eggs were collected in the morning and then kept in E3 medium (5 5 mM NaCl, 0.17 mM KCl, 0.33 mM CaCl2, 0.33 mM MgSO4) in a Petri dish at 28°C in a 14h/10h light/dark cycle. E3 was replaced daily with fresh E3 medium.

b) Experimental set-up

We designed a set-up called *Balançoire* (Figure 2.1). This setup consists of a rotating platform connected to a motor (model DMAC17, Midi ingéniérie) controlled by an Arduino board (arrow in Figure 2.1). We mounted a cylindrical water tank on the platform, into which we could introduce a larval zebrafish, immobilized in agarose and held by a capillary. Rotating the platform, we rolled the fish around its long body axis. The tank had two glass windows, one on the top for illumination and one on the bottom to image the fish behavior. To avoid visual input, experiments were performed under infrared illumination, for which the fish is blind [100]. Below the water tank we placed a mirror which projected the image of the fish to a camera (Point Grey: FLU- U3-13Y3M-C) with a 25 mm objective (Navitar 1-19912) to record tail movements. Videos were recorded at 16 frames per second (fps). The set-up was controlled by a custom-made MATLAB program. This program allowed us to rotate the platform in 3 different ways: sinusoidal, ramping and step (Figure 2.2) with a maximum rotation angle of 90°.

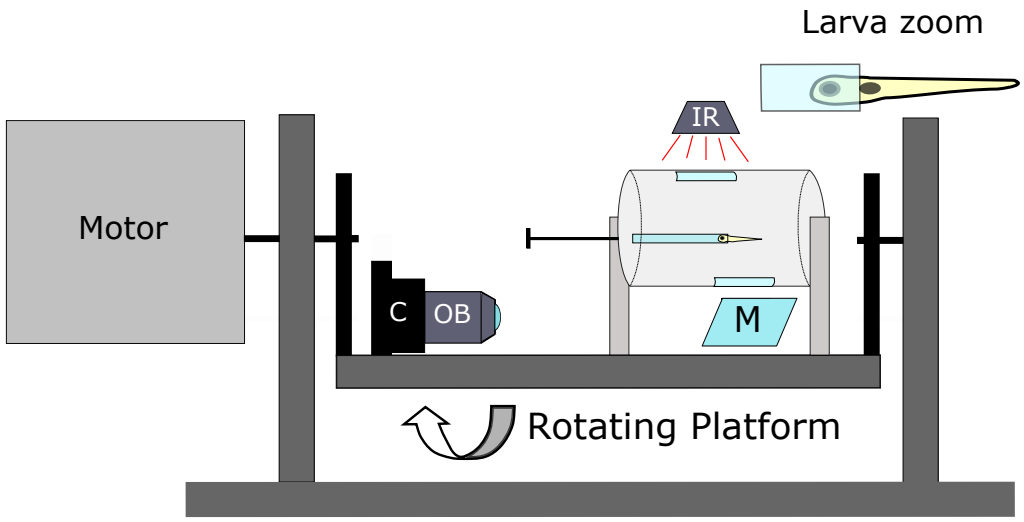

Figure 2.1 Schematic of the experimental set-up: the *Balançoire*. (A) A rotating platform was controlled by the motor. A cylindrical non-transparent water tank was placed on the platform, the tank had two openings, one on the top and one on the bottom that were both closed with a small glass window each. C: camera, OB: objective, IR: infra red led, M: mirror. **(B)** Zoom on the larva, which is mounted head-restrained in agarose and held by a capillary such that the tail is free to move.

c) Sample preparation

We used zebrafish larvae from 5 to 9 days post fertilization (dpf). The fish were embedded in 2% low melting point agarose and drawn into a capillary with a plunger. Then we removed the agar around the tail with a micro-knife at the swim bladder level. The larvae were head-fixed and the tail was free. Experiments were performed with wild-type fish and with fish in which we had removed the ear stone of the utricle in one or both ears.

d) Ear stone removal

To remove the ear stone from the fish, I used a protocol kindly shared by Dr. Masashi Tanimoto. Larvae (2 dpf) were anaesthetised with 0.04% tricaine and immobilized in 1% agarose lying on their side. The ear stone removal was done on a stereoscope using a glass capillary with a fine tip formed with a pipette puller from Narishige. I proceeded as follows: I introduced the glass-capillary in the otic

vesicle and pushed it against the ear stone. The ear stone of the utricle got attached to the capillary, then I gently pulled the capillary out with the ear stone attached to it. Next, I removed the larva from the agarose with the help of fine tip forceps (Dumont N°5). After the procedure, larvae were left to recover in a normal petri dish with E3 at 28° until experiments were performed 3 days after, at 5 dpf.

e) Vestibular stimulation protocol

With the setup we could apply various vestibular stimuli:

- *Step-wise:* This stimulation consisted in a stepwise rotation of the platform from 0° to a given angular orientation at which it was held for a given time and then rotated back to 0° followed by the same step in the opposite direction. This movement is called a step (Figure 2.2 left panel). For the first set of experiments the larvae were stimulated with a multi-step protocol (Figure 2.2 middle panel) of steps of increasing amplitude going from 2° to 30°, with a 2° increment (2°, 4°, 6°, 8°,...,30°). The transition between angles lasted less than 800 ms and the step dwell time was 20 seconds and this cycle was repeated 7 times to calculate later average behavioral responses per step amplitude. For the set of experiments with lacking ear stones, I tested the fish with a single-step protocol of 45° in amplitude and 10 seconds dwell time that was repeated 3 times (step in Figure 2.2).

- *Ramps:* This stimulus consisted in increasing the rotation angle at a constant speed of 25°/s to reach a certain angle and then go back to the initial position followed by the same movement in the opposite direction (Figure 2.2 right panel).

2.2.2 Data analysis

All the analysis was performed in MATLAB.

a) Tail tracking

In order to track the tail angle over time, raw images were first binarized using a set of filters in MATLAB [101]. Then I used a function written by Raphäel

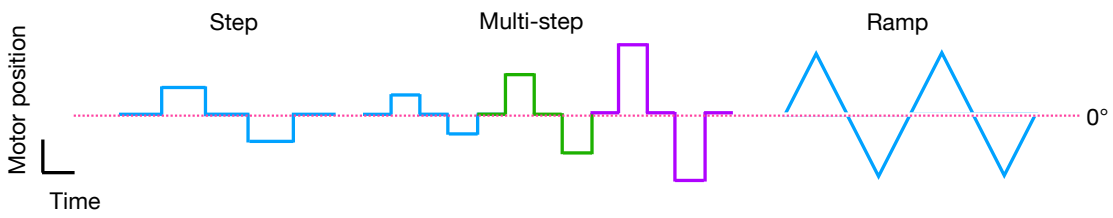

Figure 2.2 Different types of stimuli. From left to right: single step cycle, a multi-step cycle (steps of increasing amplitude) and a ramp stimulus.

Candelier (www.candelier.fr, image moments file), which uses the image moments to draw an ellipse on the binarized image. This function extracted the angle of the ellipse.

If we binarize a zebrafish larva image, we will get mainly 2 objects: the head and the trunk (Figure 2.3). We decided to draw an ellipse for each of these objects.Then we defined the tail angle as the difference between the long axis angles of the two ellipses (Figure 2.3). We analysed all frames for every video and then plotted the tail angle over time.

b) Swim bout detection

Swim bouts are fast tail movements (tail oscillations between 25 and 45 Hertz) that fish execute to swim. We detected swim bouts by calculating the derivative of measured tail angle over time to obtain the angular tail velocity. At every bout, which are fast tail movements, the angular velocity peaks. Swim bouts or other large tail movement bout types were thus detected by finding the peaks in the angular velocity data.

2.3 Results

2.3.1 Body roll drives the tail to pivot to the contraversive side

In order to study the vestibulo-spinal reflexes we designed a behavioral experiment to monitor the responsiveness of zebrafish larvae to vestibular stimulation in head-restrained conditions. We used the *Balançoire* setup that could rotate the fish about the roll axis up to ± 90° at different angular velocities. We performed

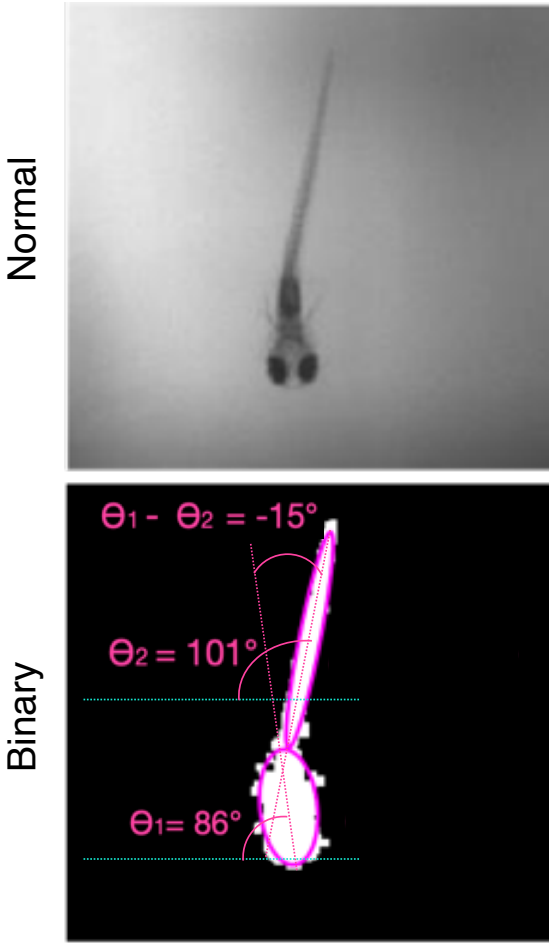

Figure 2.3 Tail tracking: image analysis to obtain the tail angle. Top: Raw image captured under infrared illumination (single frame from video). Bottom: Binarized image. Ellipses are fitted to the head and the trunk. θ_1 and θ_2 are the angles relative to the horizontal (cyan dashed lines) for the head and trunk ellipses. The difference between these two angles ($\theta_1 - \theta_2$) was taken as a measure of the tail deflection angle.

multistep stimulation protocols with step dwell times of 20 s (see Methods b) and Figure 2.4A).

We found that this body rotation drove the tail to pivot to the *contraversive* side relative to the stimulus and around a pivoting point located at the end of the swim bladder, where the trunk begins: fish rolled to the left (clockwise) pivoted their tail to the right and vice-versa (Figure 2.4B). This was true for every step along the whole cycle. The averaged trail responses (N=9) for the different step stimulation amplitudes are shown in (Figure 2.4C). The tail responses were tonic during the stimulus span for body angles higher than 10° (Figure 2.4B) but a relaxation of the tail angle towards the initial orientation during the step span was observed for smaller stimulation amplitudes (2°-6°). To quantify the tail response as a function of the stimulation amplitude we extracted the average tail angle at 2 seconds after the stimulus onset. At this time point, the tail deflection angle increased with body rotation almost linearly for stimulation angles smaller than 12°. For larger stimulation angles, the response saturated at a value of $\sim 10°$ (Figure 2.4D). The strong correlation of this robust behavioral response with the postural destabilization angle of the larva's body roll angle suggests that this behavior plays a central role in postural control.

a) Contribution of each utricle to the pivoting tail response

Since in vertebrates the vestibular system is bilateral, the brain constantly integrates inputs from both ears.

To disentangle the contribution of both ears to the pivoting tail response we removed unilaterally and bilaterally the utricle in 5 fish. Fish with missing left utricle showed no tail response when rotating the fish left ear down (phase I, blue line). Under this condition the remaining right utriclular ear stone was pulled medial by gravity. We conclude that a medial ear stone movement does not elicit a tail response. When rotating the fish right ear down the tail pivoted as in wild-type fish to the left (phase II). Here the right otolith was pulled to the lateral side. We conclude that the pivoting tail response is controlled by ear stone movements in the lateral direction. However, when rotating the fish back to its dorsal-up posture, the kinematics by which the tail relaxed back was significantly slower compared to experiments in wild-type fish (phase III). We conclude that under normal conditions

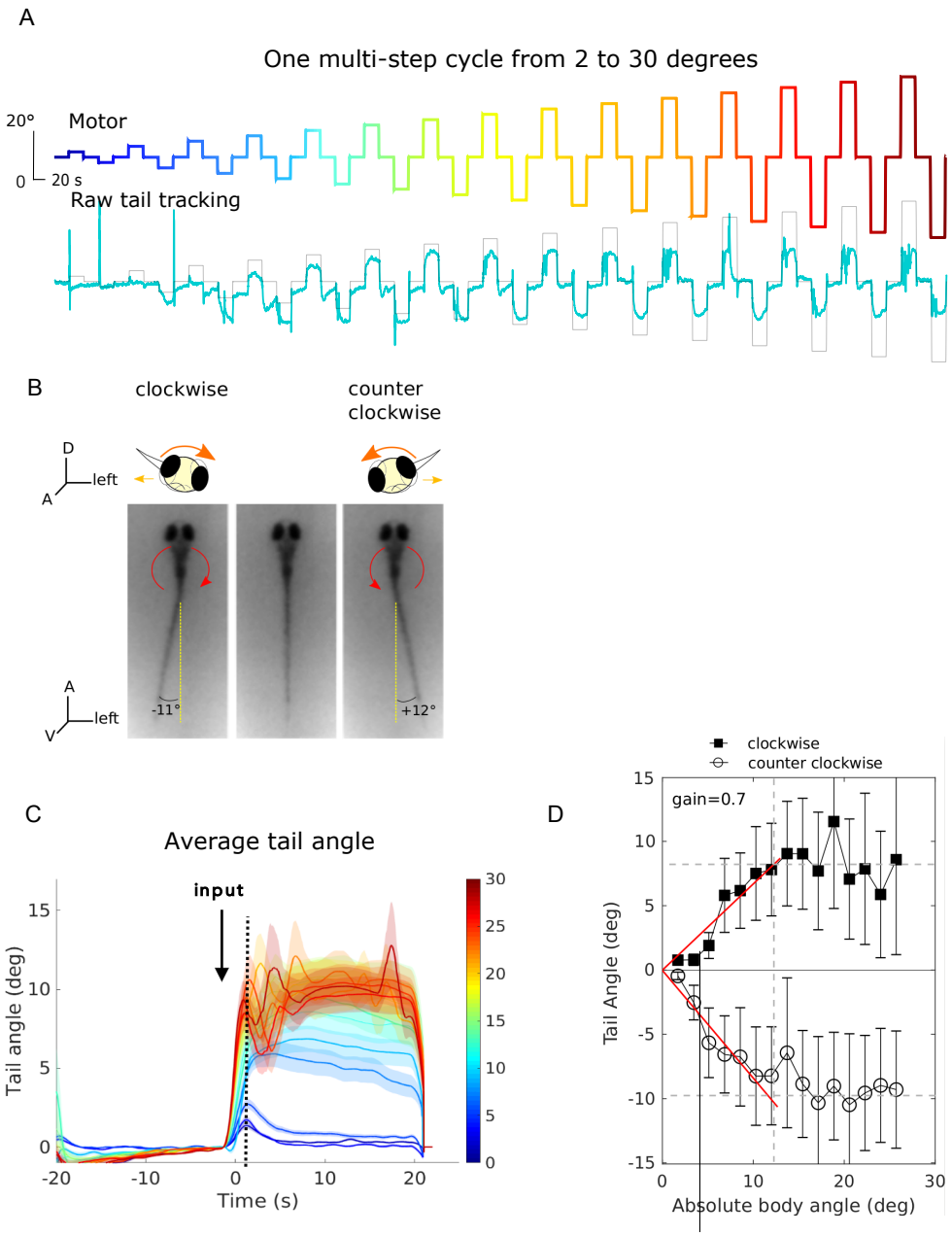

Figure 2.4 Tail deflection in response to step stimulation (A) Clockwise rotation of the fish drove the tail to pivot rightward and vice versa (red and orange arrows indicate rotation sense; yellow line indicates the reference straight position). **(B)** Absolute value of the temporal profile of the angle of the pivoting tail response averages over 9 trials recorded in a single fish. Shown are the responses to 7 different step stimulation amplitudes (color bar indicates the amplitude of the step stimulus in degrees). Red arrow indicates stimulus onset. **(C)** Trail averaged tail angle extracted 2 s after the stimulus onset (see dashed line in C) as function of the angle of the body rotation (step stimulus amplitude).

the left utricle provides a signal to pull the tail back to its center position. All these three phases of the response are shown in Figure 2.5B (blue line) together with a schematic illustrating the direction of the forces on the otoliths. Fish with bilaterally ablated utricular ear stones did not show any tail response at all to the step stimulus (Figure 2.5B, green line).

As a control, we also characterized the tail response in paralyzed fish that were treated with α-bungarotoxin, which is a neurotoxin that binds irreversibly to the nicotinic acetylcholine receptor at the neuromuscular junction [102]. The tail of paralyzed fish did not pivot when rotating the fish, only short transient deflections were observed during the rising and falling edge of the step stimulus (Figure 2.5B, black line). These movements were most probability caused by inertial forces on the tail and the water in the tank. Given the small magnitude of these tail movements, we conclude that the observed large amplitude pivoting tail movements discussed previously are all evoked by muscle contractions and not movement artifacts.

b) Multisensory nature of the pivoting tail response

It is known that the vestibular and the visual system interact during postural control [103]. A head translation or rotation leads to a movement of the visual environment in the opposite direction. The visual system can thus also inform the brain about head movements and evoke postural control movements. I performed a preliminary experiment to test if the observed pivoting tail response can also be evoked by visual whole-field motion. We attached a projector to the setup to project images inside the cylindrical water tank at 360° around the fish. As stimulus, we created a pattern of black and white strips that was controlled to move around the fish (Figure 2.6B) to simulate the movement of the visual field experienced during body roll. Indeed, the larvae tested presented a pivoting tail movement that followed the rotation of the visual pattern (Figure 2.6A). The tail movement was contraversive to the visually simulated body roll. Thus, the visual and the vestibular system control the same behavior in response to a body roll. But the observed maximal tail deflections evoked by the visual stimulus were with 3°-4° in amplitude smaller compared to the maximal responses of 11°-12° in amplitude evoked by the vestibular roll stimulus.

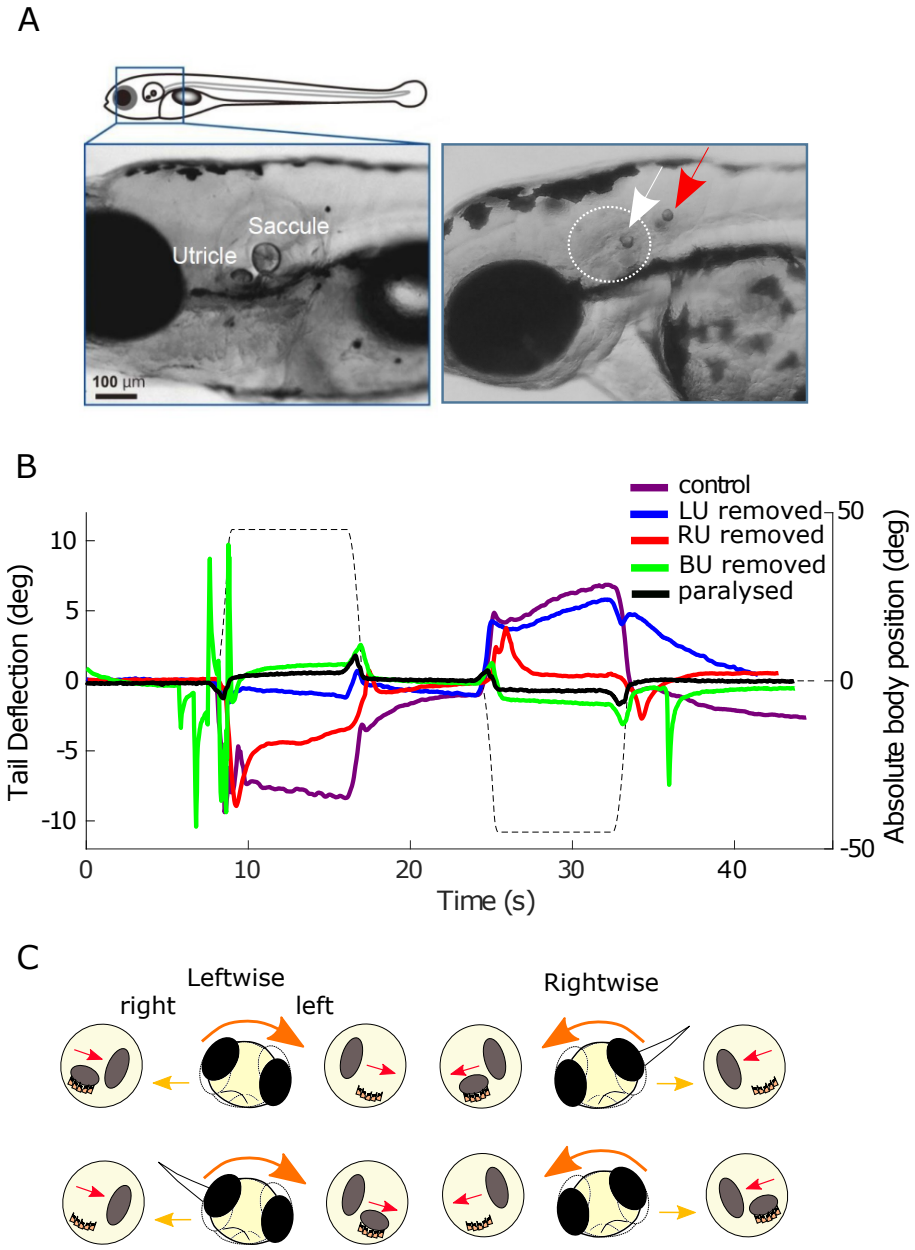

Figure 2.5 Unilateral and bilateral utricle ablation leads to different dynamics of the pivoting tail response. **(A)** Right panel: Zoom onto the otic vesicle of a 4 dpf larval zebrafish. Left panel: Removed utriclar ear stone (red arrowhead) performed in a stereoscope, only the saccule (white arrowhead) remains inside the ear. **(B)** The tail angle is shown as a function of time averaged over recordings in 5 fish and 3 stimulation cycles per fish: control (purple), left utricle removed (blue), right utricle removed (red). Positive angles correspond to a roll left ear down. **(C)** Schematic of a fish larva rolling leftward and rightward. An inset of both ears is shown in each side of the larva to display utricle movements toward the medial and lateral side of the animal.

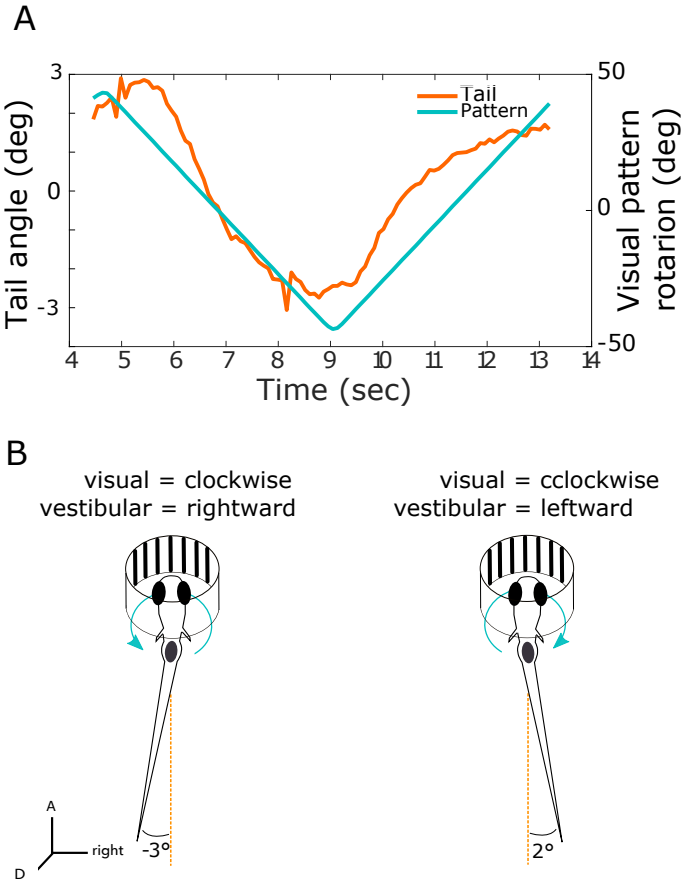

Figure 2.6 Visual pattern evokes contraversive tail deflection. **(A)** Average of 20 periods for one larva shows the tail deflection (orange) over time when a visual pattern (cyan) is moved around the fish to simulate rolling. **(B)** The scheme shows the direction of the visual pattern movement and the direction of the tail deflection. The blue arrow indicates the turning direction of the visual pattern.

2.3.2 Contribution of discrete tail bouts to postural control

Freely-swimming (non-restrained) larvae swim by performing discrete tail *bouts*, executed in average once a second [104]. Swim bouts are also observed in head-restrained larvae and can be elicited by sensory stimuli, e.g. by moving stripes under the fish (optomotor response, OMR)[105].

Next, I investigated if vestibular stimuli also trigger swim bouts and change bout kinematic as a second mechanism of postural control.

In the context of the master's internship of Muntasir Challachand, we classified the tail bout types observed during the multi-step roll stimulus protocol (Figure 2.7E). We identified three main tail bout types during the experiments:

1. Swim bouts: Characterized by a finite number of tail oscillations that propel the larva if not head-attached through water.

2. Left and right tail flips: big amplitude unilateral tail movements.

3. Struggles: stereotypical big amplitude movements from tail to head that larvae makes to free themselves from the agarose [106] (Figure 2.7F).

One of the aims of Muntasir's internship project was to develop an automated way to sort the different tail movements during the trials using the output of the tail tracking algorithm. But we found this method not easy to implement due to the low acquisition rate (16 fps) of the videos. The acquisition rate could not be improved at that time as the laboratory was closed during the lock-down forced by the pandemic, so we decided to go manually through the videos to quantify the occurrences of the different bout types for the different stimulation amplitudes.

For small rotation angles (0° – 10°), most fish did not show many spontaneous tail bout events. We observed mostly the tail to robustly pivot contraversive to the stimulus direction (Figure 2.7B and D) as described in the previous paragraph. For larger rotation angles (10°-30°), we observed that, in addition to the pivoting tail response, fish were more likely to execute swim bouts (Figure 2.7C and E) and tail flips (Figure 2.7E). The probability of swim events increased with the absolute body rotation angle (Figure 2.7F). Moreover, we observed that swim bouts were biased towards the contraversive side of the stimulus direction (Figure 2.7G), probably due to the basal pivoting movement of the tail deflection (Figure 2.7G').

Finally, we quantified the average for swim bout duration and found it to linearly increase with the stimulation angle (Figure 2.7H).

Interestingly, struggles occurred during the whole run independent of the vestibular stimulation strength (data non shown).

Many of the detected swim bouts during the step stimulation protocol were found to occur during the rising or falling edge of the step stimulus. We cannot exclude that these bouts are triggered by the vibration induced in the platform by the fast acceleration and stopping at every step. Larger steps would induce stronger vibrations thus increasing the probability to evoke a tail bout as observed during the multistep stimulus protocol.

To study if bout initiation depends on a pure angular body orientation we implemented a ramp protocol (see section 2.2.1, Figure 2.2) to exclude the vibration issue and better understand the shift from a mainly pivoting tail response at small stimulation angles to the stimulation of discrete tail bouts at higher stimulation amplitudes. In this protocol, the fish were rolled at a constant angular speed of 25°/s up to the maximum angle of ±90°. We tested 5 larvae for 4 trials each. One trial consisted of two ramps: the first one from 0° to 90° (leftwise) and back to 0°, and the second one from 0° to -90° (rightwise) and back to 0° again (Figure 2.8A) without a pause in between. For every trial, I calculated the angle at which the first swim bout occurred for each direction. I found that the first swim bout occurs most likely between 20° and 29° (Figure 2.8B). The found distribution shows that swim initiation is not random and bout initiation depends on body rotation angle. Thus, we concluded that the evoked discrete bout events are part of the postural control mechanism.

2.4 Discussion

2.4.1 Postural control on larval zebrafish

In this chapter, we have shown that zebrafish larvae present a robust pivoting tail movement that is evoked by body rotations about the roll axis. This tail movement seems to be mainly evoked by unilateral vestibular input, and it is directed to the opposite side of the stimulation (contraversive). We hypothesize that this pivoting

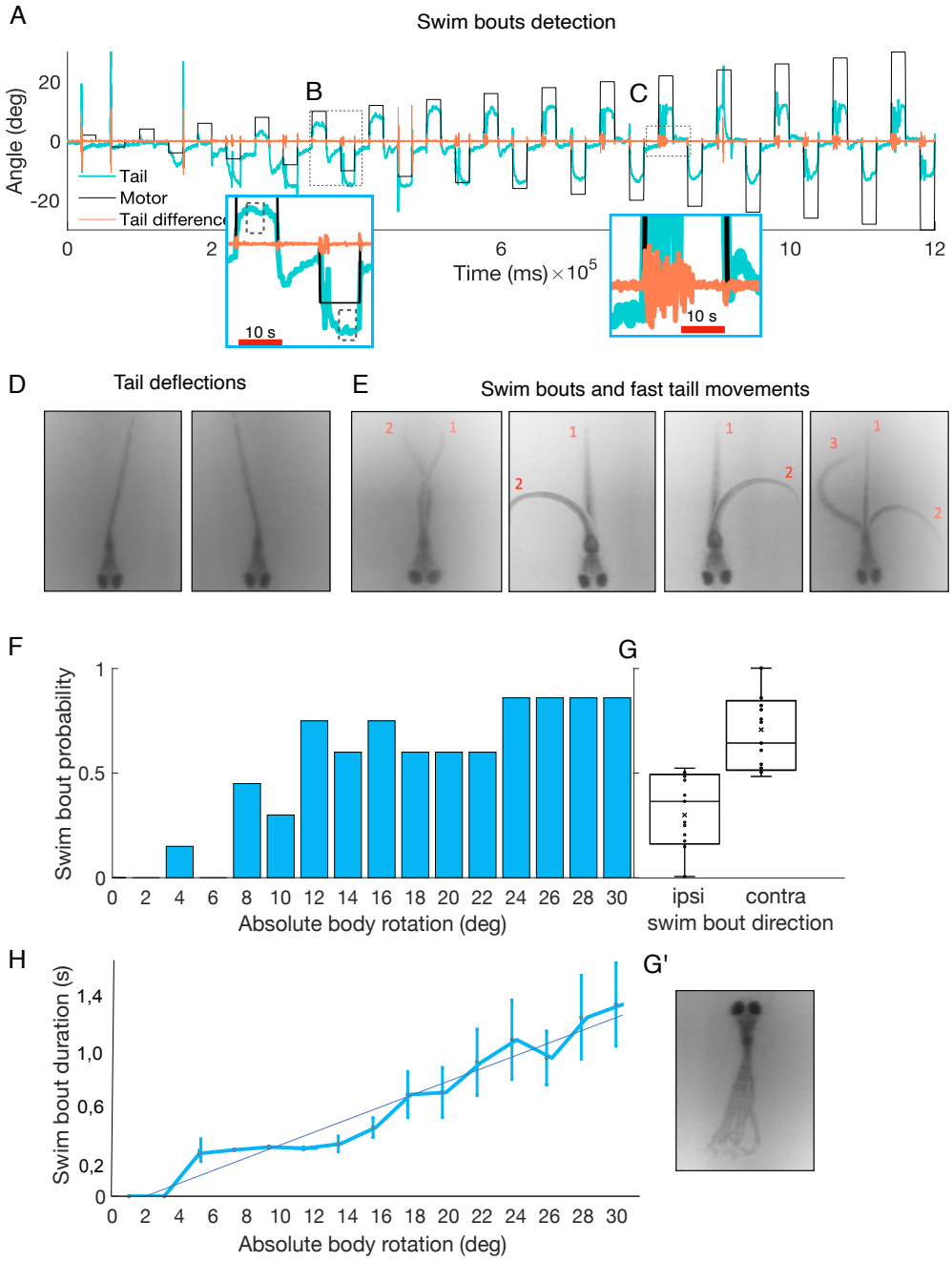

Figure 2.7 Characterization of the pivoting tail movement and of discrete tail bouts observed during the step stimulation protocol. (A) Motor angle (black), tail angle (cyan) and tail angle derivative (orange) plotted over time. **(B)** Zoom into the tail response to a 10° step stimulus. **(C)** Zoom into the response to a 22° step stimulus. **(D)** Pivoting like tail deflection in response to a left (right) roll stimulus. **(E)** Tail bout categories from left to right: swim bout, right tail flip, left tail flip, and struggling. Numbers indicate the time evolution in the sequences (caption continues in next page).

Figure 2.7 (Continued caption) **(F)** Probability of the occurrence of at least one discrete tail bout during the dwell time of the step stimulus plotted against the absolute value to the step stimulus amplitude (N = 3). **(G)** Boxplot shows the probability that a tail flip was towards the ipsiversive or contraversive direction of the step stimulus. All stimulus steps are pooled for the analysis. The probability of contraversive tail flips was significantly higher than ipsiversive (N=3, p<0,0001) flips. **(H)** Average swim bout duration (N=3) is plotted for each step. **(I)** Image shows a swim bout biased towards the left to illustrate ipsi and contraversive swim bout direction.

tail movement participates in postural control.

We observed that a fish that rolls to the right (right ear down) pivots its tail to the contraversive left side. This could be a mechanism to counterbalance a body destabilization by re-positioning the center of mass of the larva such that the fish rolls back to its dorsal up posture. This would be comparable to humans raising their left arm to restore balance when they are off balance to the right.

When larvae were rolled to larger angles, they started swimming. We propose that the observed swim bouts have the same role as the tail deflections: they serve to counterbalance the fish to its natural position when they are pushed out of equilibrium, but in a faster and more effective way. This could be comparable to humans that need to make a step to stabilize their posture when pushed too strongly out of their equilibrium position. Ehrlich et al. [1] have shown that a forward movement of a zebrafish larva can stabilize posture about the pitch axis. A similar mechanisms could help to stabilize the body orientation about the roll-axis.

In 2017, Favre-Bulle et al. [2] showed that pulling the otolith of the right ear with optical tweezers to the lateral side of the fish elicited a pivoting tail deflection to the left (Figure 2.9a). They also observed that applying a larger force onto the otolith caused a larger pivote angle (Figure 2.9b), and increased the probability of making a bout (Figure 2.9c). Finally, they showed that lateral trapping of the right otolith combined with medial trapping of the left otolith caused a pivoting movement of the tail that is the sum of the responses measured when providing these stimuli to both otoliths separately (Figure 2.9c,d). We observed the same pivoting tail movement, evoked by non-fictive (natural) vestibular stimulation. In

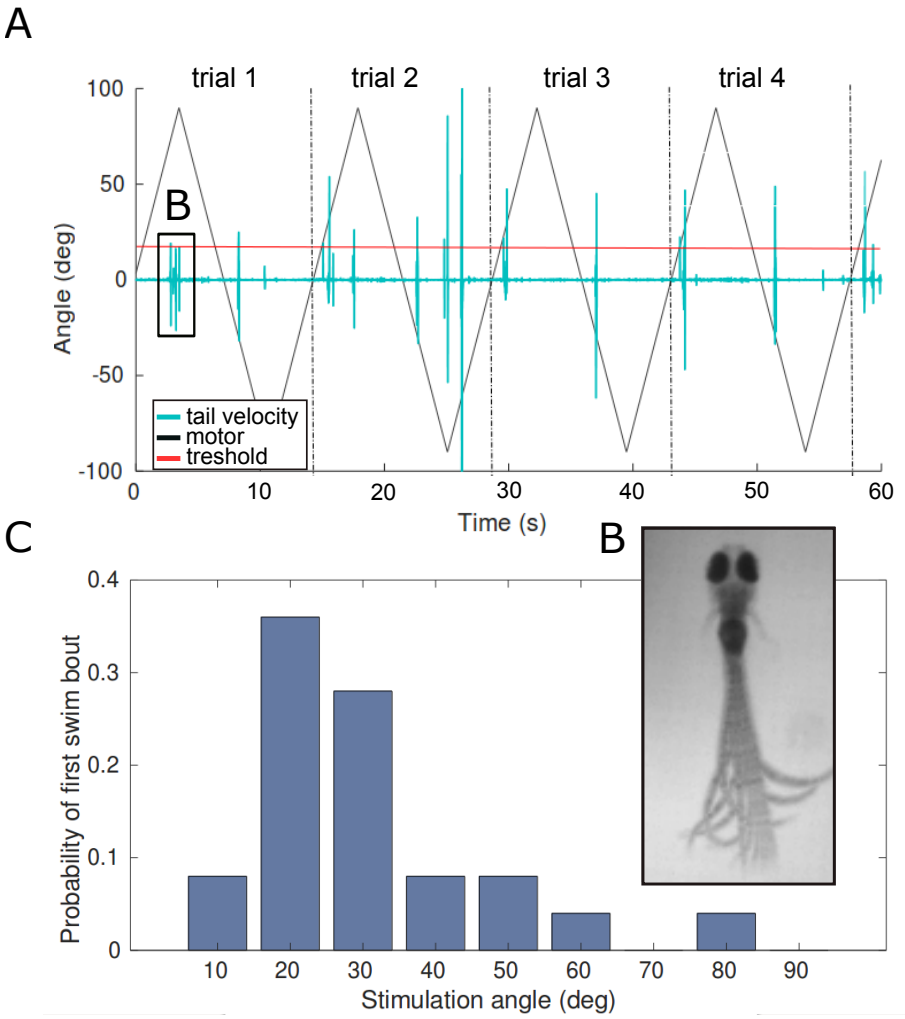

Figure 2.8 Probability of swim bout as a function of the body rotation angle. **(A)** The derivative of the tail angle (tail velocity, blue line) and the rolling angle (motor, black line) are plotted on time. The red line corresponds to 20° of stimulation to show where swim bouts occur. **(B)** The inset image shows a swim event. **(C)** The bar plot shows the occurrence of a first swim bout for every interval of 10° from 0° to 90°. The maximum probability is 0.36 in the interval between 20° and 29°, followed by 0.3 between 30 and 39° (N = 5 fish, 4 trials per fish).

addition, we removed the utricle in one ear only, to study the contribution of each ear under natural vestibular stimulation. We observed the pivoting tail response only when the intact ear was rotated downwards, which induced a lateral movement of the otolith. This is consistent with the optical tweezers experiment and confirms that unilateral utricular stimulation is sufficient to drive this compensatory tail response. Finally, we removed the utricle in both ears and demonstrated that they are necessary for this behavior, since bilateral ablated fish did not present this tail response when stimulated.

The tail deflections evoked by vestibular stimulation resemble also those elicited by optogenetic stimulation of the nucleus of the medial longitudinal fasciculus (nMLF) in larval zebrafish by Thiele et al. [80]. In this study, the authors showed that optogenetic activation of reticulospinal neurons from the nMLF led to ipsilateral deflections of the tail. When the stimulation stopped, the tail returned to the center. They also observed swim bouts in response to more powerful stimulation.

Our observations, together with the evidence previously shown by these two studies, suggest that vestibular signals from the utricle are relayed through the contralateral nMLF to motor neurons to direct a tail response. Bianco et al. proposed that this relay occurs via neurons located in the tangential nucleus [71]. In this nucleus, there are neurons with ascending commissural axons [71], thus, signals from the utricular hair cells go to the ipsilateral tangential nucleus and then to the contraleral nMLF, subserving potentially the tail responses described in this chapter.

One weakness of our set-up was the fact that the motor made a small vibration at the end of every step transition. These vibrations could have had an impact on the fish behavior, since they are probably sensed by the saccule. We were not able to solve this shortcoming mechanically, but we solved it by not considering the first 500 ms as purely vestibular behavior. We believe that removing this artifact will improve enormously the setup and will be easier to distinguish purely vestibular inputs. Another consideration to make is that we made the experiments in the absence of corresponding visual stimulation. Also, we didn't quantify the contribution (if there is any) from the lateral line. Experiments with complete ablation of the lateral line will be useful to study the pure utricular input. Also, a more detailed analysis of the tail kinematics to observe possible torsional movements [64] that were not detected

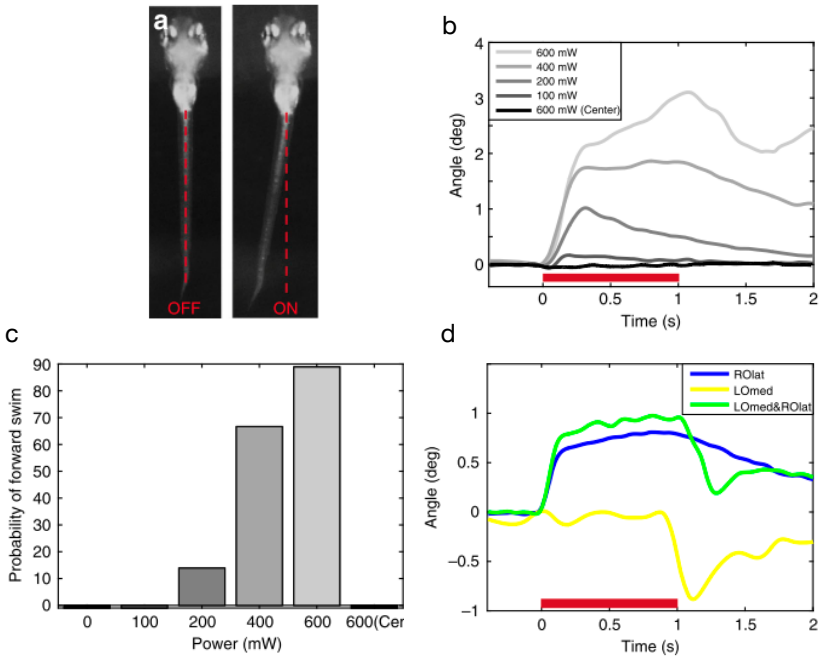

Figure 2.9 Optical trapping of otoliths drives coordinated compensatory tail movements in larval zebrafish. **(a)** Tail orientation of a larva before (left) and during (right) a 600 mW optical trap to the outside of the right otolith. **(b)** Tail deflection increases with laser power, and a 600 mW trap to the center of the otolith has no effect (average of trials from one larva). **(c)** The probability of forward swimming increases with increased laser power (n = 6 larvae, 3 trials at each power). **(d)** Average of trials from one larva. The combined tail response is roughly a linear sum of the two separate traps' effects. Figure adapted from Favre-Bulle et al. [2].

in this work (data not shown), would be necessary to understand the effects that these movements would have in free-swimming larvae.

2.4.2 Multisensory integration

The brain constantly integrates visual and vestibular inputs to stabilize gaze and posture. Optic flow provides an important sensory cue for self-motion, and it is capable of generating powerful sensations of moving even when individuals are stationary (absence of vestibular cues). Optic flow information also induces the generation of optokinetic eye movements (OKR) that complement the vestibuloocular reflex (VOR) to ensure stable gaze during self-motion [103], showing that visual stimulation can evoke a similar behavior to that evoked by the vestibular system. Our preliminary results show that purely visual stimulation also elicits the pivoting tail deflection described in this chapter. The nature of the visual response (3°-4°) is less intense compared to the vestibular (10°-12°), but it is comparable to the tail deflection angles obtained by Favre-Bulle et al. [2]. We estimate that a tail deflection of 3° is comparable to a body rotation of 5°, so we can calibrate the visual pattern rotation. In this case, we rotated the pattern between ±50 degrees to a speed of 25°/s.

One flaw of this protocol is that the larva response depends highly on the contrast and the rotation speed of the pattern, and finding the optimal parameters is not easy. But this result sets the bases of a new described behavior that could be useful to studies in multisensory integration. Further, experiments with different visual patterns to find the right stimulation parameters will allow exploring this behavior. This will shed light on deciphering neural circuits that integrate visual and vestibular cues to motor outputs.

2.4.3 Summary and Conclusions

In this chapter, we studied the vestibular system of the fish and the repertoire of tail responses elicited by vestibular cues. We were able to evoke a tail response similar to that elicited by utricle optical trapping [2]. We showed that natural vestibular stimulation evoked tail deflections four times bigger than the response elicited by optical trapping (12° compared to 3°). Moreover, we showed a positive

correlation between the tail angle and the rolling angle, with a plateau at 12°. We established a maximum tail deflection angle at 12°. These results are the first to describe this vestibulospinal reflex in detail. As expected, from the experiments done by Ehrlich et al. [1], we showed that rolling, as pitching, elicits swimming after a certain threshold. Notably, the threshold for roll (between 20° and 30°) was smaller compared to the nose-down pitch threshold (>45°). We hypothesize that this higher sensitivity to roll may be due to: 1) hair cell polarity in the macula, since the majority of the hair cells are oriented to be excited when utricle glides laterally, and 2) natural context, as fish move in the water column they need to re-orient often in the pitch axis to swim to the surface or the bottom, but in nature they do not explore or swim by rolling on their side.

By removing the utricle unilaterally we concluded that one utricle is necessary to elicit the response. In the next chapter, we will explore more in detail the neurons that could be involved in this response. We will take advantage of different transgenic lines that label neurons in the vestibular nuclei, reticulospinal system and primary motor neurons.

Study of cell types involved in vestibular behavior

3.1 Introduction

Concerning the studies done on vestibular behaviors, those about vestibulo-ocular reflex (VOR) are ahead compared to other motor responses. The three-neurons arc reflex of VOR has been studied in many vertebrates, from lamprey to humans, and we have a good understanding of how vestibular stimulation evokes compensatory eye movements [68]. The neurons and the conserved set of six extra-ocular muscles involved in this response are well described [69] and known from the extensive work done by Lorente de Nó [107, 108]. However, the memory and learning process related to it are less understood [109].

The vestibulospinal reflexes instead, which correspond to compensatory neck, body, and limbs movements to stabilize body posture, have been less studied and the neuronal circuits involved in postural control are not yet fully understood.

The second aim of my thesis was to characterize the neuronal circuits underlying postural control in larva zebrafish. In the previous chapter, I described the behavioral repertoire elicited by vestibular cues. Next, I wanted to characterize the neuronal circuits underlying these behaviors.

One of the unique characteristics of larval zebrafish is the possibility to image the whole brain *in vivo*. The recent development of the GCaMP proteins and light sheet microscopy have allowed to record the neuronal activity of thousands of neurons simultaneously [42, 46]. Nevertheless, whole-brain neuronal recordings can be difficult to analyze and identifying brain regions is not always an easy task. More-

over, in one of the most used transgenic lines: the *Tg(elavl3:GCaMP)*, almost all neurons in the larva nervous system express the calcium probe, but not all neurons. For example, the tangential nucleus and the vestibulospinal neurons—which participate in the vestibular response—are only partially labeled in this line. At the same time, one weak point of using this line in whole-brain imaging is that detailed neuronal activity can be missed out in the whole-brain response.

Therefore, generating and using different transgenic lines that express genetically encoded calcium indicators in a particular group of neurons can be useful to study the activity of specific brain regions. Other methods to observe activity of specific neurons include calcium dextran back-fill, electroporation and photoconversion [110, 71, 80]. But these can be complicated to implement, and the expression pattern is not as easy to replicate between individuals.

In this chapter, we will describe the brain response to vestibular stimuli by using a set of different transgenic lines that label different neuronal types and populations such as the vestibulospinal neurons, the reticulospinal neurons, the tangential nucleus, the granular cerebellum and the primary motor neurons (Table 3.1). For functional imaging we used the rotating light sheet microscope—developed previously in the lab by Migault et al. [3] to assess the response of specific neurons and nuclei to a sinusoidal-roll stimulus. We also ablated unilaterally the utricle to disentangle the contribution of both ears during natural stimulation, and we labeled retrogradely motor neurons to identify which muscle they innervate. The results described in this chapter are still preliminary, but provide a first step towards elucidating the neural circuits underlying postural control in the zebrafish larva.

3.2 Methods

3.2.1 Experimental methods

a) Fish lines and husbandry

All the experiments presented in this chapter were performed using 5-7 days post fertilization zebrafish larvae. Fish larvae and adults were maintained as described in the previous chapter (see section 2.2.1.a). Larvae were fed with paramecia or

powder from 5 dpf on. Calcium imaging experiments were carried out in different transgenic lines listed in Table 3.1. For better imaging, we used *nacre* fish. This fish lacked all melanophores due to a mutation in the *mitfa* gene [44].

Line name	Notes
elavl3:H2B-GCaMP6f	(1)
Tg(α-tubulin:Gal4-VP16);Tg(UAS:GCaMP7)	(2)
y249Et *Et(REX2-SCP1:GAL4FF);Tg(UAS:GCaMP7)*	(3)
Tg(mnx1:GCaMP5)	(4)
Tg(nefma-2A-KALTA4);Tg(UAS:GCaMP7)	(5)

Table 3.1: List of transgenic lines. Notes (provider and reference):
(1) Misha Ahrens (Vladimirov et al., 2014 [111])
(2) Teresa Nicolson (Koster et al., 2001 [112])
(3) Harold Burgess (Marquart et al., 2015[113])
(4) Claire Wyart (Sternberg et al., 2016 [114])
(5) François Giudicelli (Eschstruth et al., 2020 [115])

Experiments were approved by Le Comité d'Éthique pour l'Expérimentation Animale Charles Darwin C2EA-05 (02601.01 and 32423-202107121527185 v3).

b) Experimental set-up

To record whole brain neuronal activity during vestibular stimulation, we used a rotative light sheet microscope developed by Migault et al. [3](see Figure 3.1). Since the aim of my research was to describe the neuronal activity and not to develop this setup, I will explain briefly the configuration of the setup just in the extent needed to understand the research performed in this chapter.

The setup consists of a miniaturized digital scanning light-sheet unit, a fluorescence detection unit and a sample holder (see Figure 3.1). All elements were mounted onto a platform that could be rotated by a motor. Imaging was done using a 20x water immersion objective with a GFP filter and captured by a fast sCMOS camera (Hamamatsu, V2).

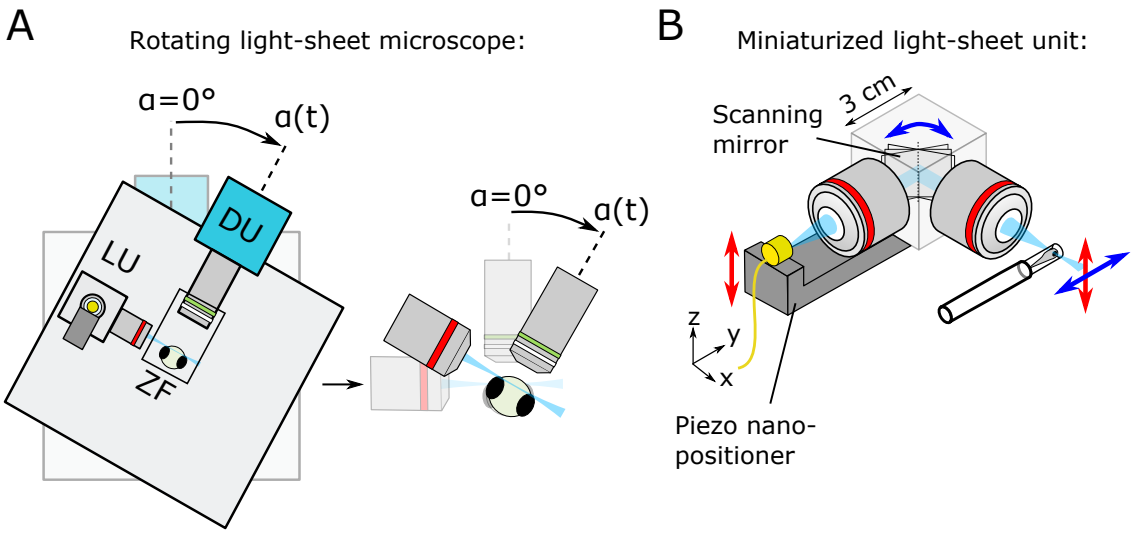

Figure 3.1 Experimental setup. Figure adapted from Migault et al. [3]. **A** Schematic of the rotating light-sheet microscope with the light-sheet unit (LU), mounted larva (ZF) and detection unit (DU). The inset illustrates how the fish co-rotates with the microscope, such that the light sheet and the detection focal plane remain static relative to the fish for any rotation angle. Angles are considered as positive in arrow direction. **B** Schematic of the miniaturized light-sheet unit. The laser is coupled via an optical fiber into the light-sheet unit. The light-sheet is created by rapidly scanning the laser in the horizontal plane using a galvanometer scanning mirror (blue arrows). For volumetric imaging, the light-sheet is scanned in the z direction through the sample by moving the fiber outlet up and down with a piezo nanopositioner (red arrows)

c) Sample preparation

5 to 7 dpf larvae were embedded in 2% low melting point agarose and drawn into a capillary with a metallic plunger. Then we removed the excess of agarose with a micro-knife. Larvae remained completely restrained in the agarose. For some experiments, the fish were paralyzed before being mounted by bathing them for 2 min in a solution of 1 mg/mL α-bungarotoxin (Thermofisher Scientific) diluted in E3. We then transferred them into pure E3 medium and waited 10 min to check for absence of motor activity but normal heart beating and blood circulation.

d) BAPTA injections

Ca^{2+} is required for hair cell transduction [116]. This cation is a necessary co-factor for the transduction apparatus located on the tip of the hair cell's stereocilia [117]. BAPTA is a calcium chelating agent, and hair cells treated with BAPTA buffered solution lose the tip-links [118], thus impairing mechanotransduction.

To perform unilateral ear stimulation, we injected BAPTA in the left ear with a glass micropipette held by a micromanipulator (Narishige MN-153) using a pneumatic pico-pump (World Precision Instruments PV830). Capillaries of 1 mm outer diameter, (GC100F-10, Warner Instruments) were pulled to obtain fine tip micropipettes (tip diameter = 1–2 μM) using the Narishige PC-100 puller with the following parameters: 2 steps, Heater N°1 = 52,4; Heater N°2 = 55,7, position 2 mm, 2 heavy and 1 light weights. The micropipettes were loaded with 2 μl of BAPTA 50 mM solution containing (in mM) 134 NaCl, 2.9 KCl, 1.2 $MgCl_2$, 2.1 $CaCl_2$, 10 HEPES, and 10 glucose, at 290 mOsm, adjusted to pH 7.8 with NaOH. 5 dpf larvae were anaesthetised in 0.04% tricaine (MS-222) and mounted on their side in 2% LMP agarose. The agarose around the ear was removed to not bend the needle tip (see Figure 3.2). We injected 3 times at 10 psi for 500 ms. After the injection, larvae were unmounted using a fine tip (Dumont n°5) and kept them in E3 medium until the experiments. Experiments were performed 3 hours after injection.

e) Motor neurons back fillings

Motor neurons were retrogradely labeled using dry Dextran-Texas Red. Larvae were embedded in methyl cellulose, and placed dorsal-up. The tip of a fine forceps (Dumont N°5) was coated with dry dextran crystals, and then used to clamp the pectoral fins. This protocol was kindly shared by Dr. Minoru Koyama.

f) Sinusoidal stimulation protocol and image acquisition

The stimulation protocol we used was a sinusoidal-roll stimulation at 10° amplitude and 0.2 Hz frequency. Image acquisition was done with the HCImage software (Hamamatsu) at a rate of 2.5 stacks per second. Every stack consisted of 20 brain sections separated by 10 μm. Images were binned down to a pixel size of

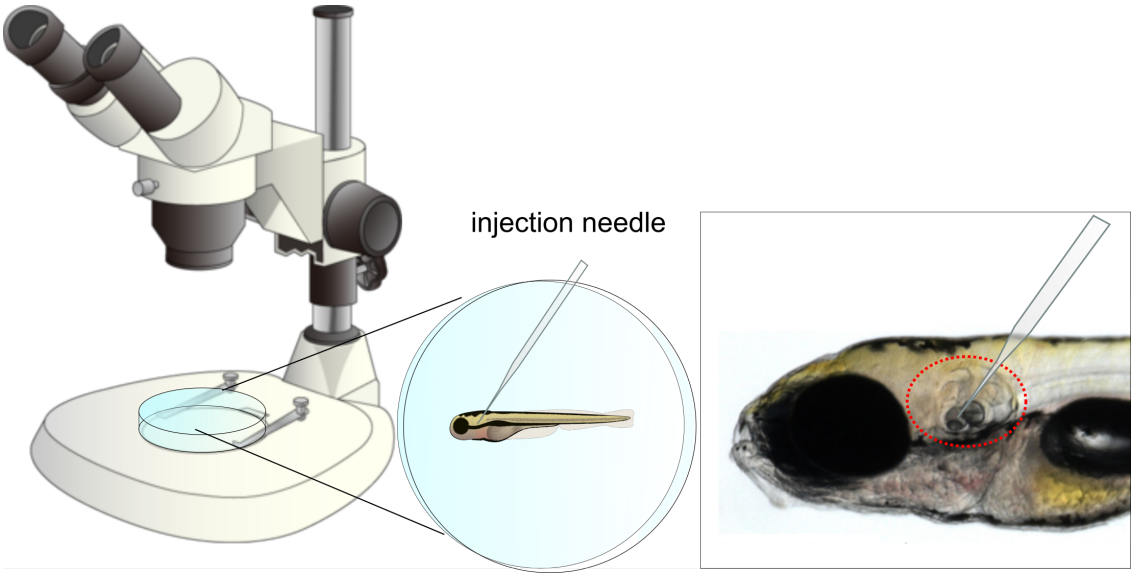

Figure 3.2 BAPTA injection in the otic vesicle. The larvae were mounted on their side in a Petri dish to easily reach the ear with the needle. The procedure was performed with a dissection stereoscope (on the left). The inset (on the right) shows the region in which the injection was done.

$0.8 \times 0.8\,\mathrm{mm}^2$. The recordings lasted 10 min, which corresponded to 120 stimulation cycles at the indicated frequency.

3.2.2 Data Analysis

a) Image processing

To analyze the functional calcium imaging data, I used a pipeline called EasyRLS (https://github.com/Pysi/easyRLS) implemented in MATLAB previously in the laboratory. This pipeline consist in many steps to obtain a multichannel matrix of the changes in fluorescence over time, either by voxel or by neuron, after image segmentation. In a preprocessing step, drift in the X and Y axis is corrected by registering each image of the stack with respect to the first image.

b) Phase map calculation

To characterize the brain response to the sinusoidal stimulation we calculated a phase map for every recording. We used the analysis described by Migault et al. [3],

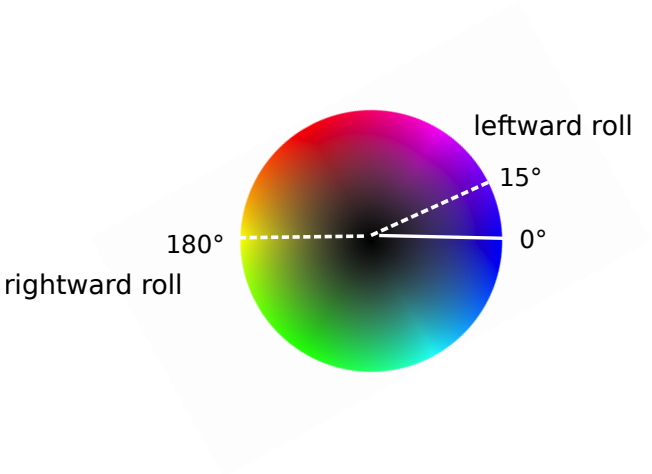

Figure 3.3 Phase map color code. Phase calculations assign hue and brightness to the fluorescence pixel value. The hue gives information about the phase with respect to the stimulus, and the brightness corresponds to the fluorescence value. Cyan to purple hues correspond to leftward rolls. Red to yellow hues correspond to rightward rolls. The maximum values between right and left roll are phase-shifted by 165°, almost anti-phasic.

which is a part of the easyRLS pipeline. To generate a phase map we calculate the power spectrum of the fluorescence time trace for every voxel of the 4D brain stack. From the power spectra, we extracted the stimulation frequency amplitude and phase of the fluorescent response relative to the stimulus waveform. These data can be graphically represented on the form of a phase map as an HSV (hue, saturation, value) image stack in which hue, saturation, and value correspond to phase, zero and amplitude respectively. Note that the measured fluorescence response is phase shifted relative to the real neuronal signal due to the convolution with the response function of the GCaMPs sensor. The induced phase shift is $\Delta\phi = arctan(-2\pi f\tau)$ with f the stimulation frequency and τ the decay time constant of the GCaMP sensor.

c) Phase map average and brain atlas registration

To average phase maps across different fish, we used the Computational Morphometry ToolKit CMTK (http://www.nitrc.org/projects/cmtk/) to compute for every fish the morphing transformation from the average brain stack (anatomical

stack) to a reference brain of the ZBrain atlas [119]. Recordings performed in fish with cytoplasmic expression of GCaMP were registered onto the Elavl3-GCaMP5G stack of the zBrain atlas, and recordings performed with the nuclear GCaMP line were mapped onto the Elavl3:H2B-RFP stack. With the found transformations, we transformed each individual phase map into the ZBrain reference frame, which allowed us to average results across specimens for every line or treatment we used.

3.3 Results

3.3.1 Sinusoidal-roll stimulus activates the vestibular nuclei and reticulospinal neurons

We used three different lines to characterize the neuronal response from specific brain regions.

- *RS:Gal4;UAS:GCaMP6f*, this line uses the Gal4;UAS system to express GCaMP6f in the reticulospinal neurons (not published and kindly provided by Isaac Bianco).
- *Tg(nefma-2A-KALTA4);Tg(UAS:GCaMP7)*, which expresses mostly in neurons with large axon caliber, including the Mautner cells, the nMLF and the vestibulospinal population of reticulospinal neurons [120]. Most of the labeled cells project to the spinal cord.
- y249Et *Et(REX2-SCP1:GAL4FF);UAS:GCaMP7* was identified in a screen of transgenic "enhancer tap" lines [113]. It labels, e.g., the tangential and the medial vestibular nucleus, vestibulospinal neurons, oculomotor neurons, the nMLF, the cerebellum granular eminence and the 8th nerve.

a) Reticulospinal labeled neurons

The reticulospinal neurons are a neuronal population, in the both midbrain and hindbrain, with descending tracts [121] and they have a main role in motor function. 5-7 dpf larvae were tested using a sinusoidal-roll stimulation protocol during 5 minutes (300 s) at 0.2 Hz and 10° amplitude (Figure 3.4B). Positive angles

are right-ear down and negative angles are left-ear down. To label specifically reticulospinal neurons we used an unpublished line from Isaac Bianco's laboratory at University College London, that we will call for now *RS:Gal4;UAS:GCaMP6f*. This line labels most of the reticulospinal neurons, e.g., the tangential vestibular nucleus (Figure 3.4A). The phase map analysis showed that a roll stimulus towards the right (right ear-down) activates the TN and vestibulospinal neurons ipsilateral to the activated ear, and the nMLF on the contralateral side. (Figure 3.4B-D). A rotation to the left side activates the mirror symmetric correlates of these brain regions. We also observed activity related to the stimulus in other reticulospinal populations, like the rostral medial (RoM) and middle ventral (MiV)[121], but they are symmetric in both sides of the brain, thus not elicited specifically by one-ear down (data not analyzed).

In addition, the MiD2 neurons of the resticulospinal population are also contralaterally activated, showing a role in vestibular processing for these neurons not previously shown.

b) *Nefma* neurons

In the *nefma* line, rolling the right ear down activated the vestibulospinal neurons and the contralateral nMLF co-activated with the vestibulospinal neurons (Figure 3.4A). This is consistent with the results found in the *RS:Gal4;UAS:GCaMP6f* line. In addition, we observed two small regions (white arrowheads in Figure 3.5A-B) that were also contralaterally active. By their position, we estimate that they correspond to the MiD3 neurons [122]. Note that this calcium indicator is expressed in the cytoplasm, making axons visible. Axons are active, e.g., in the spinal cord region and the MON.

3.3.2 Sinusoidal-roll stimulation elicits a response in the spinal cord primary motor-neurons and pectoral fins motor neurons

To study the response of motor neurons, we used the *Tg(mnx1:GCamp5)* line (kindly provided by Claire Wyart). *Mnx1* is a transcription factor specific to motor neurons in both brain and spinal cord. Our behavioral results discussed in the pre-

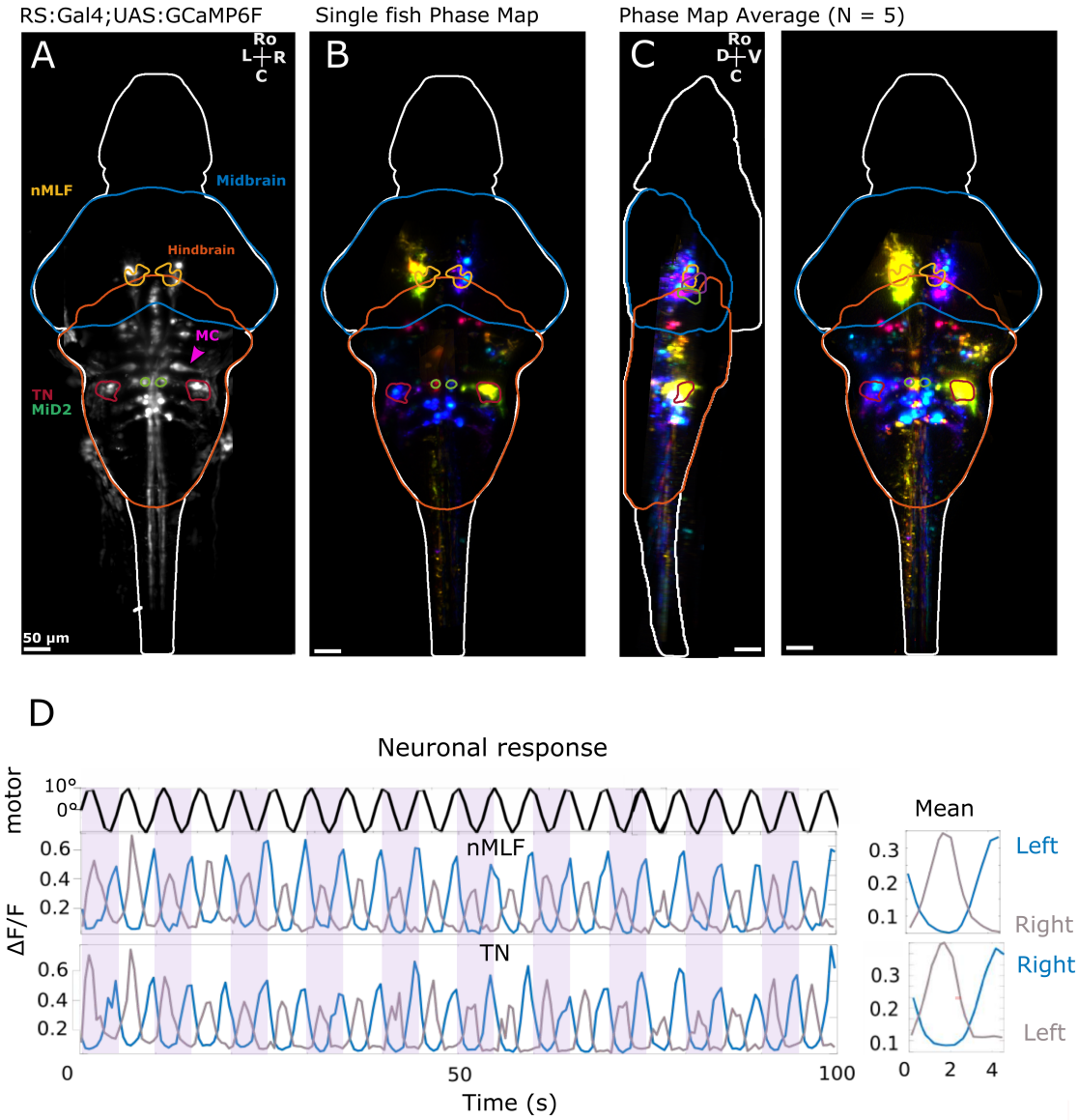

Figure 3.4 Phase map of the functional brain-wide response to a sinusoidal roll stimulus recorded in the *RS* line **(A)** Transgenic line expressing GCaMP6f in a population of the reticulospinal neurons. Mautner cells (MC) are indicated with a pink arrowhead. The tangential nucleus is outlined in red and shows also GCaMP expression. **(B)** Single fish phase map showing neurons active during sinusoidal roll. Yellow regions are active during right-ear-down roll and purple are active during left-ear-down roll. **(C)** Side and Dorsal view of the average phase map of 5 different larvae. Scale bar = 50 μm. **(D)** Fluorescence traces (raw signals and mean) of four different regions: right nMLF (blue line upper panel), left nMLF (gray line upper panel), right TN (blue line bottom panel) and left TN (gray line bottom panel).

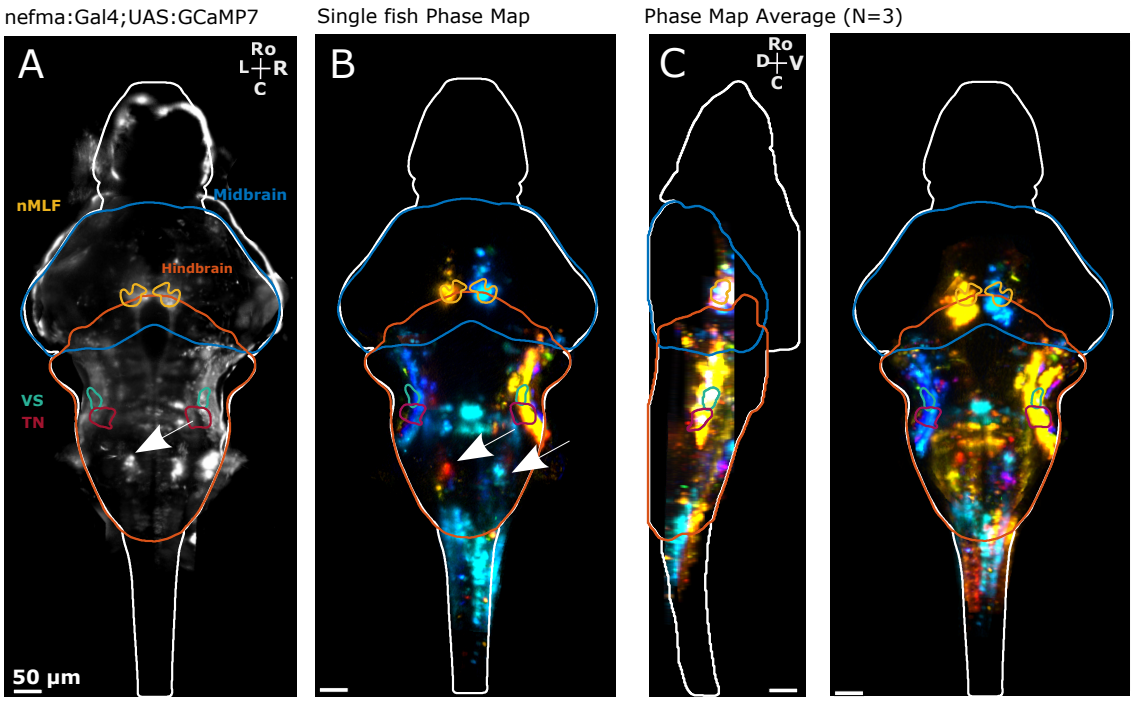

Figure 3.5 Phase map of functional brain-wide response to sinusoidal roll in the *nefma* line **(A)** Transgenic line expressing GCaMP7 driven by *nefma*. **(B)** Single fish phase map showing neurons active during sinusoidal roll. Yellow-orange regions are active during right-ear-down roll and blue are active during left-ear-down roll **(C)** Left side and dorsal view of the average phase map of 3 different larvae. Scale bar = 50 μm.

vious section showed that the tail movements elicited by vestibular roll stimulation are contraversive to the stimulus direction and consist in a pivoting motion of the tail pivoting at the swim bladder level (tail pivots to the left when the right ear rotates down).

Next, we studied which motor-neurons are recruited in the spinal cord near the swim bladder to drive this pivoting tail response during a sinusoidal-roll stimulus. We used 5-7 dpf larvae, fully embedded in agarose, thus preventing strong tail movement to avoid the generation of noise induced by movement artifact when the tail moves. Three groups of neurons were activated: 1) the oculo-motor neurons, 2) two rostral antisymmetric clutches (at the swim bladder level) and 3) two caudal antisymmetric clutches in the spinal cord (Figure 3.6A-B). The occulomotor neurons were activated, as expected, when the contralateral ear was down. The

second group was conformed by two clutches in each brain hemisphere that were activated respectively when the ipsilateral ear was down. Since the tail deflection occurs towards the contraversive side relative to the stimulated ear, we can exclude that these neurons drive this pivoting tail behavior. Finally, the third group, corresponded to primary motor-neurons in the spinal cord, that innervate trunk muscles. The response of these neurons was antisymmetric and activated contralaterally to the ear-down side. These motor-neurons should control the contraction of trunk muscles ipsilateral to their location, which is consistent with the contraversive tail deflections relative to the stimulated ear.

But what is the role of the described second group of neurons? Given their rostro-ventral position (Figure 3.6C-D), we speculated that they may correspond to motor neurons innervating the pectoral fins. To test this hypothesis, we filled the right pectoral fin with Dextran-TexasRed (sigma aldrich) using a protocol shared by Minoru Koyama. This procedure clearly backlabeled a dense population of neurons in the trunk (Figure 3.7B). The backfill was performed in the mnx1:GCaMP5 line. We found that the green fluorescence from the mnx1:GCaMP5 line and the red fluorescence from the backfilled population in the trunk colocalized (Figure 3.7C) which identified these neurons in the mnx1:GCamp5 line as the primary motor-neurons that innervate the pectoral fins. Our functional imaging results (see phase map Figure 3.6) shows thus that pectoral fin motor-neurons are recruited ipsilateral to the ear-down side during sinusoidal-roll stimulation (Figure 3.7E).

3.3.3 Only the anterior macula is active during vestibular stimulation

The hair cell patches that are attached to the otoliths are called *maculae*. In the 5-7 dpf larva there are only two of them: the anterior macula and the posterior macula, corresponding to the utricular and saccular otolith respectively. To study the activity elicited in the maculae, we used the *Tg(α-tubulin:Gal4-VP16);Tg(UAS:GCaMP7)* line, that besides neurons also labels the hair cells.

The obtained phase map and fluorescence traces showed that only the anterior macula (utricular macula) is active during sinusoidal vestibular stimulation (Figure 3.8A). The hair cells that form the crista—the mechanosensitive organ in the

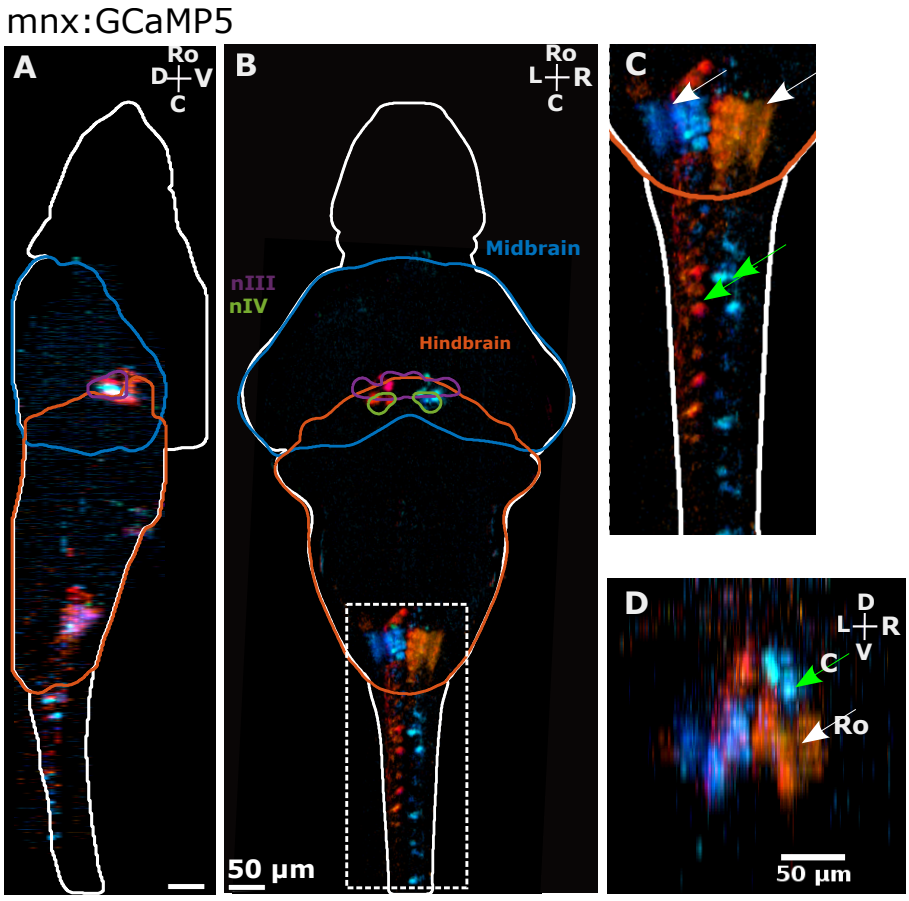

Figure 3.6 Phase map of the functional brain-wide response to a sinusoidal body roll in the *mnx1:GCaMP5* line **(A)** Transgenic line expressing GCaMP5 in the motor-neurons and some interneurons. **(B)** Side and Dorsal view of a phase map recorded in a single fish, showing neurons active during sinusoidal roll. Red and orange regions are active during right-ear-down roll, and blue regions are active during left-ear-down roll. **(C)** Inset of the caudal hindbrain and first portion of the spinal cord (obex). The rostral neurons (white arrowhead) are anti-phasic with the caudal neurons (green arrowhead). **(D)** Cross-section view of the spinal cord projected along the rostro-caudal axis. The rostral neurons are ventral with respect to the caudal ones. Scale bar = 50 μm.

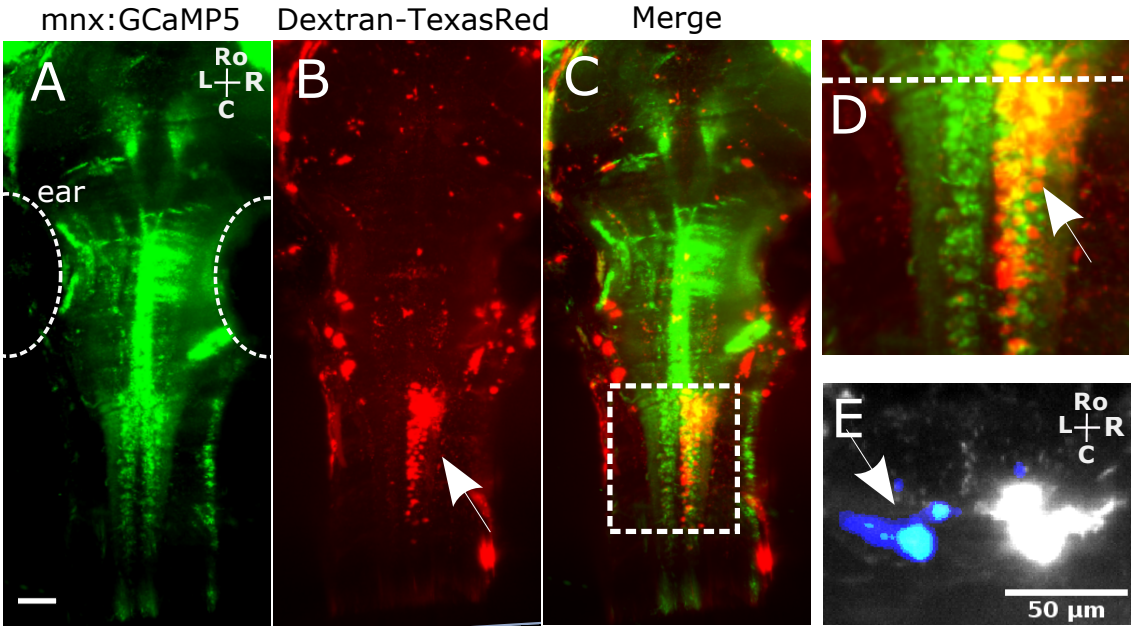

Figure 3.7 Motor neurons innervating the pectoral fins (A) GCamp5 expression driven by mnx1. **(B)** Dextran-TexasRed retrogradely labelled motor neurons. The arrowhead indicates the neurons that are backfilled by clamping the right pectoral fin. **(C)** Merge of A and B. **(D)** Zoom in the obex region and first portion of the spinal cord, showing the motor neurons that innervate the right pectoral fin. The dashed line indicates the location of the cross-section shown in E. **(E)** An overlay of the backfilled neuronal population (white) onto the phase map recorded in this fish after the backfill procedure is shown (color). The view is a cross-section through the obex at the position indicated by the dashed line in D. The neurons that got backfilled did not show a calcium signal, but the calcium signal in the mirror symmetric population could be recorded (blue).

semicircular canal—are also present by this age (Figure 3.8B), but phase map calculation and fluorescence trace did not show activity in response to sinusoidal-roll stimulus for these hair cells (Figure 3.8C).

Despite the fact that in the macula lateral hair cells present opposite polarities to those in the center and medial region (see Figure 1.5E), anti-phasic activity between hair cells in the same macula patch was not evident (Figure 3.8A).

3.3.4 Unilateral and bilateral utricle stimulation elicits similar brain-wide response

In the previous chapter, we described that one utricle is sufficient to elicit a contraversive tail deflection, and that utricles are necessary to elicit this response. Next, we wanted to check the neural response that is elicited by one utricle only. To do so, we injected BAPTA in the left ear of 5 dpf larvae *Tg(elavl3:H2B-GCaMP6f)*. BAPTA disrupts hair-cell tip-links, thus imparing mechanotransduction [118]. Despite the tip-link disruption of the left utricle, we still observed some activity in the left MON. Phase map calculation showed that the left TN was less active in the injected fish compared to the non-injected fish, as well as the right nMLF, nIII and nIV regions (white arrowheads in Figure 3.9A-C).

3.3.5 Preliminary results: y249Et neurons

The Y249Et line was identified in a screen of transgenic "enhancer tap" lines [113]. We searched the ZebraBrainBrowser (ZBB) tool (http://vis.arc.vt.edu/projects/zbb/) to find potentially interesting lines in vestibular studies. We took as a reference the phase map obtained by vestibular stimulation (Figure 3.9A) and we compared it to the lines listed on the site. We found that the y249Et line (Figure 3.10A) labeled almost identically the neurons active in the phase map. By testing this line in the RLS, we observed that all afferent neurons from the otolotiths and semicircular canals are labeled, as well as the MON region, all these neurons active during ipsilateral roll. (Figure 3.10B-C). This line is of particular interest for vestibular circuits studies, since almost all of the labeled neurons respond to vestibular stimuli (data not shown).

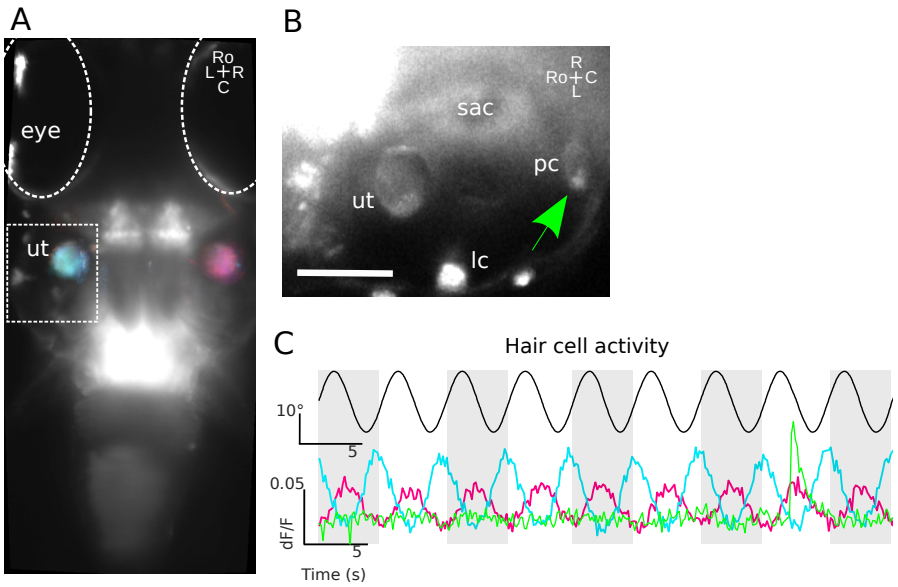

Figure 3.8 Activity elicited in the inner ear hair cells. **(A)** Phase map of the evoked calcium signal in response to a sinusodial body roll stimulus recorded in the *Tg(α-tubulin:Gal4-VP16);Tg(UAS:GCaMP7)* transgenic line. The phase map (color) is overlaid onto the anatomical stack of this line (gray scale image). The anterior macula (ut) is the only hair cell patch in the inner ear that was activated by the roll stimulus, indicated by a high brightness of the color in the phase map. The right macula and the left macula show an anti-phasic response to the roll stimulus. Magenta indicates an activation when the right ear is down, and cyan indicates when the left ear is down. **(B)** Inner ear inset. The arrowhead indicates the hair cells of the posterior crista (pc). **(C)** Fluorescence traces for the right anterior macula (magenta), the left anterior macula (cyan) and the posterior crista (green). On top: sinusoidal roll stimulus (black line). Periods are indicated with gray and white. Scale bar = 50 μm.

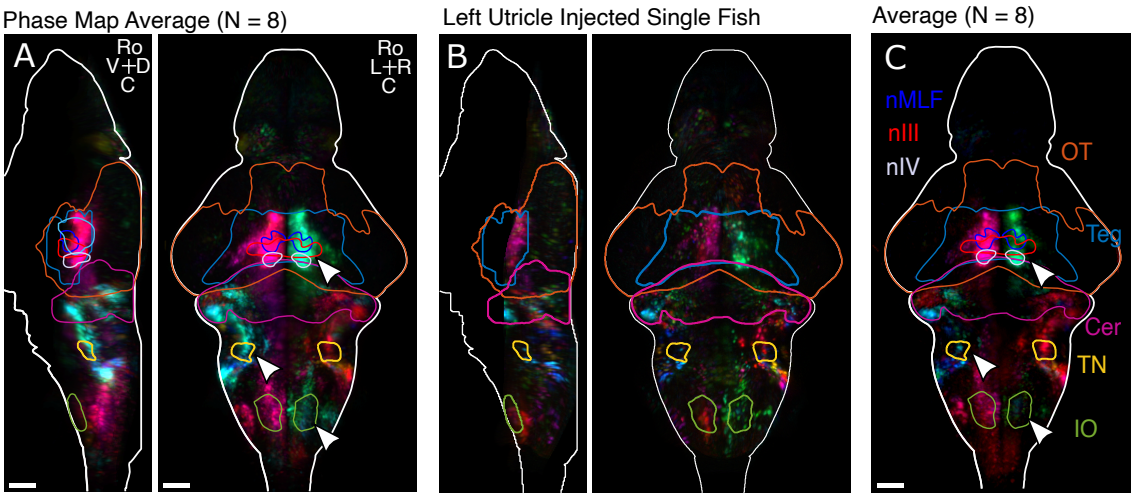

Figure 3.9 Phase map for unilateral utricle stimulation. **A** Average Phase Map of non-injected larvae. **B** Lateral and dorsal view of the Phase map of a single injected larva. **C** Average Phase Map of 8 injected larvae, white arrow heads indicated regions that are less active compared to **A**. Scale bar = 50 μm. OT: Optic Tectum; Teg: Tegmentum; Cer: Cerebellum, IO: Inferior Olive

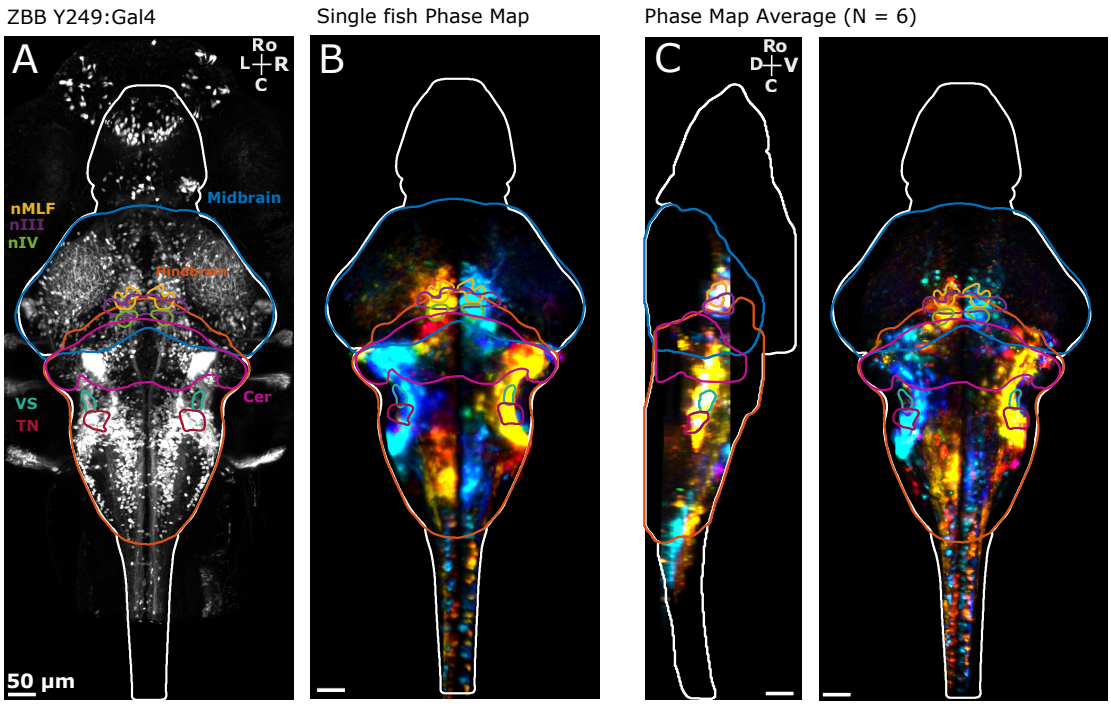

Figure 3.10 Phase map of functional brain-wide response to sinusoidal roll in the y249Et line (A) Y249Et brain stack from the ZebraBrain-Browser library. **(B)** Single fish phase map showing neurons active during sinusoidal roll. Yellow-orange regions are active during right-ear-down roll and blue are active during left-ear-down roll. **(C)** Side and Dorsal view of the average phase map of 6 different larvae. Scale bar = 50 μm. Cer: Cerebellum

3.4 Discussion

3.4.1 Different neuronal populations involved in vestibular response.

We showed that the region of the nMLF and TN are active and antisymmetric, as described by Migault et al. and Favre-Bulle et al. [3, 93]. We also described the activity in the reticulospinal neural population, identifying that vestibulospinal neurons and the MiD2 and MiD3 neurons are also active contralateral to the ear-down side. We also observed activity related to the stimulus in other reticulospinal populations, like the rostral medial (RoM) and middle ventral (MiV)[121], but they are symmetric in both sides of the brain, thus not elicited specifically by one-ear down.

For the *mnx1* line, mapping was not straightforward, so we were not able to map and average phase maps. However, we obtained good images for 6 larvae, that allowed us to calculate individual phase maps and analyse neuronal activity. We observed four clusters of motor-neurons active during sinusoidal-roll stimulus. Two antisymmetric anterior clusters and two antisymmetric posterior clusters.

The anterior cluster corresponded to the pectoral fin motor-neurons that were back-filled with Dextran-TexasRed, and they were active during ipsilateral roll. Timerick et al.[123] showed that sinusoidal-roll stimulation elicited activity of the levator and depressor muscles of the pectoral fin. The depressor activity was ipsilaterally in phase with the ear-down-side, similar to our results. The neurons activated are probably those innervating the abductor muscles [124] (which pulls the fin down, like depressors in dogfish). We hypothesise that this pectoral fin movement is a vestibular reflex, similar to that recorded from the triceps muscle of the cat, generated involuntarily by roll tilt [125]. The form of this vestibular-pectoral fin reflex — antiphasic abduction of the pectoral fins— was congruent with the expected movement to compensate for roll. In support of our hypothesis, pectoral fins are also recruited during postural correction in the pitch-axis [97]. In the present experiments, roll was imposed, but in natural situations, it will result from the active swimming of the fish and water turbulence [77].

Another difficulty we encountered in these experiments was the fact that Dex-

tran co-localization with GCaMP inhibited calcium imaging. So we were not able to record the calcium signal over time for the injected fish. Instead, we backfilled only the right pectoral fin and paired the labeled neurons with those on the contralateral side that were active.

At first, our idea was to try to correlate the vestibular-evoked tail movements with neuronal activity. Using tail-free larvae to image the neuronal activity was not simple, since tail movements destabilized the image, turning the analysis difficult. Future experiments with free-tail larvae would help to elucidate how tail movements correlate to neuronal activity during vestibular stimulation.

In this section, we used four different transgenic lines based on the Gal4:UAS system. The expression in these lines is sparse, and not always consistent (since individuals have different expression pattern of the calcium probes). Thus, mapping individuals on a reference stack and averaging them was not easy. Despite the advantages of the Gal4:UAS system, using GECIs in transgenes with a direct promoter can solve the inter-individual expression disparity.

3.4.2 Inner ear hair cells activity

In the inner ear, hair cells are arranged in distinguishable sensory patches called maculae and cristae. Maculae are the patches attached to the otoliths and cristae are the patches in the semicircular canals' cupula. By using the *Tg(α-tubulin:Gal4-VP16);Tg(UAS:GCaMP7)* line, we recorded the hair cell activity in the inner ear, elicited by sinusoidal-roll stimulus.

Despite the presence of cristaes' hair cells, the semicircular canals of 5-7 dpf larvae are not yet functional [59]. We showed that only the anterior macula hair cells respond to sinusoidal-roll stimulus. If semicircular canals were functional, we expected to observe activity, at least, in the posterior crista. Such activity was not observed, thus confirming that semicircular canals are not functional at this stage.

Even though we managed to image macula activity during vestibular stimulation, our recordings did not allow identifying individual hair cells. So we were not able to characterize in detail the activity pattern for the different hair cells. Given the hair cells polarity pattern inside a single macula [65], we were expecting to partly observe some phase shifted hair cells. Regions with antisymmetric or

anti-correlated activity were not evident within single macula.

Due to the optic opacity of the ear stones, light-sheet microscopy is not the best optical solution to image macula hair cells. Using confocal or two-photon imaging could be a more adapted technique to image this region. Unfortunately, a method that couples vestibular stimulation and this kind of microscopy is not fully developed.

3.4.3 Push-pull mechanism in the utricle

To study single-utricle contribution to the vestibular response, we impaired mechanotransduction on the left ear by injecting a calcium chelating agent (BAPTA). Surprisingly, the phase map analysis of the unilateral injected fish proved to be similar to the non-injected fish. These results coincide, to some extent, with those from Favre-Bulle et al. [93]. They observed that unilateral utricle trapping was sufficient to elicit activity bilaterally in the nMLF, the oculo-motor and the trochlear nuclei. The phase maps that we obtained show that right utricle stimulation is sufficient to elicit activity in the left MON region, even when the left utricle is not functional. Commissural neurons from the tangential nucleus communicate one ear to the other [71]. A "commissural inhibition" circuitry has been already described for cats [94, 95] and monkeys [126]. It was first described for second order neurons receiving inputs from the semicircular canals, and then it was proved to be true also for the otoliths [95]. In the first case, when hair cells from one semicircular canal are depolarized during head rotation, those in the co-planar contralateral canal are hyperpolarized. Thus, the sensitivity of vestibular neurons is potentiated by disinhibition, via commissural interactions (see Figure 3.11)

3.4.4 Summary and conclusions

In this chapter, we took advantage of the vast library of transgenic lines that has been developed in the zebrafish to look into more detail the neural substrates underlying vestibular evoked responses. And even though the results here presented are preliminary, and neural correlation analysis are still missing, we described the wide brain and spinal cord response to vestibular stimulus.

We used the setup and protocol described by Migault et al. [3]. We proved that

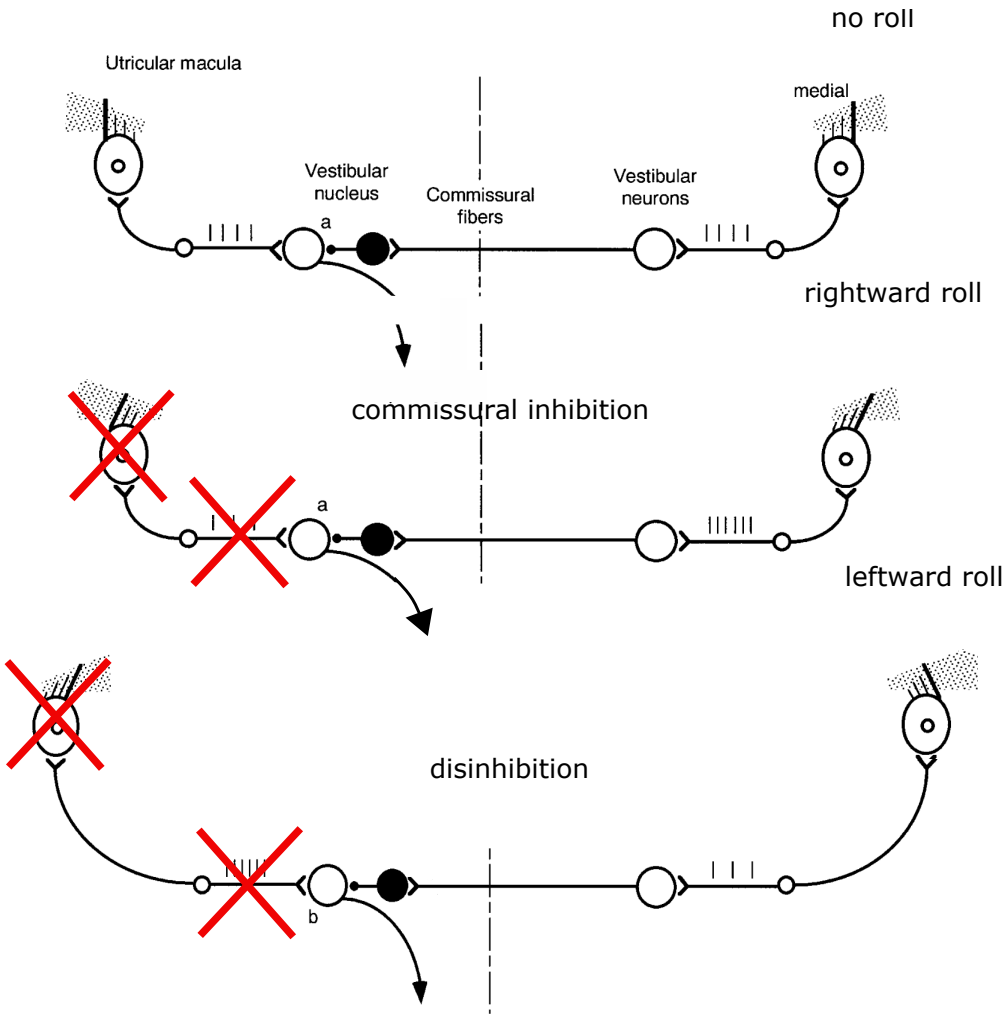

Figure 3.11 Commissural inhibition in the utricle system Schematic of commissural inhibitory pathways and of utricular maculae (Modified from Uchino et al. [95]). Hypothetical inhibitory interneurons are black circles. During rightward roll; hair cells in the right macula then depolarize. Then the vestibular neuron "a" is inhibited. In absence of left utricle, a leftward roll will not depolarize left vestibular afferents. Instead, by hyperpolarization of right hair cells, neuron b will be disinhibited generating a depolarization.

nMLF, oculomotor neurons, trochlear neurons, subpopulations of the reticulospinal neurons and spinal cord primary motor-neurons are active during contralateral roll. On the contrary, the tangential nucleus, the vestibulo spinal neurons, MON region and pectoral fins abductors' motor-neurons were active during ipsilateral roll.

In addition, we proved by mechanical means and direct measure of hair cells acitivity, that semicircular canals are not yet functional between 5 and 7 dpf. The idea that semicircular canals are not functional until 34 dpf is based on their morphology and the absence of horizontal VOR. Here, we measure the posterior crista activity during sinusoidal-roll, finding no response to the stimulus. Finally, we showed that one utricle is sufficient to generate a full response, by means of commissural disinhibition of the contralateral second order vestibular neurons.

A new method to study the vestibular system in larval zebrafish

In this section, we report a novel method to perform fictive vestibular stimulation in the zebrafish larva. Regarding the nature of the method here developed, I allow myself to quote a passage from a famous book.

The next passage tells the story of how Don Quixote and Sancho Panza are tricked into using Clavileño, a magical wooden horse, sent by the sorcerer Malambruno. Dueña Dolorida and the dukes ask them to cover their eyes, and make them believe that they have flown blindfolded. In reality, the rocking horse is inanimate and goes nowhere, meanwhile the people who tricked them use fire and bellows to simulate wind while Don Quixote and Sancho "fly".

> As Sancho heard the voices, clinging tightly to his master and winding his arms round him, he said:
>
> —Señor, how do they make out we are going up so high, if their voices reach us here, and they seem to be speaking quite close to us?
>
> —Don't mind that, Sancho —said Don Quixote—, for as affairs of this sort, and flights like this are out of the common course of things, you can see and hear as much as you like a thousand leagues off; but don't squeeze me so tight or thou wilt upset me; and really I know not what thou hast to be uneasy or frightened at, for I can safely swear I never mounted a smoother-going steed all the days of my life; one would fancy we never stirred from one place. Banish fear, my friend, for indeed everything is going as it ought, and we

Figure 4.1 *Don Quixote and Sancho Panza riding Clavileno* - Zacarias Gonzalez Velazquez (Madrid, 1763 - 1834)

have the wind astern.

—That's true —said Sancho—, for such a strong wind comes against me on this side, that it seems as if people were blowing on me with a thousand pair of bellows—; which was the case; they were puffing at him with a great pair of bellows; for the whole adventure was so well planned by the duke, the duchess, and their majordomo, that nothing was omitted to make it perfectly successful.[1].

[1]Miguel de Cervantes, 1615, *Don Quixote, Pt.2, Chapter XLI, Of The Arrival Of Clavileno And The End Of This Protracted Adventure*

4.1 Introduction

In the previous chapters, we described the vestibulospinal reflexes and the neurons that are active during sinusoidal-roll stimulus. However, the fine details of how utricular input controls this tail movements remain unknown and questions are still open. For example, which are the second and third order vestibular neurons that participate in this behavior? which are the motor-neurons responsible for the tail deflections? will inhibition of the nMLF impair this behavior during vestibular stimulation? what is the role of the vestibulospinal tracts in producing reflexes in response to a whole range of vestibular stimuli?

To dissect and decipher neural circuits, one of the current paradigms in neuroscience, is to manipulate via optogenetic tools specific brain regions, to see whether they elicit or inhibit a certain behavioural output [127, 84, 86]. So far, these studies have been convenient to link neurons to behavior, but they have not considered the vestibular system in the equation, due to the complexity of coupling an optogenetic setup with vestibular stimulation. To stimulate the vestibular system, the animal's head needs to be rotated or translated in space, making it incompatible with setups that required head-fixed animals. To solve this problem, we developed a method to accomplish fictive vestibular stimulation via magnetic forces in head-restrained larva. The present chapter deals with the development and proof of principle of this new method. The results are attached in a scientific article format, this article was submitted for peer-reviewed publication.

4.2 Submitted Article

Magnetic actuation of otoliths allows behavioral and brain-wide neuronal exploration of vestibulo-motor processing in larval zebrafish

Natalia Beiza-Canelo[1] **Hippolyte Moulle**[1] **Thomas Pujol**[1,2] **Thomas Panier**[1,3]

Geoffrey Migault[1] **Guillaume Le Goc**[1] **Pierre Tapie**[1] **Nicolas Desprat**[4] **Hans Straka**[5]

Georges Debrégeas[1]

Volker Bormuth[1,*]

[1] Sorbonne Université, CNRS, Institut de Biologie Paris-Seine (IBPS),
Laboratoire Jean Perrin (LJP), Paris, France.
[2] IBENS, Département de Biologie, Ecole Normale Supérieure, CNRS, Inserm,
PSL Research University, Paris, France.
[3] Sorbonne Université, CNRS, Institut de Biologie Paris-Seine (IBPS),
Plateforme d'Imagerie, Paris, France.
[4] Laboratoire de Physique de l'École normale supérieure, ENS,
Université PSL, CNRS, Sorbonne Université, Université Paris Cité, F-75005 Paris, France
Paris Diderot University, 10 rue Alice Domon et Leonie Duquet, 75013, Paris, France
[5] Faculty of Biology,
Ludwig-Maximilians-University Munich, Grosshadernerstr. 2, 82152 Planegg, Germany

[*] Corresponding : volker.bormuth@sorbonne-universite.fr

April 13, 2022

Version Wednesday 22nd June, 2022, 14:47

Abstract

The vestibular system in the inner ear plays a central role in sensorimotor control by informing the brain about the orientation and linear acceleration of the head. However, most neurophysiological experiments are performed using head-fixed configurations depriving animals of vestibular inputs. To overcome this limitation, we decorated the utricular otolith of the vestibular system with paramagnetic nanoparticles. This procedure effectively endowed the animal with magneto-sensitive capacities: applied magnetic field gradients induced forces on the otoliths resulting in robust behavioral responses comparable to that evoked by rotating the animal by up to 20°. We recorded the whole-brain neuronal response to this fictive vestibular stimulation using light-sheet functional imaging. Experiments performed in unilaterally injected fish revealed the activation of a commissural inhibition between the brain hemispheres. This magnetic-based stimulation technique opens new perspectives to functionally dissect the neural circuits underlying vestibular processing and to develop multisensory virtual environments including vestibular feedback.

***K*eywords** zebrafish · vestibular system · ferrofluid · magnetic actuation · zebrafish · whole-brain imaging · light-sheet microscopy

1 Introduction

The vestibular system continuously informs the brain about self motion and body orientation within the gravitational field. The vestibular apparatus is located in the inner ear and comprises several organs that report on the various components of the acceleration forces. Rotational acceleration of the head induces an endolymph flow in the semicircular canals, which is detected by mechanosensitive structures called cupulae, respectively. Translational acceleration, as well as gravitational forces, act on two otolithic structures overlaying on the utricular and saccular epithelia, and whose motion is transduced by mechanosensitive hair cells to which they are coupled.

Neuronal signals encoding the head orientation and movement are relayed to neuronal circuits that drive compensatory movements in order to stabilize gaze and posture. Vestibular information is first processed in the brainstem vestibular nucleus and the cerebellum, which receive direct vestibular afferent input. Information is further distributed to oculomotor, skeletomotor, and autonomous motor systems, and in mammals, also via the thalamus to cortical systems [1]. At the various stages of signal processing, vestibular information is integrated with non-vestibular sources of self-motion information such as visual, somatosensory and proprioceptive inputs as well as locomotor efference copies [2].

In spite of the central role played by the vestibular system in sensorimotor tasks, most neuronal recordings are currently performed in animals deprived of any vestibular signals, i.e., under head- or body-fixed stationary conditions. This is due to the inherent challenge of combining neural recordings and natural vestibular stimulation as the latter necessitates to rotate or translate the animal's head in space, and is thus incompatible with head-fixed recording configurations required for most functional calcium imaging techniques.

Our knowledge on the vestibular system thus essentially derives from electrophysiological experiments in which the spike activity of a small number of neurons is sequentially monitored using implanted electrodes.

As vestibular processing is widely distributed across the brain, zebrafish constitutes a promising model animal to study the neuronal substrate of this highly conserved sensory system. The small size and transparency of the larval zebrafish brain indeed offers the unique opportunity to record cell-resolved brain-wide neuronal activity using light-sheet based calcium imaging [3, 4, 5, 6]. With the exception of the semicircular canals, which are still immature in young larvae [7], the vestibular system is mostly functional in larval zebrafish as early as 6 days post-fertilization [8], an age at which whole-brain imaging is routinely performed. This is evidenced by the capacity of the larvae to efficiently stabilize their posture and gaze in response to body rotation, via vestibulo-ocular and vestibulo-spinal reflexes [8, 4, 9, 10, 11].

Two experimental methods to provide controlled vestibular stimulation, while performing functional whole-brain imaging, were recently introduced. In the work from Migault *et al.* [4], we solved the problem by co-rotating the fish and the (miniaturized) light-sheet microscope, thus keeping the imaging volume unchanged during the stimulation. Favre-Bulle et al.[9, 5] generated a fictive vestibular stimulus using optical tweezers to displace the utricular otolith. Although these two approaches enable simultaneous neural recording, they both involve demanding optical developments that may hamper their broad diffusion among groups employing neurophysiological methods. Furthermore, the accessible stimulation range, in terms of maximal acceleration that they can emulate, is limited.

Here we present an alternative approach based on the magnetic actuation of the otoliths after surface coating by ferromagnetic nanoparticles. These superparamagnetic iron oxide nanoparticles are available in the form of colloïdal solutions called ferrofluids [12]. Although they do not carry a permanent magnetic moment, these particles acquire a magnetization in an externally applied magnetic field and can be manipulated by magnetic field gradients. Their magnetic susceptibility is several orders of magnitude larger than biological tissues [13], allowing the application of large forces. Biocompatible ferrofluids have been used to study mechanical properties inside living tissues *in vivo* [14, 15, 16, 17, 18] and functionalized nanoparticles have allowed targeting cellular components such as DNA and proteins with high specificity [19, 20] or to deliver drugs into compartments that are difficult to access as e.g., the inner ear [13].

Magnetic actuation offers several advantages over optical tweezers in the context of biological systems. First, biological tissues are fully transparent to magnetic fields. Forces can thus be exerted in a controlled way deep within the specimen regardless of its optical transparency. Second, magnetic fields do not induce heating, and, with the exception of magnetoreceptive species [21], most animals are insensitive to this physical parameter. Thus, besides the injection itself, this technique is physiologically non-invasive even for extremely large magnetic intensity.

Here we show that the injection of ferrofluid into the otic vesicle of larval zebrafish allows controlled magnetic forces to be exerted on the otolith, mimicking naturally occurring gravitational and acceleration forces. This fictive vestibular stimulation elicits strong and robust compensatory eye and tail movements, comparable to those evoked by roll or tilt motion of the animal over large angles. We simultaneously recorded the brain-wide neuronal activity evoked by this fictive vestibular stimulation using functional light-sheet microscopy. By

injecting the ferrofluid into a single ear we disentangled the contribution of each utricle to the brain-wide neuronal response, which is not possible under natural conditions when rotating the animal [4]. This constitutes the first use of a ferrofluid to stimulate a sensory system *in vivo*. The method is inexpensive, easy to implement and compatible with most neurophysiological recording methods such as optogenetics or electrophysiology.

2 Results

After ferrofluid injection into the otic vesicle, vestibular-driven behaviors can be evoked through magnetic stimulation

We injected a custom-made ferrofluid [22] into both inner ears of zebrafish larvae 5 days after fertilization (dpf). The ferrofluid consisted of 11 nm in diameter iron oxide (γ-Fe_2O_3) particles with citric acid surface functionalization to make them stable in water (pH 7, see Methods). After the injection, the otic vesicle maintained its shape and the ferrofluid was visible as a red-orange tinge (Figure 1A). The otolith itself, once dissected out and washed, also displayed a slight orange coloration, indicating that some of the injected ferrofluid particles had permanently bound to the otolith. The otolith was thus magnetized, as could be confirmed by approaching a permanent magnet to its proximity. The otolith immediately moved towards the magnet as shown in the Supplementary Figure S1.

Next, we tested whether this nanoparticle coating of the otolith could yield magnetic forces *in vivo* on the otolith comparable to the gravitational force that acts on it when the head/body is rolled or tilted in space (Figure 1B). To do so, we examined the behavioral response (compensatory eye and tail movements) that were induced through magnetic actuation. We thus immobilized a bilaterally injected fish in a drop of 2% low melting point agarose on a thin glass slide and removed the agarose around the eyes and tail to allow free movements (Figure 1C). The specimen was placed in a chamber filled with the embryonic medium E3. A front and a side camera were used to monitor the eyes and tail movements evoked by the in-plane movement of a small permanent neodymium magnet positioned beneath the fish.

We observed two distinct responses depending on the orientation of the movement with respect to the body axis. When the magnet was moved along the medio-lateral axis, the eyes rolled and the tail bent in a direction opposite to the magnet (Movie 4 Part I). Such movements are characteristic of responses elicited by a roll motion of the animal (i.e., a rotation along its longitudinal axis) via vestibulo-ocular and vestibulo-spinal reflexes [4, 8]. In this case, the magnetic force acted laterally on the otolith, as does the gravitational force during a roll motion. When the magnet was moved along the antero-posterior axis, the eyes rotated along the tilt axis and discrete swim bouts were triggered. Here the response to the magnetic stimulation was in line with compensatory eye movements and tail kinematics elicited upon tilting the fish [8] (see Movie 4 Part II).

To quantify these responses, we imposed controlled sinusoidal displacements to the magnet using a two-axis motorized stage either along the lateral axis (fictive roll stimulus) or along the antero-posterior axis (fictive tilt stimulus). We used a frequency of 0.5 Hz and an amplitude of 2.5 mm corresponding to the radius of the magnet (see the following section describing the numerical simulations for an estimation of the corresponding magnetic force). Typical behavioral responses of such recordings are shown in the Movie 4. We found the

behavioral response to be strong in 80 % of the tested fish, which confirmed the robustness of the method. Importantly, the observed vestibular behaviors were reproducible and stable over time with only small variability over 150 stimulus repetitions in the same fish (Figure 1D). From the averaged cyclic ocular rotation signal, we extracted an angular range of $\alpha = 13.2° \pm 7.4°$ (mean ± standard deviation) during simulated roll motion and $\beta = 8° \pm 4.3°$ for simulated tilt motion (Figure 1). Interestingly, the behavioral responses were stronger for lower concentrations of injected ferrofluid (Figure 1E).

These values can be compared to those obtained during natural vestibular stimulation in which the animal is actually rolled or tilted in space. As an illustration, we show in Figure 1E the angular range ($\alpha = 14.1° \pm 5.8°$ (mean ± standard deviation) of eye rotation measured in larvae exposed to a sinusoidal roll motion of ±15°. One may notice that both the mean and the standard deviation are comparable in both experiments, indicating that the large variability across specimen is not specific to the fictive ferromagnetic stimulation. From the roll motion-evoked responses, we calculated a gain of the roll vestibulo-ocular response in darkness of $g_{roll} = 0.5 \pm 0.2$ and for the ocular motor tilt response a gain of $g_{tilt} = 0.3$ is reported [8]. From this calibration, we thus estimated that the fictive magnetic vestibular roll and tilt stimuli corresponded to a peak-to-peak stimulus of $\alpha/g_{roll} \approx \pm 14° \pm 27°$ (mean ± std) and $\beta/g_{tilt} \approx \pm 7° \pm 4°$ (mean ± std), respectively.

Ferrofluid injection into the inner ear does nor impair vestibular function.

Hair cells in the vestibular system are sensitive to mechanical and chemical stress, which can lead to cell death, thus impairing sensory function [23]. We assessed possible damage induced by either the injection procedure or by the ferrofluid itself using a simple behavioral assay. Fish use their vestibular system to keep their dorsal side-up posture stable during swimming. Therefore, uncorrected rolling along the rostro-caudal body axis during a swim bout can be used as an indication of vestibular dysfunction [24, 25, 26] (Figure 2A). We quantified the outcome of this procedure by calculating a roll ratio, i.e., the proportion of roll events over a total of 5 swimming events after a mechanically evoked startle response [27] (see Methods). The roll ratio was measured at 2, 24 and 48 hours after the injection had been performed at 5 dpf.

Control (non-injected) fish had a mean roll ratio of 0.44 ± 0.36 (mean ± std, N = 10) at 5 dpf (Figure 2B). Although the vestibulo-ocular reflex is fully established at 5 dpf [8], vestibular-driven postural control is still being refined between 5 to 7 dpf as evidenced by the decrease of the roll ratio during this period. As a second (negative) control, we performed a similar assay on larvae injected bilaterally with the calcium chelator BAPTA (5 mM), which disassociates hair cell tip-links and disrupts the mechano-electrical transduction [28]. Two hours after the injection, the roll ratio was close to one (mean roll ratio: 0.93 ± 0.11, see Movie 4), indicative of an almost complete loss of vestibular-driven postural control. Tip links have been shown to regenerate in 8 to 24 hours [29]. Hence, 48 h after BAPTA injection, the roll ratio of the larvae were significantly lowered and not significantly different anymore to control fish, reflecting a progressive recovery of posture control by tip link regeneration.

Next, we performed similar tests on buffer- and ferrofluid-injected fish, in order to disentangle the effect of the injection procedure from the ferrofluid itself on the vestibular system. Two hours after injection, the roll ratio (0.51 ± 0.31 and 0.65 ± 0.21, respectively) for both conditions were not significantly different from that of control fish (Tukey test $p > 0.1$). This remained so at 24 h and 48 h post injection. Finally, we injected

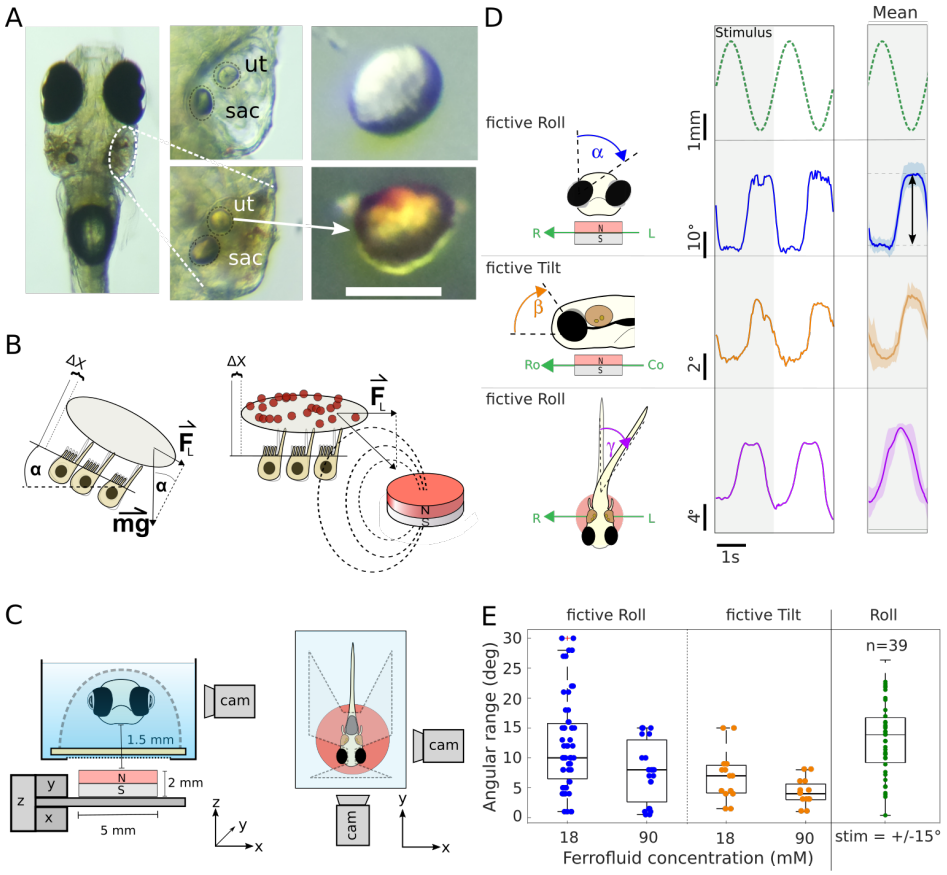

Figure 1: Magnetic actuation of the otoliths after surface coating by ferromagnetic nanoparticles. **A** Top view of a 5 dpf zebrafish larva after bilateral intra-otic ferrofluid injection. Middle column: Zoom onto the otic vesicle with injected ferrofluid (bottom) and before injection (top). The otoliths of the utricle, ut, and of the saccule, sac, are visible. Right: Bright-field image of an utricular otolith dissected from a control fish (top) and from a fish after ferrofluid injection (bottom). Attached iron nanoparticles appear in red-orange. Scale bar = 50 μm. **B** The diagram on the left illustrates the lateral force experienced by an otolith when the head is rotated relative to the gravitational field, $F_L = g \cdot sin(\alpha)$ (top). The right side illustrates an otolith covered with nanoparticles that exert a lateral force onto the otolith when placed in a magnetic field gradient. **C** Left: Diagram of the setup in front view. An x,y-motorized stage and a manual z-stage (black) move the magnet (red) under the head-tethered fish, mounted in agarose (outlined by a dashed line). Right: Top view of the setup illustrating the front and side cameras (cam) for eye motion tracking. The magnet center is aligned with the center of mass of the fish inner ears (not drawn to scale). **D** Evoked eye and tail movements in response to the magnet motion along different directions in a sinusoidal manner beneath a fish injected with 18 mM ferrofluid solution. Left column shows the two first cycles of a 150 repetition trial and right columns shows the average trial response and standard deviation. **E** Angular range of evoked eye rotation angles (peak-to-peak, see arrow in 1D) in response to fictive roll and tilt stimuli plotted for two concentrations of ferrofluid bilaterally injected into the inner ears ($N_{roll,18mM}$=24, $N_{roll,90mM}$=11, N_{tilt} = 9 for both concentrations).

DiASP that fluorescently labels functional hair cells as it diffuses through the mechanotransduction channels if mechanotransduction is functional. Hair cells became clearly labeled after the injection (see inset Figure 2B). Thus, neither the injection procedure itself nor the ferrofluid seem to significantly affect the function of the vestibular organs.

Finally, we examined the kinematics of free swimming behavior in ferrofluid-injected fish compared to uninjected control larvae. We found that inter-bout interval and turn angle distributions were not significantly different from control fish, while the average displacement per swim bout was only marginally increased (Figure S2 and Movie 4). The various tests confirmed that the ferrofluid injection procedure has a very limited impact on the functionality of the vestibular system and on the locomotor behavior.

Numerical simulations of the magnetic force exerted onto the magnetized otolith.

To evaluate the impact of magnetic forces on the nanoparticle-covered otolith and its dependency on the magnet position relative to the larva, we resorted to numerical simulations (Figure 3A). This approach revealed the existence of a range of magnet positions within which the force exerted onto the magnetized particle varies linearly with the radial distance to the center of the magnet. The force is maximal when the particle is located above the edge of the magnet beyond which it decreases and eventually vanishes. The maximal lateral force and the extent of the linear regime increases with magnet diameter, while the maximal force decayed as z^{-4} as expected for a magnetic dipole, where z is the vertical distance to the magnet. These results suggest that the magnet should be placed as close as possible beneath the fish and that horizontal displacements should remain smaller than the radius of the magnet. Under these conditions, the force-displacement relationship is expected to be linear.

To estimate the maximum force that can be imposed onto the otolith, we measured the velocity in water of an isolated otolith (obtained after dissection of an injected larva) submitted to a comparable magnetic field as in the *in vivo* experiment. Taking into account the otolith diameter, that controls the drag force, we obtained an estimated force of $\sim 1\,\mathrm{nN}$. We can then compare this value to the gravitational forces exerted on the otolith *in vivo* when the head is tilted in space. The utricular otolith in fish is a calcium carbonate (aragonite) crystal with a density of $2.83\,\mathrm{g.cm^{-3}}$ and a diameter of $\sim 55\,\mu m$ at the age of 6 dpf [9]. From these values, we estimated that under natural conditions, the maximal gravitational force experienced by the utricular otolith is $\sim 1.6\,\mathrm{nN}$ when the fish is rolled 90°. The magnetic and gravitational forces acting on the otolith are thus in the same range, which *a posteriori* explains the capacity to drive large vestibular-like behavioral responses as detailed above.

Our simulations can also be used to evaluate the number of nanoparticles attached to the otolith. A single particle experiences $\sim 0.007\,\mathrm{fN}$ of lateral force when placed at the edge of a 5 mm in diameter magnet positioned 2 mm beneath the particle. Therefore, approximately $1.4{\cdot}10^8$ particles are required to produce a total of 1 nN force. This corresponds to a ~ 1 monolayer of particles bound to the otolith. This fine coating represents only 0.2 ‰ of the mass of the otolith and is thus unlikely to interfere with the vestibular function, in agreement with our observations.

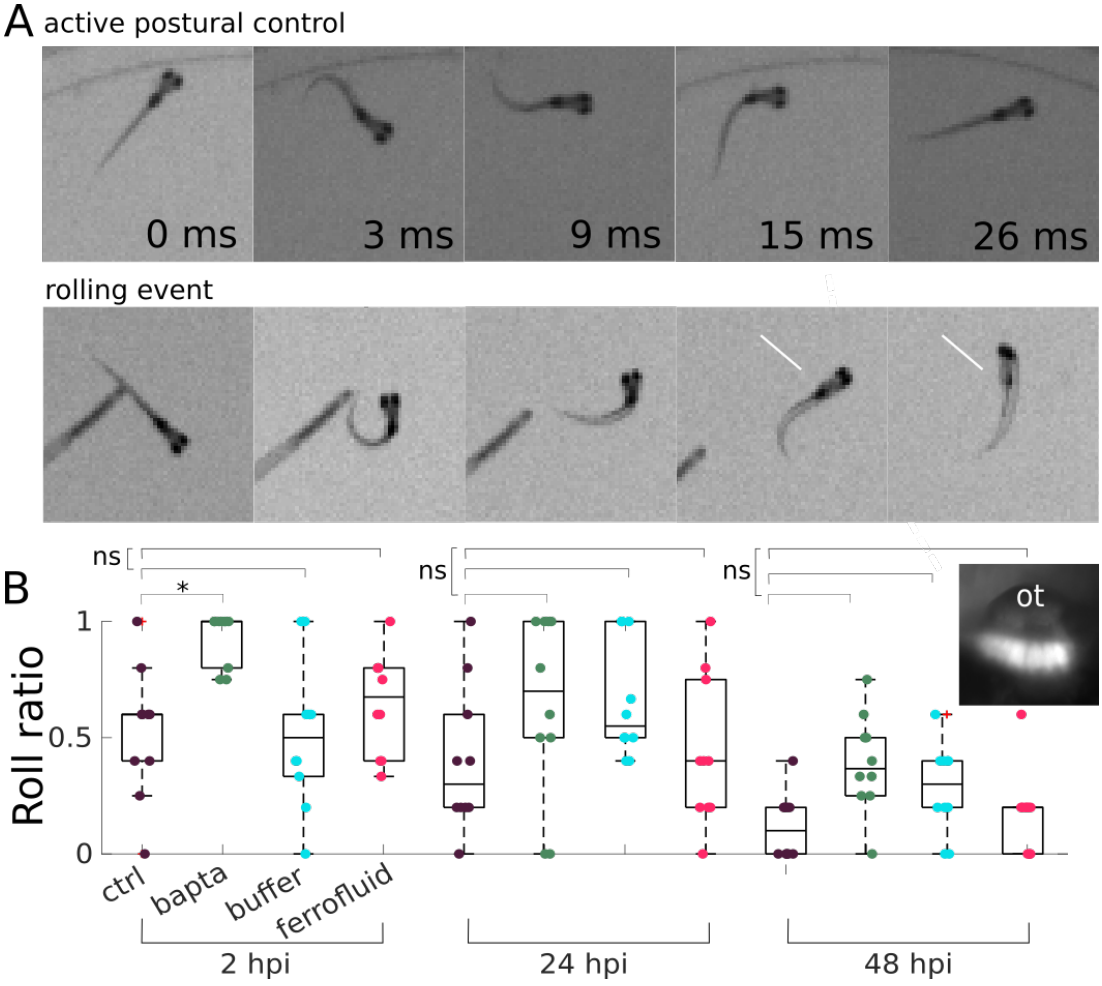

Figure 2: Control experiments probing the impact of the injection procedure on vestibular functionality **A** Image sequence recorded during evoked startle response behaviors for a non-injected control fish illustrating active postural control (top) as well as for BAPTA injected fish illustrating a roll event (bottom). **B** Roll ratio during an evoked startle response measured 2, 24 and 48 hours post bilateral injection (hpi) of BAPTA, ferrofluid or buffer compared to non-injected control fish from the same batch, respectively.

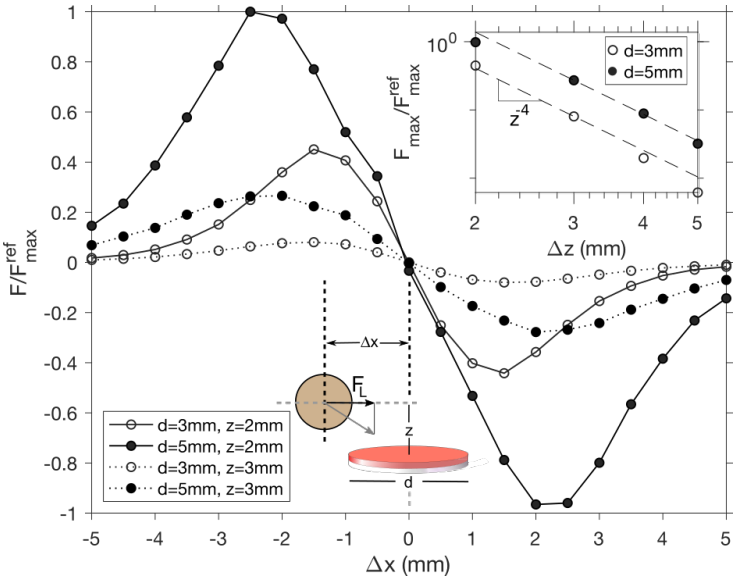

Figure 3: Simulations. Finite element simulation of the lateral force, F, exerted on a paramagnetic particle by a magnet as a function of the lateral distance (Δx) of the particle to the magnet's center axis. Shown are force-displacement relationships for two magnet diameters, d, and two z-distances, z, between the magnet and the particle. The calculated forces were normalized by the maximum of the force-displacement relation, F^{ref}_{max}, extracted from the configuration with the 5 mm in diameter magnet positioned at a distance of 2 mm. Inset: Dependency of the maximal lateral magnetic force, F_{max}, as function of the z-distance between the particle and the magnet, calculated for two magnet diameters.

Brain-wide functional imaging during magnetic vestibular stimulation and behavioral monitoring

One of the assets of our stimulation technique is its low footprint, which facilitates a combination with any functional recording technique. Here we used a setup that enables the application of controlled fictive vestibular stimuli in head-tethered larval zebrafish while recording the behavioral responses as well as the evoked brain-wide neuronal activity using light-sheet imaging (Figure 4A).

We first recorded the neuronal activity, evoked in mechanosensitive inner ear hair cells. In order to do so, we used the transgenic line *α-tubulin:Gal4-VP16;UAS:GCaMP7*, which expresses the GCaMP7 calcium indicator in hair cells of the inner ear [30]. Both inner ears of these fish were injected with ferrofluid, embedded in agarose, and placed in the experimental setup one day after the injection. We generated a fictive vestibular roll stimulus by moving the magnet sinusoidally along the left-right body axis at 0.5 Hz and 2.5 mm amplitude. Hair cells in the anterior macula (AM, utricle) showed a modulation of the fluorescence signal, phase-coupled to the stimulus (Figure 4B). In contrast, hair cells in the posterior macula (PM), which are part of the saccule that senses vertical oscillations at higher (auditory) frequencies, showed no detectable response indicating that they were likely not stimulated. These observations are consistent with the anatomical orientation of the mechanosensitive axes of the two vestibular organs.

Next, we recorded the brain-wide neuronal dynamics elicited upon fictive vestibular stimulation using the pan-neuronal nuclear localized *Tg(elavl3:H2B-GCaMP6f)* transgenic line. This stimulus evoked neuronal activity throughout the brain (see Movie 5). As an example, we show activity time traces recorded from vestibulo-spinal neurons and from the oculomotor nucleus nIII (Figure 4C). We quantified the brain-wide vestibular response pattern by computing a phase map as described in Migault *et al.* [4]. Briefly, we estimated, for each voxel (0.6x0.6x10μm), the amplitude and the phase relation of the evoked signal relative to the stimulus waveform. These two parameters were displayed in the form of a phase map, where color represents the relative phase of the neuronal response to the stimulus and intensity encodes the amplitude of the response. Hence, a phase shift of 0° applies to neurons whose activity is locked to the applied force, whereas a phase shift of 90° corresponds to neurons responding to the time-derivative of the force signal. Figure 4D shows the phase map for several selected layers and their z-projection, recorded in a single fish and registered on the Z-brain atlas [31]. Vestibular-induced activity is clearly visible in the tangential vestibular nucleus and in vestibulo-spinal neurons. The observed ocular motoneuron activity is consistent with the monitored compensatory eye movements. Active regions also include the nucleus of the medial longitudinal fascicle, as well as hindbrain pre-motor neuronal populations involved in tail motion. Cerebellar and inferior olivary neurons were also clearly recruited. This response map was found to be stereotypic and reproducible for all injected fish as shown by the sharpness of the average phase map, which combines the observations in 14 larvae (Figure 4E). This average phase map shows a close similarity with the brain-wide response recorded during natural vestibular stimulation using a rotating light-sheet microscope (Figure 4F and Figure 4 in Migault *et al.* [4].

This new stimulation method offers, as optical tweezers but in contrast to a natural stimulation, the opportunity to stimulate a single ear at a time, by injecting the ferrofluid only unilaterally. Figure 4G show the average phase map for fish injected with ferrofluid into the right ear only. Interestingly, the response appears rather similar to that evoked by bilateral fictive vestibular stimulation, albeit with a relatively lower intensity. The marked antisymmetric activity in the medial octovolateralis nucleus (MON) reflects a strong activity of commissural connections between both sides of the brain and suggests a pronounced contralateral inhibitory connectivity in the hindbrain.

We finally performed control experiments with non-injected fish. At the stimulation frequency, no signal was detectable in the average phase map (Figure 4H). This rules out the possibility that the recorded activity may in part reflect the visual stimulus caused by the moving magnet, which could have been possible as the blue (488 nm) laser forming the light sheet also illuminates the sample chamber.

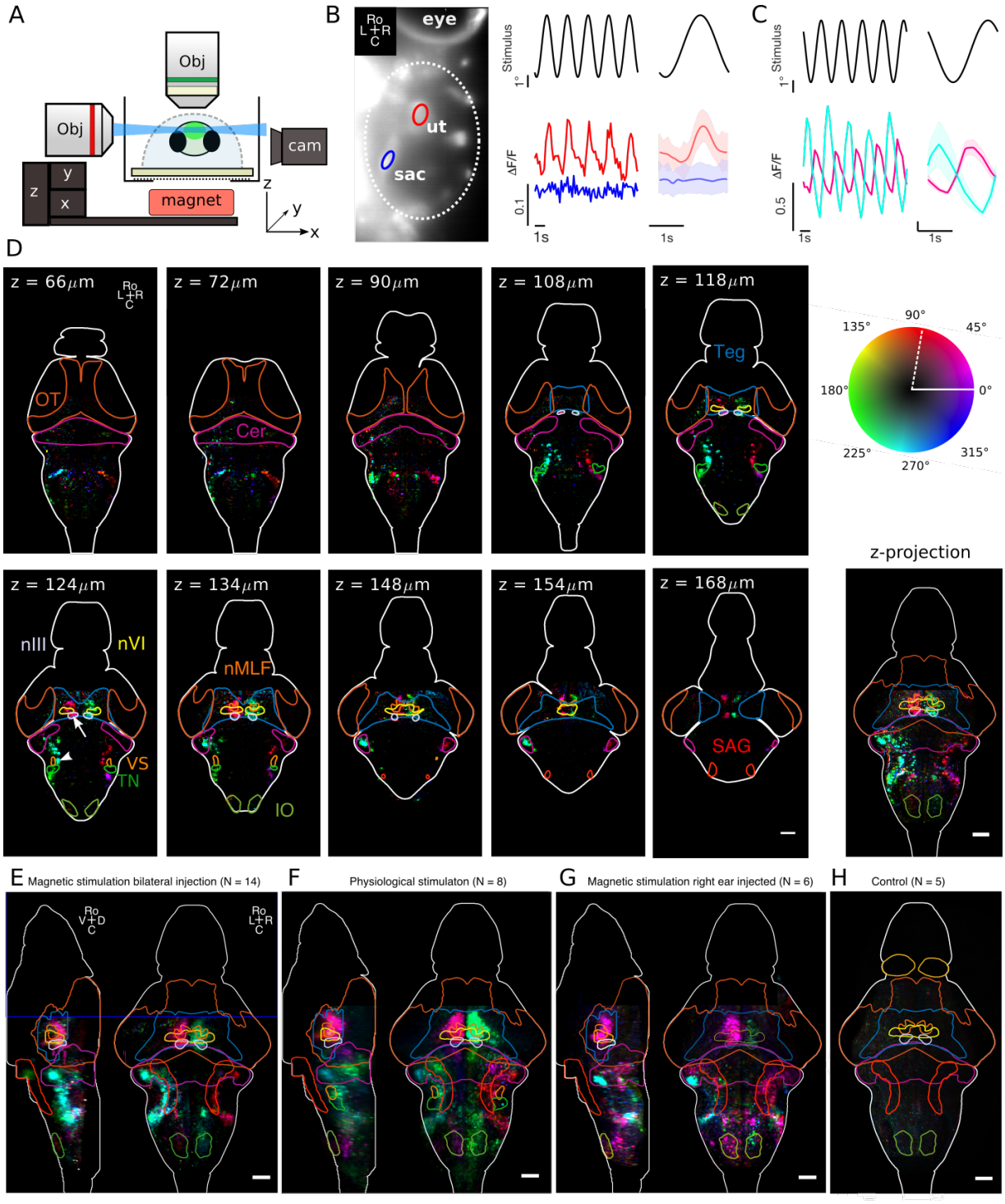

Figure 4: Brain-wide neuronal responses evoked by magnetic vestibular stimulation. Caption continues next page.

Figure 4: (Continued) **A** For functional imaging a light-sheet (blue) excites the fluorescence GCaMP6 sensor genetically encoded in the brain (green). The fluorescence is collected by an objective perpendicular to the light-sheet. **B** Calcium responses recorded in the otic vesicle from the utricle (red) and the saccule (blue) in response to a sinusoidal fictive roll stimulus (black). The trial-averaged response with std (N = 75 repetitions) is shown on the right. The ROIs from which the fluorescent signals were extracted are indicated with red and blue circles respectively. **C** Neuronal responses to the same stimulus as in **B** but measured in vestibulo-spinal neurons (white arrowhead in panel D) and extraocular motoneurons in the oculomotor nucleus (white arrow in panel **D** bottom left). **D** Selected layers of the phase map of the brain-wide response recorded in one fish. OT: optic tectum, Cer: cerebellum, Teg: tegmentum, nIII and nIV: oculomotor and trochlear nucleus, nMLF: nucleus of the medial longitudinal fascicle, SAG: statoacoustic ganglion, IO: inferior olive, TN: tangential nucleus, VS: vestibulo-spinal neurons. The color map indicates the phase of the neuronal response relative to the stimulus after correction for the phase delay introduced by the GCaMP6f calcium sensor $\Delta\phi = \arctan(-2\pi f \tau_{GCaMP6f})$(decay time $\tau_{GCaMP6f} \approx 1.8\,\mathrm{s}$). Without this correction the zero degree phase shift would be at the position indicated by the dashed white line. Bottom right: Maximum z-projection of the entire phase map shown of this fish. **E** Average phase map in response to bilateral fictive vestibular stimulation (N = 14 fish). **F** Average phase map recorded during natural vestibular stimulation with a rotating light-sheet microscope [4]. **G** Average phase map in response to unilateral (only right ear injected) fictive vestibular stimulation. **H** Control phase map recorded under the same conditions as **E and H** but without injected ferrofluid into the inner ear. Transgenic lines: *Tg(a-tubulin:Gal4-VP16 ;UAS:GCaMP7a)* panel B, *Tg(elavl3:H2B-GCaMP6f)* panel C-H.

3 Discussion

Our work demonstrates that injecting a ferrofluid solution into the inner ears of larval zebrafish allows to subsequently apply controlled forces to the utricular otolith *in vivo*, thus mimicking natural motion-like vestibular stimuli in immobilized animals. A small permanent magnet was sufficient to elicit robust motor responses to both fictive vestibular roll and tilt stimulation that were indistinguishable from those observed during natural motion stimulation. Cross-talk between the two stimulus directions was negligible, provided that the magnet was well centered beneath the fish.

Control experiments confirmed that the injection procedure did not damage the vestibular system and left the swimming behavior and postural control performance unaffected 24 hours after the injection. This robustness of the method reflects the minor interference of the injection procedure with the functionality of the system but may in part be related to the capacity of non-mammalian hair cells for self-repair [29]. Hence, even if tip-links were damaged by the injection procedure, the vestibular apparatus is likely fully functional 24 - 48 h post injection. In addition to potential tip-link repair, non-mammalian inner ear hair cells can regenerate destroyed hair cell bundles [32] and even full hair cells with restored sensory function after cell death [33, 34, 35]. In the adult zebrafish utricle, the full regeneration of the utricular macula after induced damage takes about 13 days [36]. This is too slow to explain the observed high performance of the vestibular system after injections leading to the conclusion that the injections did not cause substantial and functionally detrimental cell death.

Our proposed mechanism underpinning the fictive stimulation is based on the irreversible binding of nanoparticles onto the surface of the otolith. This thin magnetized coating can then be acted upon using magnetic field gradients. We reported direct evidence of the effective magnetization of the otolith and that the corresponding magnetic force is in the same order of magnitude as the gravitational force imposed during macroscopic body rotation. In the present study, we only tested two different concentrations of injected ferrofluid, and the strongest response was obtained already at the lowest concentration. This observation suggests that a relatively small number of nanoparticles is sufficient to entirely cover the otolith with a compact monolayer. Any further particles are then likely to be repelled from the surface due to electrostatic repulsion between the citric acid-coated nanoparticles.

A complementary mechanism may be at play that would rely on the magnet-induced motion of freely floating nanoparticles in the endolymphatic otic environment. The induced fluid motion would then impose a drag force onto the otolith. Given the nano-bead dimensions, the associated flow would be in the low Reynolds number regime and the particles are thus expected to reach their terminal velocity in less than a millisecond when placed in a field gradient. The resulting drag force, proportional to this particle velocity, would vary with the magnet position and could not be distinguished from the direct magnetic actuation on the otolith. However, an estimate of the particle terminal velocity results in a value of $\approx 0.1\,\mu m/s$, which in turn yields a drag force orders of magnitude smaller than the force exerted by the particles attached to the otolith. This suggests that this second mechanism is probably negligible.

In zebrafish, the utricular otolith is spherical. For a spherical mass, the gravitational force grows with the radius cubed while the magnetic force acting on a thin surface coating grows with the radius squared. One may thus anticipate that this magnetic actuation method should become relatively inefficient for larger animals (with larger otoliths). However, in most animals other than teleost fish, the otolithic membrane is covered with small carbon crystals called otoconia yielding a flat meshwork of extended mass. This leads to a much higher surface to volume ratio, which is more favorable for the actuation via surface-bound nanoparticles. Our method could thus work also in larger animals such as for instance *Xenopus* larvae, lampreys or even mammalian species provided that sufficiently strong magnetic fields and field gradients can be delivered. In fact, a pilot study on an isolated *in vitro* preparation of *Xenopus* tadpoles at mid-larval stage, demonstrated that solutions of citrate-coated ferromagnetic nanoparticles can be reliably injected and distributed throughout the duct system of the inner ear. Repetitive displacement of a permanent point magnet above the transparent otic capsule in different directions, elicited faithful and robust eye movements also in these animals (see Movie 4), which are an order of magnitude larger than larval zebrafish. The known functionality of all inner ear organs at this developmental stage ([37]), however, renders an identification of the recruited vestibular organ(s) more difficult but potentially derives from the magnetic stimulation of multiple inner ear organs.

This magnetic actuation method was implemented to fictively stimulate a slow tilt or roll of the fish body. However, the same approach could be used to mimic translational accelerations experienced by the larvae during free swimming. Larval zebrafish swimming patterns consist of discrete swim bouts that last for $100 - 200\,\text{ms}$ interspersed by $\sim 1\,\text{s}$-long resting periods. Owing to the Einstein principle, otoliths are

actuated during these transient linear accelerations: forward acceleration of the animal produces a backwards pointing force on the otolith while a deceleration corresponds to a forward pointing force. The reported peak acceleration during a bout is in the range of $0.3 - 2\,\mathrm{m/s^2} = 0.03 - 0.2\,\mathrm{g}$ [38, 39], which corresponds to a force on the otolith in the range of $50 - 300\,\mathrm{pN}$, i.e., within the accessible range of our instrument. To mimic acceleration forces encountered during a swim bout, the magnet has to be moved by $0.3 - 2\,\mathrm{mm}$ in about 50 ms, which is also compatible with the performance of our mechanical stages. Our system can thus be used to emulate vestibular signals associated with fictive self motion in head-fixed animals. It could thus be included into closed-loop virtual reality assays, mitigating sensory mismatch and enhancing the quality of virtual environments. This will open new possibilities to study sensorimotor processing.

Unlike other approaches, such as optical tweezers, the reported method could potentially be implemented in freely swimming configurations as well. A large scale magnetic field gradient could be used to create a sufficiently large force onto the magnetized otolith coating to counteract the gravitational force acting on it. One could thus create a zero gravity condition or mimic inverted gravity and study how fish adapt to and learn to cope with this change of physical parameters. As only injected fish will be sensitive to the applied magnetic field gradients, social behavior experiments can be envisioned to study how conspecific fish react to behavioral changes of a single fish when the latter experiences a perturbation of the vestibular sensation. But one may even go beyond and investigate how animals can learn to use this novel sensation of magnetic field gradients, e.g. for navigational strategies.

We have demonstrated that our vestibular stimulation method is compatible with simultaneous whole-brain functional imaging using light-sheet microscopy. In response to the fictive vestibular stimulus, we observed consistent neuronal activity in the vestibular nucleus and in downstream nuclei throughout the brain. The evoked neuronal response map in bilaterally injected fish was comparable to the one that was obtained during actual vestibular motion stimulation with a rotating light-sheet microscope. This confirms that the magnetic force acts without delay onto the otolith in the same manner as gravitational forces when the animal is e.g., rolled along its longitudinal body axis. The recorded average phase maps during unilateral stimulation suggests the presence of a pronounced commissural inhibition between the two vestibular nuclei, typically conserved in all vertebrates [40]. Sinusoidal magnetic stimulation of the right ear shows that pulling the right otolith laterally activates neurons located in the right vestibular nucleus and downstream regions such as the ipsilateral vestibular cerebellum, and on the contralateral side oculomotor motoneurons, neurons in the nMLF as well as hindbrain neuronal populations probably projecting to the spinal chord. This activity pattern and profile is consistent with the highly conserved axonal projections from the vestibular nucleus to these brain regions [41, 42]. This activation pattern has a mirror-symmetric counterpart with a mean activity that is 180 degrees phase-shifted and thus exhibits a mean activity that is minimal when the mirror-symmetric neuronal correlate is maximally active. This suggests that the vestibular nucleus inhibits the contralateral vestibular nucleus, which leads to a reduced activity in downstream nuclei. The latter result is consistent with the description of inhibitory commissural projections in cats between vestibular neurons of the utricular pathway [43], which are thought to contribute to the sensitivity of vestibular neurons through a disinhibition [43]. In larval zebrafish, commissural projections have been described as originating from the tangential vestibular nucleus [8], with a likely inhibitory function as evidenced by our results.

In summary, our magnet-based vestibular stimulation method is inexpensive, easy to implement, and can be developed as an add-on device for existing microscopes and visual virtual reality setups. Since the magnet is small and operates beneath the fish, the whole experimental chamber is accessible for all types of microscopes, optogenetic tools, electrophysiological setups, other sensory stimulation methods or behavioral monitoring. Accordingly, our method uniquely expands the toolbox of widely accessible sensory stimulation methods for zebrafish systems neuroscience but also for neuroscientific studies in other species.

4 Movie legends

Movie 1

Behavioral responses to fictive magnetic vestibular stimulation with a hand-held magnet.
Part I: Behavioral response to fictive vestibular roll stimulation recorded by top view monitoring. The fish is tethered with the agarose that was removed around the tail and eyes to allow free movements. The movie was obtained with a stereomicroscope immediately after ferrofluid injection. The magnet was hand-held and moved beneath the fish along the left-right body axis to mimic a vestibular roll stimulus.
Part II: Same fish as in Part I, with the magnet moved along the rostro-caudal body axis to mimic a tilt stimulus (nose-up, nose-down).
Eyes and tail perform marked compensatory movements in response to these fictive vestibular stimuli.

Movie 2

Behavioral responses to fictive vestibular roll and tilt stimuli generated and recorded in an automatized setup. Ferrofluid was bilaterally injected at 5 dpf and movies were recorded the next day at 6 dpf. The magnet was moved sinusoidally at 0.5 Hz and with 2.5 mm amplitude. **Part I:** Front view of evoked eye movements in response to a fictive roll stimulus.
Part II: Side view of evoked eye movements in response to a fictive roll stimulus. The eye rotates only along the roll axis and not along the tilt axis, demonstrating the absence of cross-talk between the two stimulation axes.
Part III: Side view of evoked eye movements in response to a fictive tilt stimulus. **Part IV:** Top view of evoked tail movements in response to a fictive roll stimulus. Note that the magnet created a shadow under the fish, which allows to see the correlation between magnet displacement and tail movement.

Movie 3

Impaired postural control along the roll axis after BAPTA injection compared to wild-type control fish with an intact vestibular system.
Part I: The movie shows a fish two hours after bilateral injection of the calcium chelator BAPTA. The fish was placed freely in a Petri dish filled with embryonic medium E3 and recorded from the top. A startle response was elicited by touching the fish with a fine glass tip. During the startle response and also during successive swimming bouts, the fish lost its dorsal position and rolled around its longitudinal body axis.

Part II: Recording of a wild-type control fish under the same conditions as in Part I. Throughout the sequence and including the startle response, the fish maintained its dorsal side-up posture.

Movie 4

Free swimming behavior of fish, injected bilaterally with ferrofluid, compared to wild-type control fish (Recording frame rate = 70 fps):
Part I: Wild-type fish (N = 10) swimming freely in a Petri dish.
Part II: Fish after bilateral injection of ferrofluid into the inner ears (N = 7), swimming freely in a Petri dish.

Movie 5

Brain-wide neuronal responses during a fictive sinusoidal roll stimulus.
The movie shows in a loop the neuronal response averaged over 40 stimulus cycles. Six sections of the brain are shown.
Experimental parameters: Ferrofluid was injected bilaterally at 5 dpf into a fish of the Tg(elav3-H2B:GCaMP6f) transgenic line. The movie was recorded the next day at 6 dpf. The magnet was moved sinusoidally at a frequency of 0.5 Hz and with an amplitude of 2.5 mm.

The phase map in Figure 4D was calculated from this recording.

Movie 6

Pilot study in a *Xenopus* tadpole.
The movie shows a dorsal view of an isolated *in vitro* preparation of a *Xenopus* tadpole prepared following the protocol in Lambert *et al.* 2008 [37]. Ferrofluid was injected into the left inner ear (red-orange color). A permanent point magnet was displaced in close proximity above the inner ear. The magnet motion provoked eye rotations via the vestibulo-ocular reflex. Only the left eye responded as the right eye was partly immobilized to hold the preparation in place.

5 Materials and Methods

5.1 Key resources table

REAGENT OR RESOURCES	SOURCE	IDENTIFIER
Chemicals		
Low melting point agarose	Sigma-Aldrich	A9414-50G
Tricaine	Sigma-Aldrich	E10521-10G
Ferrofluid	custom made	[22]
BAPTA	Sigma-Aldrich	14510-100MG-F
2-Di-4-Asp	Sigma-Aldrich	D3418-500MG
Ultrapure Low Melting Point Agarose	Invitrogen	16520050
Experimental Models: Organisms/Strains		
Tg(a-tubulin:Gal4-VP16 ;UAS:GCaMP7a)		Köster and Fraser 2001 [30]
Tg(elav3-H2B:GCaMP6f)		Vladimirov et al. 2014 [44]
Software and Algorithms		
Matlab	The MathWorks	https://www.mathworks.com/products.html
CMTK	Rohlfing and Maurer, 2003 (citation)	https://www.nitrc.org/projects/cmtk/
FIJI	(ImageJ) NIH	https://fiji.sc/
ZBrain atlas	Randlett et al., 2015	https://zebrafishexplorer.zib.de/home/
Comsol Multiphysics	Comsol	https://www.comsol.com/
Other		
Pneumatic PicoPump	World Precision Instruments	SYS-PV830
Glass capillaries to pull micropipettes	Warner Instruments	GC100F-10
Micropipette puller	Narishige	PC-100
Motorized stages	Physik Instrumente PI	PIMag® Linear Stage: V-408.132020, V-408.232020
Behavior tracking: Camera	Point Grey	BFLY-U3-05S2M-CS
Behavior tracking: Objective	Navitar	1-61449
Behavior tracking: 2x Adaptor	Navitar	1-61450
Magnet (D=5 mm, thickness 1 mm, 3 magnets stacked)	RS Components	N837RS
Micro knife 22,5° cutting angle	Fine Science Tools	10316-14

Table 1: Key resource table

5.2 Animal husbandry

All experiments were performed on 5-7 dpf larvae. Adult fish were maintained at 28°C in system water (ph 7-7.5 and conductivity between 300 and 350 μS)) in the fish facility of the Institut de Biologie Paris-Seine. Eggs were collected in the morning and then kept in a Petri dish with E3 at 28°C in a 14h/10h light/dark cycle. Larvae were fed with paramecia or powder from 5 dpf on. Calcium imaging experiments were carried out in two different transgenic lines: *elavl3:H2B-GCaMP6f* [44] (kindly provided by Misha Arhens) and *α-tubulin:Gal4-VP16 ;UAS:GCaMP7* [30] (kindly provided by Teresa Nicolson) both in Nacre background. Experiments were approved by Le Comité d'Éthique pour l'Expérimentation Animale Charles Darwin C2EA-05 (02601.01 and 32423-202107121527185 v3).

5.3 Ferrofluid

The ferrofluid, a suspension of γ-Fe_2O_3 iron oxide nanoparticles, was produced by Christine Ménager and Aude Michel Tourgis (Sorbonne Université, Laboratoire PHENIX, CNRS UMR 8234) following the protocol described by Massart et al. [22] and kindly provided to us for our experiments. The hydrodynamic diameter measured by dynamic light scattering (DLS) was 22 nm with a polydispersity index of 0.15. This corresponds to a physical diameter of 11 nm, usually measured by TEM after drying the sample. The particles were dispersed in water and stabilized with citrate molecules at pH 7 to prevent agglomeration.

5.4 Ear injections

Either ferrofluid, BAPTA or 4-Di-1-ASP were injected into the inner ear with a glass micropipette held by a micromanipulator (Narishige MN-153) using a pneumatic Pico-pump (World Precision Instruments PV830). Capillaries (1 mm outer diameter, Warner Instruments GC100F-10) were pulled to obtain fine tip micropipettes (tip diameter = 1 - 2 μm) using a Narishige PC-100 puller with the following parameters: 2 steps, Heater N°1 = 52,4; Heater N°2 = 55,7, position 2 mm, 2 heavy and 1 light weights. Micropipettes were loaded with 2 μL of ferrofluid diluted in buffer (NaCl 0.178 M, sodium citrate 0.023 M, HEPES 0.01 M) at 0,019 μM. Injections were performed in 5 dpf fish. Larvae were mounted dorsal side up in 2 % LMP agarose on top of a microscope glass slide. Using a small piece of metal as support, the slide was rolled 45 degrees to access the fish's left ear. For the ferrofluid, 3 pulses (10 psi for 500 ms) were injected into the otic vesicle, corresponding to a total volume of 1,2 nL. After the left ear injection, the glass slide was rolled onto the other side to inject the right ear. For injection of BAPTA and DiASP the protocol was the same except for different concentrations of the solutions. We used 50 mM BAPTA dissolved in extracellular solution containing (in mM) 134 NaCl, 2.9 KCl, 1.2 $MgCl_2$, 2.1 $CaCl_2$, 10 HEPES, and 10 glucose, at 290 mOsm, adjusted to a pH 7.8 with NaOH. For 4-Di-1-ASP, a 50 mM solution of diluted E3 medium containing 1% ethanol was injected. After the injections, larvae were freed from the agarose using a fine tip (Dumont n°5) and maintained in E3 medium until the experiments commenced.

5.5 Free swimming control

We analyzed the free swimming behavior of ferrofluid-injected and control fish. Seven larvae were injected at 5 dpf. 24 hours later they were placed in a Petri dish to record the swimming behavior during 1 hour at 30 fps. The movies were tracked using FastTrack [45]. Individual fish were not tracked throughout the whole movie but rather split into wall-to-wall trajectories. For each trajectory, discrete swim bouts were detected when the instantaneous swim speed exceeded two times the overall variance of the speed. Putative bouts were then filtered on a distance criterion: bouts with a linear displacement – measured in a time window of $\pm$0.5 s centered on the bout velocity peak – less than 0.3 mm or greater than 18 mm were rejected) and on a temporal criterion (bouts occurring within 0.4 s after a bout were rejected. Bout onset was defined at 80 ms before the velocity peak. From positions, time and body angles before and after an event, the inter-bout interval, displacement and turn angles associated with each bout were computed. These values were then averaged over trajectories and the means were displayed as boxplots. Mean square displacement (MSD) was

computed using the MATLAB package msdanalyzer [46]. (x,y) sequences were pooled by condition (control and injected), a MSD was computed for each sequence and the ensemble average is presented along with the standard error of the mean.

5.6 Roll ratio essay

The larvae were placed in a 5 cm Petri dish positioned under a high magnification objective and recorded at 300 fps. Approaching the larvae with a fin glass tip evoked a startle response. Each larva was subjected to five trials. The roll behavior was assessed for each trial. The roll ratio was calculated as the number of trials the animal rolled during an escape divided by the number of trials the animal attempted an escape [27].

5.7 Finite element simulations and force generation mechanism

Force of a ferrofluid particle in a magnetic field gradient The ferrofluid particles are so small that nanoparticles consist only of a single magnetic domain giving the particle a giant magnetic moment. In the absence of an external magnetic field, the direction of this moment changes randomly depending on the temperature. The average magnetisation is zero and the particle is in a superparamagnetic state. In an external magnetic field, the giant magnetic moment becomes progressively aligned against the thermal agitation, and the average net magnetization increases. The macroscopic magnetization of a ferrofluid particle or of a ferrofluid droplet is characterized by the macroscopic magnetic moment, $\vec{m}$, which depends on the volume V of the particle or of a ferrofluid droplet, and the external field B. In a weak magnetic field the macroscopic magnetization is given by

$$\vec{m}(\vec{B}) = \frac{V\chi}{\mu_0}\vec{B}$$

with χ the magnetic susceptibility and μ_0 the vacuum permeability. And the force exerted on the droplet reads

$$\vec{F} = \nabla\left(\vec{m}(\vec{B})\cdot\vec{B}\right) = \nabla\left(\frac{V\chi}{\mu_0}\vec{B}^2\right) = 2\frac{V\chi}{\mu_0}\vec{B}\nabla\vec{B}$$

In a strong field that saturates the magnetization the force exerted on the droplet is

$$\vec{F} = \nabla\left(\vec{m}_{sat}\cdot\vec{B}\right) = \vec{m}_{sat}\nabla\vec{B}$$

Finite element simulations We used Comsol Multiphysics to calculate the magnetic force applied by the magnet to the ferrofluid. Lateral force-displacement curves were calculated for cylindrical magnets of different diameters and z-distance to a spherical droplet of the ferrofluid with a diameter of 200 μm. The spherical droplet was considered perfectly rigid. The droplet volume was chosen arbitrarily. The force, acting on the droplet depends linearly on the volume of the droplet. Therefore uncertainty with respect to the droplet volume will change the maximum force reached but not the linear dependence of force on the magnet position. The relationship between magnetic flux density and magnetic field strength (B-H curve) is defined

for the ferrofluid by a magnetization curve (Figure S3). The magnetic flux density is fixed for the magnets. For the simulations, we started with a mesh size of 500 μm and then iteratively reduced the mesh size until the results converged. Parametric sweeps were realized for different distances and diameters.

The simulation gives a maximal lateral force of $F_{D=200\,\mu} = 4 \cdot 10^{-4} N$ exerted on the ferrofluid droplet with a diameter of $D = 200\,\mu m$ placed 2 mm above our 5 mm in diameter magnet. As the force depends linearly on the volume we estimated that the force exerted on a single nanoparticle with a diameter of $D = 11\,nm$ is $F_p = 0.007\,\text{fN}$.

Drag force on an otolith pulled through water To estimate the maximum force that can be delivered to the otolith, we measured the velocity in water of an isolated otolith (obtained after dissection of an injected larvae) submitted to a comparable magnetic field as in the *in vivo* experiment. Taking into account the otolith diameter that controls the drag force, we obtained an estimated force of

$$F_{drag} = 6\pi\eta R v = 0.9\,\text{nN}$$

with η the viscosity of water $R = 27.5\,\mu$m, the radius of the otolith and v the speed at which the otolith was dragged by the magnet through the aqueous solution.

Given the force that the magnet exerts on a single particle of the ferrofluid suspension $F_p = 0.007\,\text{fN}$ we can estimate the number of particle bound to the otolith

$$N = \frac{F_{drag}}{F_p} = 1.3 \cdot 10^8$$

A monolayer of particles on the otolith surface corresponds to

$$N \approx \frac{4\pi R_{otolith}^2}{D_p} = 0.8 \cdot 10^8$$

particles. Thus we estimate that ~ 1.6 monolayers of particles have bound to the otolith.

However, due to the small diameter of the particles, the mass change of the otolith is negligible with

$$\frac{m_{monolayer}}{m_{otolith}} = \frac{4\pi R_{otolith}^2 D_p \cdot \rho_{Fe_2O_3}}{4/3\pi R_{otolith}^3} = 2 \cdot 10^{-4}$$

Gravitational force F_g exerted onto the otolith during roll motion When the fish is rolled under natural conditions along the rostro-caudal body axis, gravity acts on the otoliths pulling them along the left-right body axis. The magnitude of this lateral component of the gravitational force F_g depends on the roll angle and on the density of the otolith

$$F_g = (\rho_o - \rho_w) V_o g \sin(\alpha)$$

with the density of the otolith $\rho_o = 2.83\,\mathrm{g\,cm^{-3}}$, the density of water $\rho_o = 1\,\mathrm{g\,cm^{-3}}$, the otolith volume $V_o = \frac{4}{3}\pi R_o^3$, the otolith radius $R_o = 27\,\mathrm{nm}$, the gravitational acceleration $g = 9.81\,\mathrm{m\,s^{-2}}$ and the angle α by which the animal is rolled relative to its dorsal side-up position.

At $\alpha = 90°$ the lateral force on the otolith is maximal with:

$$F_g(\alpha = 90°) = 1.6\,nN$$

Because the mean behavioral response in the fictive roll motion experiments compares to the mean evoked response when rolling fish with a sinusoidally modulated excursion of ±15°, we can estimate that we exerted *in vivo* with our experimental parameters in average a force of $< F_{max} >= 1.6\,\mathrm{nN} \cdot \sin(15°) = 400\,\mathrm{pN}$ on the otolith when displacing the magnet $2.5\,mm$.

Time constant at which a particle reaches its terminal velocity when accelerated by a constant force in a viscous solution. Freely floating particles in the inner ear will be accelerated by the magnet. However, due to the interaction with the surrounding water molecules they will reach a terminal velocity after a characteristic time

$$\tau = \frac{m_p}{6\pi\eta R_p} = \frac{2\rho_p R_p^2}{9\eta} = 516\,\mathrm{ps}$$

with the particle mass m_p, the hydrodynamic particle radius $R_p = 22\,nm$ and the viscosity of water η. The terminal velocity reached is

$$v = \frac{F}{6\pi\eta R_p} = 0.1\,\mu\mathrm{m\,s}{-}1$$

with the hydrodynamic particle radius $R_p = 22\,nm$ and the viscosity of water η and with the estimated maximal force $F_p = 0.007\,\mathrm{fN}$ exerted on a ferrofluid nanoparticle placed 2 mm over the edge of our 5 mm in diameter magnet.

5.8 Sample preparation

24 hours after ferrofluid injection larvae were mounted in 2 % low melting point agarose dorsal side-up on top of a small acrylic holder (1mm thick). Then, the holder was placed inside an acrylic chamber filled with E3. For behavioral experiments, the agarose was removed from the eyes and tail using a micro knife (FST Micro Knife - Plastic Handle/22.5° Cutting Angle).

5.9 The setup

We built a platform with two motorized stages (PI instruments) to precisely control the magnet position and hence the fictive vestibular stimulation. A third manual stage allowed to position the magnet beneath the fish as close as possible in the vertical plane in order to maximize the accessible range of force. For the experiments shown in Figure 1 and 4 we used a magnet 5 mm in diameter and 3 mm in height. Injected

fish were mounted in a drop of 2% low melting point agarose on top of a transparent acrylic holder (1 mm thick). The agarose was removed from around the eyes and tail to allow unimpaired movements. Then, the holder was placed into the sample chamber filled with embryonic medium E3. The bottom of the sample chamber was formed by a 220μm thick coverslip glass. A front and a side camera were installed to record eye movements. To record tail movements, we used the same camera as for the neural recordings, equipped with a 4x objective. The entire platform was mounted on a light-sheet microscope system to perform simultaneous brain-wide neuronal activity recordings.

5.10 Behavioral protocol

In order to move the magnet in a controlled manner, we used 2 stages for x and y axis movements (Physik Instrumente, V-408 PIMag Linear Stage). To simulate a roll-like motion, we moved the magnet along the transverse axis, starting from the center and extending 2.5 mm towards each side of the fish. To simulate a tilt-like motion, we moved the magnet along the longitudinal axis, using the same amplitude. The stimulation frequency was 0.5 Hz.

5.11 Imaging Setup

The imaging setup was built around a microscope frame (Scientifica Slicescope Pro) fitted with an Olympus BX-URA fluorescence illuminator and a custom light-sheet forming unit adapted from Migault et al. [4]. Functional imaging was performed with a Leica HC FLUOTAR L 25x/0,95 W VISIR objective and a Hamamatsu Orca-Flash4.0 V3. Images were recorded with HCImage software (Hamamatsu) and the light-sheet was controlled with a custom application written in Matlab (MathWorks). Top view behavioral recordings used the microscope's light path and camera with a Nikon CFI Achro 4x objective. Side and front view behavioral recordings used separate systems of Point Grey cameras (BFLY-U3-05S2M-CS) with Navitar Precise Eye objectives (1-61450 with 1-61449).

5.12 Registration onto the Z-Brain atlas

We used the Computational Morphometry ToolKit CMTK (http://www.nitrc.org/projects/cmtk/) to compute for every fish the morphing transformation from the average brain stack (anatomical stack) to the Elavl3:H2B-RFP stack of the zBrain atlas [31]. This allowed mapping the functional data onto the Z-Brain Viewer, to overlay the region outlines and to calculate averages across animals.

We computed first the affine transformation, which we used then as initialization to compute the warp transformation between the two stacks. The used commands and options are listed in table 2.

5.13 Data and code availability

Data and code are available on request to the lead author: volker.bormuth@sorbonne-universite.fr

Tool	Options	Description
cmtk registration	–Initxlate –dofs 6,9,12 –sampling 3 –coarsest 25 –omit-original-data –accuracy 3 –exploration 25.6	Calculate affine transformation
cmtk warp	-v -–fast –grid-spacing 40 –refine 2 –jacobian-weight 0.001 –coarsest 6.4 –sampling 3.2 –accuracy 3.2 –omit-original-data	Use affine transformation as initialization
reformatx		Apply transformation to other stacks

Table 2: CMTK commands and options

Acknowledgements

We thank Christine Ménager and Aude Michel Tourgis (Sorbonne Université, Laboratoire PHENIX, CNRS UMR 8234) who kindly provided the ferrofluid. We thank the IBPS fish facility staff for the fish maintenance, in particular Stéphane Tronche and Alex Bois. We thank Misha Ahrens and Teresa Nicolson for providing transgenic fish lines. We are grateful to Carounagarane Dore for his contribution to the design of the experimental setup. We thank Claire Wyart and Marcus Ghosh for their comments on the manuscript. This project has received funding from the European Research Council (ERC) under the European Union's Horizon 2020 research innovation program grant agreement number 715980, and was partially funded by the CNRS, Sorbonne Université, and by the German Science Foundation through the collaborative research center 870 (CRC 870). H.M., G.M., and P.T. had a PhD fellowship from the Doctoral School in Physics, Ile de France (EDPIF). G.L.G. had a PhD fellowship from the Systems Biology Network of Sorbonne Université.

Authors contribution

N.B., H.S., N.D, G.D. and V.B designed the project. N.B., H.M., G.M. and P.T. performed the zebrafish experiments. N.B. T.Panier, T. Pujol, G.M, and V.B. built the experimental setup. T.Pujol performed the finite element simulations. N.B., H.M., G.M., G.L.G., P.T., G.D., V.B. analyzed the data, N.D. and H.S. performed the *Xenopus* experiment. N.B., G.D., V.B wrote the manuscript with input from all the authors.

Declaration of interests

The authors declare no competing interests.

References

1. Angelaki DE and Cullen KE. Vestibular system: the many facets of a multimodal sense. English. Annual review of neuroscience 2008; 31:125–50. DOI: 10.1146/annurev.neuro.31.060407.125555
2. Cullen KE. The vestibular system: Multimodal integration and encoding of self-motion for motor control. Trends in Neurosciences 2012; 35:185–96. DOI: 10.1016/j.tins.2011.12.001. Available from: http://dx.doi.org/10.1016/j.tins.2011.12.001
3. Panier T, Romano SA, Olive R, Pietri T, Sumbre G, Candelier R, and Debrégeas G. Fast functional imaging of multiple brain regions in intact zebrafish larvae using Selective Plane Illumination Microscopy. English. Frontiers in neural circuits 2013; 7:65. DOI: 10.3389/fncir.2013.00065
4. Migault G, Plas TL van der, Trentesaux H, Panier T, Candelier R, Proville R, Englitz B, Debrégeas G, and Bormuth V. Whole-Brain Calcium Imaging during Physiological Vestibular Stimulation in Larval Zebrafish. Current Biology 2018. DOI: 10.1016/j.cub.2018.10.017
5. Favre-Bulle IA, Vanwalleghem G, Taylor MA, Rubinsztein-Dunlop H, and Scott EK. Cellular-Resolution Imaging of Vestibular Processing across the Larval Zebrafish Brain. Current Biology 2018 Dec; 28:3711–3722.e3. DOI: 10.1016/j.cub.2018.09.060
6. Ahrens MB, Orger MB, Robson DN, Li JM, and Keller PJ. Whole-brain functional imaging at cellular resolution using light-sheet microscopy. English. Nature methods 2013; 10:413–20. DOI: 10.1038/nmeth.2434
7. Beck JC, Gilland E, Tank DW, and Baker R. Quantifying the ontogeny of optokinetic and vestibuloocular behaviors in zebrafish, medaka, and goldfish. Journal of Neurophysiology 2004 Dec; 92:3546–61. DOI: 10.1152/jn.00311.2004. Available from: https://www.physiology.org/doi/10.1152/jn.00311.2004
8. Bianco IH, Ma LH, Schoppik D, Robson DN, Orger MB, Beck JC, Li JM, Schier AF, Engert F, and Baker R. The tangential nucleus controls a gravito-inertial vestibulo-ocular reflex. Current Biology 2012; 22:1285–95. DOI: 10.1016/j.cub.2012.05.026
9. Favre-Bulle IA, Stilgoe AB, Rubinsztein-Dunlop H, and Scott EK. Optical trapping of otoliths drives vestibular behaviours in larval zebrafish. Nature Communications 2017; 8. DOI: 10.1038/s41467-017-00713-2. Available from: http://dx.doi.org/10.1038/s41467-017-00713-2
10. Mo W, Chen F, Nechiporuk A, and Nicolson T. Quantification of vestibular-induced eye movements in zebrafish larvae. BMC neuroscience 2010; 11:110. DOI: 10.1186/1471-2202-11-110
11. Ehrlich DE and Schoppik D. Control of Movement Initiation Underlies the Development of Balance. Current Biology 2017 Feb; 27:334–44. DOI: 10.1016/j.cub.2016.12.003

12. Voit W, Kim DK, Zapka W, Muhammed M, and Rao KV. Magnetic behavior of coated superparamagnetic iron oxide nanoparticles in ferrofluids. MRS Online Proceedings Library 2011; 676:78. DOI: 10.1557/PROC-676-Y7.8. Available from: https://doi.org/10.1557/PROC-676-Y7.8

13. Shapiro B, Kulkarni S, Nacev A, Sarwar A, Preciado D, and Depireux D. Shaping Magnetic Fields to Direct Therapy to Ears and Eyes. Annual Review of Biomedical Engineering 2014; 16:455–81. DOI: 10.1146/annurev-bioeng-071813-105206

14. Desprat N, Supatto W, Pouille PA, Beaurepaire E, and Farge E. Tissue Deformation Modulates Twist Expression to Determine Anterior Midgut Differentiation in Drosophila Embryos. Developmental Cell 2008; 15:470–7. DOI: 10.1016/j.devcel.2008.07.009

15. Doubrovinski K, Swan M, Polyakov O, and Wieschaus EF. Measurement of cortical elasticity in Drosophila melanogaster embryos using ferrofluids. Proceedings of the National Academy of Sciences of the United States of America 2017 Jan; 114:1051–6. DOI: 10.1073/PNAS.1616659114

16. Fernández-Sánchez ME, Barbier S, Whitehead J, Béalle G, Michel A, Latorre-Ossa H, Rey C, Fouassier L, Claperon A, Brullé L, Girard E, Servant N, Rio-Frio T, Marie H, Lesieur S, Housset C, Gennisson JL, Tanter M, Ménager C, Fre S, Robine S, and Farge E. Mechanical induction of the tumorigenic β-catenin pathway by tumour growth pressure. Nature 2015; 523:92–5. DOI: 10.1038/nature14329. Available from: https://doi.org/10.1038/nature14329

17. Mitrossilis D, Röper JC, Le Roy D, Driquez B, Michel A, Ménager C, Shaw G, Le Denmat S, Ranno L, Dumas-Bouchiat F, Dempsey NM, and Farge E. Mechanotransductive cascade of Myo-II-dependent mesoderm and endoderm invaginations in embryo gastrulation. Nature Communications 2017; 8:13883. DOI: 10.1038/ncomms13883. Available from: https://doi.org/10.1038/ncomms13883

18. Serwane F, Mongera A, Rowghanian P, Kealhofer DA, Lucio AA, Hockenbery ZM, and Campàs O. In vivo quantification of spatially varying mechanical properties in developing tissues. Nature Methods 2017; 14:181–6. DOI: 10.1038/nmeth.4101. Available from: https://doi.org/10.1038/nmeth.4101

19. Strick TR, Allemand JF, Bensimon D, Bensimon A, and Croquette V. The Elasticity of a Single Supercoiled DNA Molecule. Science 1996; 271:1835–7. DOI: 10.1126/science.271.5257.1835. eprint: https://science.sciencemag.org/content/271/5257/1835.full.pdf. Available from: https://science.sciencemag.org/content/271/5257/1835

20. Adhikari AS, Chai J, and Dunn AR. Mechanical Load Induces a 100-Fold Increase in the Rate of Collagen Proteolysis by MMP-1. Journal of the American Chemical Society 2011 Feb; 133:1686–9. DOI: 10.1021/ja109972p. Available from: https://doi.org/10.1021/ja109972p

21. Nimpf S, Nordmann GC, Kagerbauer D, Malkemper EP, Landler L, Papadaki-Anastasopoulou A, Ushakova L, Wenninger-Weinzierl A, Novatchkova M, Vincent P, Lendl T, Colombini M, Mason MJ, and Keays DA. A Putative Mechanism for Magnetoreception by Electromagnetic Induction in the Pigeon Inner Ear. Current Biology 2019; 29:4052–4059.e4. DOI: 10.1016/j.cub.2019.09.048

22. Massart R, Dubois E, Cabuil V, and Hasmonay E. Preparation and properties of monodisperse magnetic fluids. Journal of Magnetism and Magnetic Materials 1995; 149:1–5. DOI: 10.1016/0304-8853(95)00316-9

23. Schuknecht HF and Montandon P. Pathology of the ear in pneumococcal meningitis. Archiv für klinische und experimentelle Ohren-, Nasen-und Kehlkopfheilkunde 1970; 195:207–25

24. Riley BB and Moorman SJ. Development of utricular otoliths, but not saccular otoliths, is necessary for vestibular function and survival in zebrafish. Journal of Neurobiology 2000 Jun; 43:329–37. DOI: 10.1002/1097-4695(20000615)43:4<329::AID-NEU2>3.0.CO;2-H

25. Bagnall MW and McLean DL. Modular organization of axial microcircuits in zebrafish. Science 2014; 343:197–200. DOI: 10.1126/science.1245629

26. Roberts R, Elsner J, and Bagnall MW. Delayed Otolith Development Does Not Impair Vestibular Circuit Formation in Zebrafish. JARO - Journal of the Association for Research in Otolaryngology 2017; 18:415–25. DOI: 10.1007/s10162-017-0617-9

27. Hubbard JM, Böhm UL, Prendergast A, Tseng PEB, Newman M, Stokes C, and Wyart C. Intraspinal Sensory Neurons Provide Powerful Inhibition to Motor Circuits Ensuring Postural Control during Locomotion. Current Biology 2016; 26:2841–53. DOI: 10.1016/j.cub.2016.08.026

28. Assad JA, Shepherd GM, and Corey DP. Tip-link integrity and mechanical transduction in vertebrate hair cells. Neuron 1991; 7:985–94. DOI: 10.1016/0896-6273(91)90343-X

29. Zhao YD, Yamoah EN, and Gillespie PG. Regeneration of broken tip links and restoration of mechanical transduction in hair cells. Proceedings of the National Academy of Sciences of the United States of America 1996 Dec; 93:15469–74. DOI: 10.1073/pnas.93.26.15469. Available from: /pmc/articles/PMC26428/%20/pmc/articles/PMC26428/?report=abstract%20https://www.ncbi.nlm.nih.gov/pmc/articles/PMC26428/

30. Köster RW and Fraser SE. Tracing transgene expression in living zebrafish embryos. Developmental Biology 2001 May; 233:329–46. DOI: 10.1006/dbio.2001.0242

31. Randlett O, Wee CL, Naumann EA, Nnaemeka O, Schoppik D, Fitzgerald JE, Portugues R, Lacoste AMB, Riegler C, Engert F, and Schier AF. Whole-brain activity mapping onto a zebrafish brain atlas. Nature methods 2015; 12:1039–46. DOI: 10.1038/nmeth.3581

32. Harris Ja, Cheng AG, Cunningham LL, MacDonald G, Raible DW, and Rubel EW. Neomycin-induced hair cell death and rapid regeneration in the lateral line of zebrafish (Danio rerio). Journal of the Association for Research in Otolaryngology : JARO 2003 Jun; 4:219–34. DOI: 10.1007/s10162-002-3022-x. Available from: http://www.pubmedcentral.nih.gov/articlerender.fcgi?artid=3202713&tool=pmcentrez&rendertype=abstract

33. Cotanche DA. Regeneration of hair cell stereociliary bundles in the chick cochlea following severe acoustic trauma. Hearing research 1987; 30:181–95

34. Girod DA, Duckert LG, and Rubel EW. Possible precursors of regenerated hair cells in the avian cochlea following acoustic trauma. Hearing research 1989; 42:175–94

35. Jones JE and Corwin JT. Regeneration of sensory cells after laser ablation in the lateral line system: hair cell lineage and macrophage behavior revealed by time-lapse video microscopy. eng. The Journal of neuroscience : the official journal of the Society for Neuroscience 1996 Jan; 16:649–62. DOI: 10.1523/JNEUROSCI.16-02-00649.1996

36. Jimenez E, Slevin CC, Colón-Cruz L, and Burgess SM. Vestibular and Auditory Hair Cell Regeneration Following Targeted Ablation of Hair Cells With Diphtheria Toxin in Zebrafish. Frontiers in Cellular Neuroscience 2021; 15:721950. DOI: 10.3389/fncel.2021.721950

37. Lambert FM, Beck JC, Baker R, and Straka H. Semicircular Canal Size Determines the Developmental Onset of Angular Vestibuloocular Reflexes in Larval Xenopus. Journal of Neuroscience 2008; 28:8086–95. DOI: 10.1523/jneurosci.1288-08.2008

38. Ehrlich DE and Schoppik D. A primal role for the vestibular sense in the development of coordinated locomotion. eLife 2019 Oct; 8. DOI: 10.7554/eLife.45839

39. Pozo Ad, Manuel R, Gonzalez ABI, Koning HK, Habicher J, Zhang H, Allalou A, Kullander K, and Boije H. Behavioral Characterization of dmrt3a Mutant Zebrafish Reveals Crucial Aspects of Vertebrate Locomotion through Phenotypes Related to Acceleration. eNeuro 2020; 7:ENEURO.0047–20.2020. DOI: 10.1523/eneuro.0047-20.2020

40. Malinvaud D, Vassias I, Reichenberger I, Rossert C, and Straka H. Functional Organization of Vestibular Commissural Connections in Frog. Journal of Neuroscience 2010; 30:3310–25. DOI: 10.1523/jneurosci.5318-09.2010

41. Highstein SM, Goldberg JM, Moschovakis AK, and Fernandez C. Inputs from regularly and irregularly discharging vestibular nerve afferents to secondary neurons in the vestibular nuclei of the squirrel monkey. II. Correlation with output pathways of secondary neurons. Journal of Neurophysiology 1987; 58:719–38. DOI: 10.1152/jn.1987.58.4.719

42. Straka H and Baker R. Vestibular blueprint in early vertebrates. Frontiers in Neural Circuits 2013; 7:1–9. DOI: 10.3389/fncir.2013.00182. Available from: http://journal.frontiersin.org/article/10.3389/fncir.2013.00182/abstract

43. Uchino Y, Sato H, Zakir M, Kushiro K, Imagawa M, Ogawa Y, Ono S, Meng H, Zhang X, Katsuta M, Isu N, and Wilson VJ. Commissural effects in the otolith system. Experimental Brain Research 2001; 137:421–30. DOI: 10.1007/s002210000611

44. Vladimirov N, Mu Y, Kawashima T, Bennett DV, Yang CT, Looger LL, Keller PJ, Freeman J, and Ahrens MB. Light-sheet functional imaging in fictively behaving zebrafish. English. Nature methods 2014; 11:883–4. DOI: 10.1038/nmeth.3040

45. Gallois B and Candelier R. FastTrack: An open-source software for tracking varying numbers of deformable objects. PLoS Computational Biology 2021; 17:e1008697. DOI: 10.1371/journal.pcbi.1008697. eprint: 2011.06837

46. Tarantino N, Tinevez JY, Crowell EF, Boisson B, Henriques R, Mhlanga M, Agou F, Israël A, and Laplantine E. TNF and IL-1 exhibit distinct ubiquitin requirements for inducing NEMO–IKK supramolecular structures. The Journal of Cell Biology 2014; 204:231–45. DOI: 10.1083/jcb.201307172

Supplementary Information

Supplementary figures

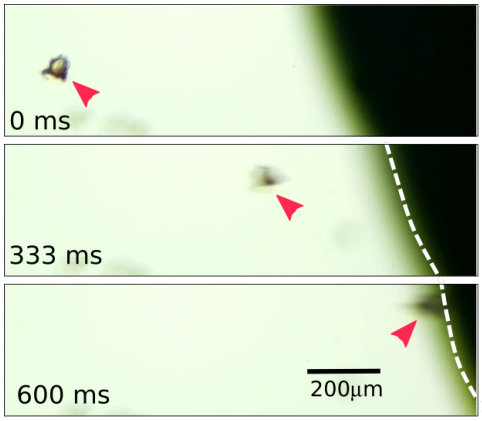

Figure S1: Image sequence of the dissected otolith (red arrowheads) with attached magnetic nanoparticles being attracted by a magnet (d = 5 mm) over time (dashed line indicates the magnet's edge).

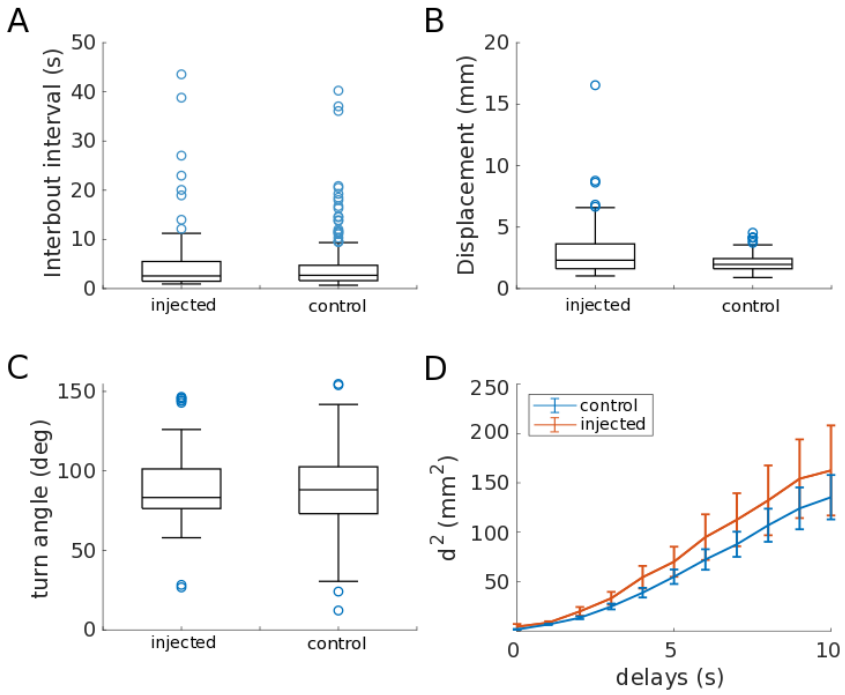

Figure S2: Effect of ferrofluid injection on swimming behavior. **(A-C)** Boxplots showing: **(A)** the distribution of the inter-bout interval, which is the time in seconds elapsed between two consecutive swimming events, **(B)** the mean displacement after a swim bout in mm, and **(C)** the turn angle in degrees. **(D)** Plot showing the mean of the mean square distance for 10 different time delay. The results were obtained by tracking two different batches of injected and non-injected fish. The fish were filmed swimming freely during 1 h (75 fps). P-values : ib-interval p = 0.846, displacement p = 0.00077, turn angle p = 0.366. N = 6 injected fish, 11 control non-injected fish.

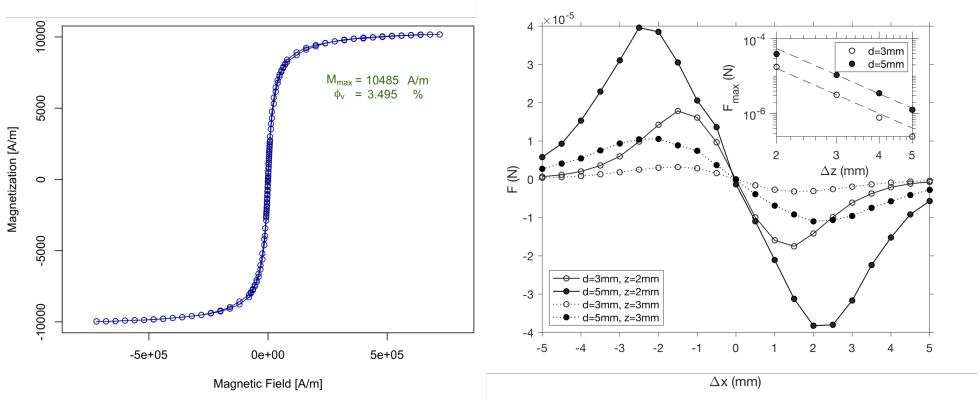

Figure S3: Left: Magnetization of the ferrofluid as a function of the magnetic field intensity (H). In vacuum, magnetic field intensity and magnetic flux density are linked by $\vec{B} = \mu_0 \vec{H}$. Right: Non-normalized simulation results from Figure 3.

Conclusions and perspectives

5.1 Summary

As discussed in the previous chapters, circuits underlying postural control rely on specific connectivity to process vestibular, visual and somatosensory signals to appropriate motor outputs. The focus of my work was not the interaction and integration of the different sensory modalities, but rather to study the role of the vestibular system in postural control and describe vestibular-evoked behaviors that sub-serve balance, using the model organism of the zebrafish larva.

One important advantage of the zebrafish larva is that it represents a simpler model to study the vestibular system. The semicircular canals are not yet functional between 5-7 dpf [59], and only utricular otoliths are responsible for detecting vestibular stimuli [23], meaning that we can stimulate the whole functional vestibular circuits of the larva and study them.

In this animal, research on vestibular-driven postural circuits has lagged behind that of vestibulo-ocular gaze-stabilizing circuits. Compared to the VOR, which relies on a set of six extra-ocular muscles [68], the mechanisms that operate in the spinal cord are richer and more complex, usually involving larger sets of muscles. However, these two kind of reflexes likely share neural substrates [128], and VOR develops contemporaneously with consistent postural orientation [71].

Being aware of the lack of research regarding the mechanisms of postural control, this work was dedicated to describe the different postural responses elicited by vestibular input and to elucidate the neural circuit involved in these behaviors. This thesis was divided in three chapters that aimed to study postural control and the vestibular system of the zebrafish larva at three levels: (i) behavioral, (ii) neuronal

and (iii) brain-wide.

In the first part of the results, we described a set of behaviors that are elicited by roll stimulus. Step-wise stimulation evoked a tonic pivoting tail deflection, opposite to the ear-down side (contraversive). This response is comparable to those obtained by Thiele et al. [80] and Favre-Bulle et al. [2] by fictive stimulation. Here, we showed that natural vestibular stimulation elicits this behavior. Moreover, we quantified the corresponding body angle rotation, finding that angles larger than 20° evoked swim bouts.

In the second part, we described the brain response to sinusoidal-roll vestibular stimulus by using a set of different transgenic lines. This method allowed us to study populations such as the vestibulospinal neurons, the reticulospinal neurons, the tangential nucleus and the primary motor neurons. To perform functional calcium imaging, we used the rotating light sheet microscope—developed previously in the lab by Migault et al. [3].

We also backfilled the pectoral fins to retrogradely label motor-neurons. This allowed us to identify two ipsilateral-activated neuronal clutches in the rostral spinal cord.

Finally, we impaired mechanotransduction in the left utricle to disentangle the contribution of both ears during natural stimulation. The results described in this chapter are still preliminary, but provide a first step towards elucidating the neural circuits underlying postural control in the zebrafish larva.

In the third chapter, we combined magnetic stimulation of the utricular otoliths with light-sheet calcium imaging to produce a brain-wide map of vestibular responses in the larval zebrafish similar to that reported by Migault et al. [3] and Favre-Bulle et al. [93].

The aim of magnetic stimulation via ferrofluid injections was to stimulate the vestibular system without moving the animal, to make a set-up compatible with optogenetic, electrophysiology and microscopy techniques that may require head-fixed animals. During my PhD work, I developed a new method to stimulate the utricle via magnetic forces, proving that this technique works using a set of different experiments. By this approach, we obtained VOR movements, comparable to those

evoked by natural vestibular stimulation [71, 3]. However, matching the magnetic force exerted to real roll angle was not easy, since fish response is highly variable, even in natural stimulation.

The next step will be to couple this set-up with other techniques that allow neuronal manipulation, to dissect in detail the circuits responsible for postural control. For example, an interesting experiment would be to exert magnetic forces in the utricle while inhibiting optogenetically vestibulo-spinal tracts. This kind of protocol would serve to unveil how vestibular input coordinates the motor response in the trunk.

In addition, the method developed here allowed us to stimulate only one or both otoliths, enabling to separate individual utricle contribution to the global brain response, unlike traditional experiments, in which otoliths need to be removed to achieve unilateral stimulation [71] or injected with hair cell ablating agents [91].

5.2 Future perspectives

The pivoting tail movement elicited by vestibular stimulation was also elicited by a visual stimulus, suggesting that multisensory integration processes underlay this behavior. We believe that studying the neural substrates of this behavior may shed lights on multi-sensory-motor integration mechanisms.

While fish swim, motor action and sensory perception couple and participate in a sensory-motor feedback loop. For example, during forward swimming, fish receive translational vestibular input generated by inertia. This input is lost in head-restrained animals. The magnetic stimulation method developed here could be used in virtual reality environments to make them more realistic, by creating a closed feedback loop in the vestibular system of head-fixed animals. This will help to resolve questions such as: are larvae learning better when both systems (visual and vestibular) are engaged?

This system is easy to implement and low-cost, making it compatible with neuronal manipulating techniques that require restrained animals in other setups. The small unit used for magnet movement can be easily implemented as an add-on onto any microscope that is already working.

The ontogeny of the vestibular response has been already studied in the VOR.

Instead, how fish ameliorate their balance in time and the dynamics of this process is not fully understood. By assessing the roll ratio during startling response, we showed that it decreases from 0.5 to almost 0 between 5 and 7 dpf, indicating an improvement in postural control. It would be interesting to study how the dynamics of the vestibular neural network evolves after swim onset: is it just learning, or are anatomical/morphological processes involved?

5.3 Main conclusions

- We described a behavioral repertoire for different vestibular stimulation, we showed that vestibular stimulation evokes a spinal reflex that leads to contraversive tail movements.
- Vestibular response acts in two different mechanisms: 1) for low amplitude rolling, the fish responds with small pivoting tail movements that seem like a passive reflex, and 2) for higher rolling angles, when the pivoting reflex saturates, the fish perform high frequency swim bouts and tail flips to counterbalance.
- The pivoting tail deflection evoked by step-wise vestibular stimulation was evoked also with less amplitude by a visual whole-field rotating around the fish, suggesting that multisensory integration underlies this behavior.
- One ear is sufficient for VSR and VOR in rolling condition, and utricles are necessary for VSR response in zebrafish larva.
- We assessed single-utricle (unilateral) stimulation by two different means. The overall elicited neural response was similar to that of the bilaterally stimulated fish. Our results confirm that commissural fibers communicate with vestibular nuclei, most likely by disinhibition mechanisms.
- Finally, we described the activity of the reticulospinal population and primary motor neurons in response to sinusoidal-roll stimulus.

Bibliography

[1] D. E. Ehrlich & D. Schoppik; "Control of Movement Initiation Underlies the Development of Balance"; Current Biology **27**, pp. 334–344 (2017). ISSN 09609822. iv, 15, 19, 25, 39, 44

[2] I. A. Favre-Bulle, A. B. Stilgoe, H. Rubinsztein-Dunlop & E. K. Scott; "Optical trapping of otoliths drives vestibular behaviours in larval zebrafish"; Nature Communications **8** (2017). ISSN 20411723. http://dx.doi.org/10.1038/s41467-017-00713-2. v, 15, 20, 22, 39, 42, 43, 104

[3] G. Migault, T. L. van der Plas, H. Trentesaux, T. Panier, R. Candelier, R. Proville, B. Englitz, G. Debrégeas & V. Bormuth; "Whole-Brain Calcium Imaging during Physiological Vestibular Stimulation in Larval Zebrafish"; Current Biology (2018). ISSN 09609822. vi, 20, 22, 46, 47, 48, 50, 63, 65, 104, 105

[4] T. G. Deliagina, P. V. Zelenin, I. N. Beloozerova & G. N. Orlovsky; "Nervous mechanisms controlling body posture"; Physiology and Behavior **92**, pp. 148–154 (2007). ISSN 00319384. 1, 2

[5] T. G. Deliagina, G. N. Orlovsky, P. V. Zelenin & I. N. Beloozerova; "Neural bases of postural control"; Physiology **21**, pp. 216–225 (2006). ISSN 15489213. 1, 2, 3

[6] J. Massion; "Postural control systems in developmental perspective"; Neuroscience and Biobehavioral Reviews **22**, pp. 465–472 (1998). ISSN 01497634. 1

[7] L. Vinay, F. F. Ben-Mabrouk, F. Brocard, J.-X. Clarac, E. Pearlstein & J.-F. Pflieger; "Perinatal Development of the Motor Systems Involved in Postural Control"; NEURAL PLASTICITY **12** (2005). 1

[8] M. L. Shik; "Control of walking and running by means of electrical stimulation of the midbrain"; Biophysics **11**, pp. 659–666 (1966). 1

[9] P. E. Musienko, O. V. Gorskii, V. A. Kilimnik, I. B. Kozlovskaya, G. Courtine, V. R. Edgerton & Y. P. Gerasimenko; "Regulation of Posture and Locomotion in Decerebrate and Spinal Animals"; Neuroscience and Behavioral Physiology **45**, pp. 229–237 (2015). ISSN 1573-899X. https://doi.org/10.1007/s11055-015-0062-3. 1

[10] T. Iwahara, Y. Atsuta, E. Garcia-Rill & R. Skinner; "Spinal cord stimulation-induced locomotion in the adult cat"; Brain research bulletin **28**, pp. 99–105 (1992). 1

[11] F. Horak & J. Macpherson; "Postural orientation and equilibrium. In: Shepard J, Rowell I, eds. Handbook of Physiology." (1996). 2

[12] F. B. Horak; "Postural orientation and equilibrium: What do we need to know about neural control of balance to prevent falls?" Age and Ageing **35**, pp. 7–11 (2006). ISSN 00020729. 2

[13] F. B. Horak & J. M. Macpherson; *Postural Orientation and Equilibrium*; pp. 255–292 (John Wiley & Sons, Ltd) (2011); ISBN 9780470650714. https://onlinelibrary.wiley.com/doi/abs/10.1002/cphy.cp120107; https://onlinelibrary.wiley.com/doi/pdf/10.1002/cphy.cp120107. 2, 4

[14] R. Magnus; *Körperstellung, Experimentell-Physiologische Untersuchungen über die Einzelnen bei der Körperstellung in Tätigkeit Tretenden Reflexe, über ihr Zusammenwirken und ihre Störungen* (Springer, Berlin, Heidelberg) (1924). 2

[15] G. M. Jones & J. H. Milsum; "Spatial and dynamic aspects of visual fixation." IEEE transactions on bio-medical engineering **12 2**, pp. 54–62 (1965). 2

[16] V. J. Wilson & B. W. Peterson; "Peripheral and central substrates of vestibulospinal reflexes"; Physiological Reviews **58**, pp. 80–105 (1978). ISSN 00319333. 2, 14

[17] E. von HOLST; "Ueber den Lichtruckenreflex bei Fischen"; Pubbl. Statz. zool. Napoli **15**, pp. 143–158 (1935). 2

[18] R. S. Snell; *Clinical neuroanatomy* (Lippincott Williams & Wilkins) (2010). 3

[19] I. D. Loram; "Postural Control and Sensorimotor Integration"; in "Grieve's Modern Muscoskeletal Physiotherapy, 4th Edition," (2015). https://evolve.elsevier.com/cs/product/9780702051524?role=student. 4

[20] P. F. Smith & I. S. Curthoys; "Mechanisms of recovery following unilateral labyrinthectomy: a review"; Brain Research Reviews **14**, pp. 155–180 (1989). ISSN 01650173. 4

[21] N. Vibert, A. Bantikyan, A. Babalian, M. Serafin, M. Mühlethaler & P. P. Vidal; "Post-lesional plasticity in the central nervous system of the guinea-pig: A 'top-down' adaptation process?" Neuroscience **94**, pp. 1–5 (1999). ISSN 03064522. 4

[22] P. Flourens; *Expériences sur le système nerveux* (Crevot, Paris) (1825). 5

[23] K. von Frisch & H. Stetter; "Untersuchungen über den Sitz des Gehorsinnes bei der Eiritze"; Zeitschrift für vergleichende Physiologie **17**, p. 686–801 (1932). 5, 10, 103

[24] C. M. Rovainen; "Electrophysiology of vestibulospinal and vestibuloreticulospinal systems in lampreys"; Journal of Neurophysiology **42**, pp. 745–766 (1979). ISSN 00223077. 5

[25] N. Dieringer & W. Precht; "Mechanisms of compensation for vestibular deficits in the frog"; Experimental Brain Research **36**, pp. 311–328 (1979). ISSN 1432-1106. https://doi.org/10.1007/BF00238914. 5

[26] P. Flourens; "Expériences sur les canaux semi-circulaires de l'oreille, dans les mammifères"; Mémoires de l'Académie des sciences de l'Institut de France **9**, pp. 467–477 (1828). 5

[27] W. Graf & F. Klam; "Le système vestibulaire : anatomie fonctionnelle et comparée, évolution et développement"; Comptes Rendus - Palevol **5**, pp. 637–655 (2006). ISSN 16310683. 5, 11

[28] H. Straka & R. Baker; "Vestibular blueprint in early vertebrates"; Frontiers in Neural Circuits **7**, pp. 1–9 (2013). ISSN 1662-5110. http://journal.frontiersin.org/article/10.3389/fncir.2013.00182/abstract. 5, 10, 12

[29] H. Straka, A. Zwergal & K. E. Cullen; "Vestibular animal models: contributions to understanding physiology and disease"; Journal of Neurology **263**, pp. 10–23 (2016). ISSN 14321459. 5

[30] N. Bussières & R. Dubuc; "Phasic modulation of vestibulospinal neuron activity during fictive locomotion in lampreys"; Brain Research **575**, pp. 174–179 (1992). ISSN 00068993. 5

[31] T. G. Deliagina & P. Fagerstedt; "Responses of Reticulospinal Neurons in Intact Lamprey to Vestibular and Visual Inputs"; Journal of Neurophysiology **83**, pp. 864–878 (2000). https://doi.org/10.1152/jn.2000.83.2.864; pMID: 10669500; https://doi.org/10.1152/jn.2000.83.2.864. 5

[32] G. Streisinger, C. Walker, N. Dower, D. Knauber & F. Singer; "Production of clones of homozygous diploid zebra fish (Brachydanio rerio)"; Nature **291**, pp. 293–296 (1981). ISSN 1476-4687. https://doi.org/10.1038/291293a0. 6

[33] C. Houart; *Zebrafish as an Experimental Organism* (John Wiley & Sons, Ltd) (2001). 6

[34] C. B. Kimmel, J. Patterson & R. O. Kimmel; "The development and behavioral characteristics of the startle response in the zebra fish"; Developmental Psychobiology **7**, pp. 47–60 (1974). ISSN 10982302. 6

[35] R. Willemsen, S. v. Padje, J. C. van Swieten & B. A. Oostra; *Zebrafish (Danio rerio) as a Model Organism for Dementia*; pp. 255–269 (Humana Press, Totowa, NJ) (2011); ISBN 978-1-60761-898-0. https://doi.org/10.1007/978-1-60761-898-0_14. 6

[36] A. M. Stewart, O. Braubach, J. Spitsbergen, R. Gerlai & A. V. Kalueff; "Zebrafish models for translational neuroscience research: from tank to bedside"; Trends in neurosciences **37**, pp. 264–278 (2014). ISSN 1878-108X. https://pubmed.ncbi.nlm.nih.gov/24726051https://www.ncbi.nlm.nih.gov/pmc/articles/PMC4039217/. 6, 7

[37] G. Sumbre & G. G. de Polavieja; *The world according to zebrafish: how neural circuits generate behavior*; volume 8 (2014); ISBN 9782889193288. http://journal.frontiersin.org/article/10.3389/fncir.2014.00091/abstract. 6, 16

[38] R. Friedrich, C. Genoud & A. Wanner; "Analyzing the structure and function of neuronal circuits in zebrafish"; Frontiers in Neural Circuits **7** (2013). ISSN 1662-5110. https://www.frontiersin.org/article/10.3389/fncir.2013.00071. 6, 16

[39] A. V. Kalueff, M. Gebhardt, A. M. Stewart, J. M. Cachat, M. Brimmer, J. S. Chawla, C. Craddock, E. J. Kyzar, A. Roth, S. Landsman, S. Gaikwad, K. Robinson, E. Baatrup, K. Tierney, A. Shamchuk, W. Norton, N. Miller, T. Nicolson, O. Braubach, C. P. Gilman, J. Pittman, D. B. Rosemberg, R. Gerlai, D. Echevarria, E. Lamb, S. C. Neuhauss, W. Weng, L. Bally-Cuif, Schneider & H. the Zebrafish Neuroscience Research Consortium (ZNRC); "Towards a Comprehensive Catalog of Zebrafish Behavior 1.0 and Beyond"; Zebrafish **10**, pp. 70–86 (2013). https://doi.org/10.1089/zeb.2012.0861; pMID: 23590400; https://doi.org/10.1089/zeb.2012.0861. 7

[40] K. Watt, A. Achilleos, C. Neben, A. Merrill & P. Trainor; "The Roles of RNA Polymerase I and III Subunits Polr1c and Polr1d in Craniofacial Development and in Zebrafish Models of Treacher Collins Syndrome"; PLOS Genetics **12**, p. e1006187 (2016). 8

[41] P. Antinucci & R. Hindges; "A crystal-clear zebrafish for in vivo imaging"; Scientific Reports **6**, pp. 1–10 (2016). ISSN 20452322. http://dx.doi.org/10.1038/srep29490; NIHMS150003. 8

[42] T. Panier, S. A. Romano, R. Olive, T. Pietri, G. Sumbre, R. Candelier & G. Debrégeas; "Fast functional imaging of multiple brain regions in intact zebrafish larvae using Selective Plane Illumination Microscopy." Frontiers in neural circuits **7**, p. 65 (2013). 7, 8, 18, 45

[43] K. Kawakami, A. Shima & N. Kawakami; "Identification of a functional transposase of the Tol2 element, an Ac-like element from the Japanese medaka fish, and its transposition in the zebrafish germ lineage"; Proceedings of the National Academy of Sciences **97**, pp. 11403–11408 (2000). https://www.pnas.org/doi/abs/10.1073/pnas.97.21.11403; https://www.pnas.org/doi/pdf/10.1073/pnas.97.21.11403. 7

[44] J. A. Lister, C. P. Robertson, T. Lepage, S. L. Johnson & D. W. Raible; "nacre encodes a zebrafish microphthalmia-related protein that regulates neural-crest-derived pigment cell fate"; Development **126**, pp. 3757–3767 (1999). ISSN 09501991. 7, 47

[45] J. Nakai, M. Ohkura & K. Imoto; "A high signal-to-noise Ca2+ probe composed of a single green fluorescent protein"; Nature Biotechnology **19**, pp. 137–141 (2001). ISSN 1546-1696. https://doi.org/10.1038/84397. 7

[46] M. B. Ahrens, M. B. Orger, D. N. Robson, J. M. Li & P. J. Keller; "Whole-brain functional imaging at cellular resolution using light-sheet microscopy." Nature methods **10**, pp. 413 – 420 (2013). 7, 18, 45

[47] F. Ahmad, L. P. Noldus, R. A. Tegelenbosch & M. K. Richardson; "Zebrafish embryos and larvae in behavioural assays"; Behaviour **149**, p. 1241 (2012). 7

[48] A. Scarpa; *Anatomicae disquisitiones de auditu et olfacto* (Milan, Josephi Galeatti) (1789). 9

[49] S. RINKWITZ, E. BOBER & R. BAKER; "Development of the Vertebrate Inner Ear"; Annals of the New York Academy of Sciences **942**, pp. 1–14 (2001). https://nyaspubs.onlinelibrary.wiley.com/doi/abs/10.1111/j.1749-6632.2001.tb03730.x; https://nyaspubs.onlinelibrary.wiley.com/doi/pdf/10.1111/j.1749-6632.2001.tb03730.x. 9

[50] B. FRITZSCH; "Evolution of the vestibulo-ocular system"; Otolaryngology - Head and Neck Surgery (1998). ISSN 01945998. 9, 11

[51] V. J. WILSON; "Physiological Pathways Through the Vestibular Nuclei"; pp. 27–81 (Academic Press) (1972). https://www.sciencedirect.com/science/article/pii/S0074774208603281. 9

[52] L. ABBAS & T. T. WHITFIELD; *The zebrafish inner ear*; volume 29 (Elsevier) (2010). http://dx.doi.org/10.1016/S1546-5098(10)02904-3. 10, 12

[53] M. INOUE, M. TANIMOTO & Y. ODA; "The role of ear stone size in hair cell acoustic sensory transduction"; Scientific Reports **3**, pp. 1–5 (2013). ISSN 20452322. 10

[54] R. R. FAY & A. N. POPPER; "Comparative hearing: Fish and amphibians." in "Springer Handbook of Auditory Research," , volume 11 (Springer, New York). 10

[55] B. B. MILLIMAKI, E. M. SWEET, M. S. DHASON & B. B. RILEY; "Zebrafish atoh1 genes: classic proneural activity in the inner ear and regulation by Fgf and Notch"; Development **134**, pp. 295–305 (2007). ISSN 0950-1991. https://doi.org/10.1242/dev.02734; https://journals.biologists.com/dev/article-pdf/134/2/295/1527179/295.pdf. 10

[56] C. B. KIMMEL, W. W. BALLARD, S. R. KIMMEL, B. ULLMANN & T. F. SCHILLING; "Stages of embryonic development of the zebrafish." Developmental dynamics : an official publication of the American Association of Anatomists **203**, pp. 253–310 (1995). ISSN 1058-8388. http://www.ncbi.nlm.nih.gov/pubmed/8589427. 10

[57] C. Haddon & J. Lewis; "Early ear develpment in the embryos of the zebrafish, Danio rerio"; The Journal of Comparative Neurology **365**, pp. 113–128 (1996). 10

[58] C. Platt; "Zebrafish inner ear sensory surfaces are similar to those in goldfish"; Hearing Research **65**, pp. 133–140 (1993). ISSN 03785955. 10

[59] J. C. Beck, E. Gilland, D. W. Tank & R. Baker; "Quantifying the ontogeny of optokinetic and vestibuloocular behaviors in zebrafish, medaka, and goldfish"; Journal of Neurophysiology **92**, pp. 3546–3561 (2004). ISSN 00223077. https://www.physiology.org/doi/10.1152/jn.00311.2004. 10, 14, 25, 64, 103

[60] F. M. Lambert, J. C. Beck, R. Baker & H. Straka; "Semicircular Canal Size Determines the Developmental Onset of Angular Vestibuloocular Reflexes in Larval Xenopus"; Journal of Neuroscience **28**, pp. 8086–8095 (2008). ISSN 0270-6474. https://www.jneurosci.org/content/28/32/8086; https://www.jneurosci.org/content/28/32/8086.full.pdf. 10

[61] J. C. Beck, E. Gilland, D. W. Tank & R. Baker; "Quantifying the Ontogeny of Optokinetic and Vestibuloocular Behaviors in Zebrafish, Medaka, and Goldfish"; Journal of Neurophysiology **92**, pp. 3546–3561 (2004). https://doi.org/10.1152/jn.00311.2004; pMID: 15269231; https://doi.org/10.1152/jn.00311.2004. 10

[62] P. K. Von Frisch; "The Sense of Hearing in Fish*"; Technical report (1938). 10, 25

[63] W. Mo, F. Chen, A. Nechiporuk & T. Nicolson; "Quantification of vestibular-induced eye movements in zebrafish larvae." BMC neuroscience **11**, p. 110 (2010). ISSN 1471-2202. 10, 14, 19, 25

[64] M. W. Bagnall & D. L. McLean; "Modular organization of axial microcircuits in zebrafish"; Science **343**, pp. 197–200 (2014). ISSN 10959203. 12, 15, 25, 41

[65] C. Haddon, C. Mowbray, T. Whitfield, D. Jones, S. Gschmeissner & J. Lewis; "Hair cells without supporting cells: Further studies in the ear of the zebrafish mind bomb mutant"; Journal of Neurocytology **28**, pp. 837–850 (1999). ISSN 03004864. 13, 64

[66] M. M. Bever & D. M. Fekete; "Atlas of the developing inner ear in zebrafish"; Developmental Dynamics **223**, pp. 536–543 (2002). ISSN 10588388. 14

[67] J. Szentagothai; "Pathway and synaptic articulation patterns connecting vestibular receptors and oculomotor nuclei in the oculomotor system"; Ed. M. Bender. Harper & Row, New-York (1964). 12

[68] H. Straka, B. Fritzsch & J. C. Glover; "Connecting ears to eye muscles: Evolution of a 'Simple' reflex arc"; Brain, Behavior and Evolution **83**, pp. 162–175 (2014). ISSN 00068977. 12, 14, 45, 103

[69] J. Szentágothai; "The elementary vestibulo-ocular reflex arc"; Journal of neurophysiology **13**, pp. 395–407 (1950). 12, 45

[70] B. B. Riley & S. J. Moorman; "Development of utricular otoliths, but not saccular otoliths, is necessary for vestibular function and survival in zebrafish"; Journal of Neurobiology **43**, pp. 329–337 (2000). ISSN 1097-4695. 12, 15, 25

[71] I. H. Bianco, L. H. Ma, D. Schoppik, D. N. Robson, M. B. Orger, J. C. Beck, J. M. Li, A. F. Schier, F. Engert & R. Baker; "The tangential nucleus controls a gravito-inertial vestibulo-ocular reflex"; Current Biology **22**, pp. 1285–1295 (2012). ISSN 09609822. 14, 16, 22, 25, 41, 46, 65, 103, 105

[72] H. SUWA, E. GILLAND & R. BAKER; "Otolith Ocular Reflex Function of the Tangential Nucleus in Teleost Fish"; Annals of the New York Academy of Sciences **871**, pp. 1–14 (1999). https://nyaspubs.onlinelibrary.wiley.com/doi/abs/10.1111/j.1749-6632.1999.tb09171.x; https://nyaspubs.onlinelibrary.wiley.com/doi/pdf/10.1111/j.1749-6632.1999.tb09171.x. 14

[73] S. Cajal; "Sur un noyau spécial du nerf vestibulaire des poissons et des oiseaux"; Trabajos del Laboratorio de Investigaciones Biologicas de la Universidad de Madrid **6**, p. 1–20 (1908)https://books.google.fr/books?id=YlT6ygEACAAJ. 14

[74] H. Straka & R. Baker; "Vestibular System Anatomy and Physiology"; p. 244–251 (Academic press) (2011). 14

[75] T. D. M. Roberts; *Neurophysiology of Postural Mechanisms* (1978); ISBN 9780608180090. 14

[76] G. R. Barnes; "Vestibular control of oculomotor and postural mechanisms"; Clinical Physics and Physiological Measurement **1**, pp. 3–40 (1980). https://doi.org/10.1088/0143-0815/1/1/001. 14

[77] P. W. Webb & D. Weihs; "Stability versus maneuvering: Challenges for stability during swimming by fishes"; Integrative and Comparative Biology **55**, pp. 753–764 (2015). ISSN 15577023. https://academic.oup.com/icb/article/55/4/753/635906. 15, 63

[78] T. Deliagina, F. Ullen, M. Gonzalez, H. H. Ehrsson, G. Orlovsky & S. Grillner; "Initiation of locomotion by lateral line photoreceptors in lamprey: Behavioural and neurophysiological studies (Journal of Experimental Biology 198 (2581-2591))"; Journal of Experimental Biology **198**, pp. 2581–2591 (1995). ISSN 00220949. 15

[79] M. W. Bagnall & D. Schoppik; "Development of vestibular behaviors in zebrafish"; Current Opinion in Neurobiology **53**, pp. 83–89 (2018). ISSN 09594388. https://linkinghub.elsevier.com/retrieve/pii/S0959438818300850. 15, 17

[80] T. R. Thiele, J. C. Donovan & H. Baier; "Descending Control of Swim Posture by a Midbrain Nucleus in Zebrafish"; Neuron **83**, pp. 679–691 (2014). ISSN 10974199. http://dx.doi.org/10.1016/j.neuron.2014.04.018; NIHMS150003. 15, 18, 19, 22, 41, 46, 104

[81] P. J. Keller & M. B. Ahrens; "Visualizing Whole-Brain Activity and Development at the Single-Cell Level Using Light-Sheet Microscopy"; Neuron **85**, pp. 462–483 (2015). ISSN 0896-6273. https://www.sciencedirect.com/science/article/pii/S0896627314011489. 18

[82] W. Zong, R. Wu, M. Li, Y. Hu, Y. Li, J. Li, H. Rong, H. Wu, Y. Xu, Y. Lu, H. Jia, M. Fan, Z. Zhou, Y. Zhang, A. Wang, L. Chen & H. Cheng; "Fast high-resolution miniature two-photon microscopy for brain imaging in freely behaving mice"; Nature Methods **14**, pp. 713–719 (2017). ISSN 1548-7105. https://doi.org/10.1038/nmeth.4305. 18

[83] J. Huisken, J. Swoger, F. Del Bene, J. Wittbrodt & E. H. Stelzer; "Optical sectioning deep inside live embryos by selective plane illumination microscopy"; Science **305**, pp. 1007–1009 (2004). ISSN 00368075. 18

[84] C. Wyart, F. D. Bene, E. Warp, E. K. Scott, D. Trauner, H. Baier & E. Y. Isacoff; "Optogenetic dissection of a behavioural module in the vertebrate spinal cord"; Nature **461**, pp. 407–410 (2009). ISSN 00280836. http://www.nature.com/authors/editorial_policies/license.html#terms. 18, 71

[85] A. Vaziri & V. Emiliani; "Reshaping the optical dimension in optogenetics"; Current Opinion in Neurobiology **22**, pp. 128–137 (2012). ISSN 18736882. http://dx.doi.org/10.1016/j.conb.2011.11.011. 18

[86] M. dal Maschio, J. C. Donovan, T. O. Helmbrecht & H. Baier; "Linking Neurons to Network Function and Behavior by Two-Photon Holographic Optogenetics and Volumetric Imaging"; Neuron **94**, pp. 774–789.e5 (2017). ISSN 10974199. http://dx.doi.org/10.1016/j.neuron.2017.04.034. 18, 71

[87] N. Vladimirov, C. Wang, B. Höckendorf, A. Pujala, M. Tanimoto, Y. Mu, C.-T. Yang, J. D. Wittenbach, J. Freeman, S. Preibisch, M. Koyama, P. J. Keller & M. B. Ahrens; "Brain-wide circuit interrogation at the cellular level guided by online analysis of neuronal func-

tion"; Nature Methods **15**, pp. 1117–1125 (2018). ISSN 1548-7105. https://doi.org/10.1038/s41592-018-0221-x. 18

[88] S. S. Easter & J. N. Gregory Nicola; "and "Encephalization"; Dev Psychobiol **31**, pp. 267–276 (1997). 19, 25

[89] T. Whitfield, M. Granato, F. van Eeden, U. Schach, M. Brand, M. Furutani-Seiki, P. Haffter, M. Hammerschmidt, C. Heisenberg, Y. Jiang, D. Kane, R. Kelsh, M. Mullins, J. Odenthal & C. Nusslein-Volhard; "Mutations affecting development of the zebrafish inner ear and lateral line"; Development **123**, pp. 241–254 (1996). ISSN 0950-1991. https://doi.org/10.1242/dev.123.1.241; https://journals.biologists.com/dev/article-pdf/123/1/241/1130221/241.pdf. 19

[90] M. Granato, F. J. Van Eeden, U. Schach, T. Trowe, M. Brand, M. Furutani-Seiki, P. Haffter, M. Hammerschmidt, C. P. Heisenberg, Y. J. Jiang, D. A. Kane, R. N. Kelsh, M. C. Mullins, J. Odenthal & C. Nüsslein-Volhard; "Genes controlling and mediating locomotion behavior of the zebrafish embryo and larva"; Development **123**, pp. 399–413 (1996). ISSN 0950-1991. https://journals.biologists.com/dev/article/123/1/399/39337/Genes-controlling-and-mediating-locomotion. 19

[91] K. R. Hamling, K. Harmon, M. Greaney, Z. Dobler, Y. Kimura, S.-I. Higashijima & D. Schoppik; "Synaptic Encoding of Vestibular Sensation Regulates Movement Timing and Coordination"; bioRxiv (2021). https://doi.org/10.1101/2021.07.05.451142. 19, 105

[92] Z. Liu, Y. Kimura, S. ichi Higashijima, D. G. Hildebrand, J. L. Morgan & M. W. Bagnall; "Central Vestibular Tuning Arises from Patterned Convergence of Otolith Afferents"; Neuron **108**, pp. 748–762.e4 (2020). ISSN 10974199. 19

[93] I. A. Favre-Bulle, G. Vanwalleghem, M. A. Taylor, H. Rubinsztein-Dunlop & E. K. Scott; "Cellular-Resolution Imaging of Vestibular Process-

ing across the Larval Zebrafish Brain"; Current Biology **28**, pp. 3711–3722.e3 (2018). ISSN 09609822. 20, 63, 65, 104

[94] M. Kasahara & Y. Uchino; "Selective mode of commissural inhibition induced by semicircular canal afferents on secondary vestibular neurones in the cat"; Brain Research **34**, pp. 366–369 (1971). ISSN 00068993. 22, 65

[95] Y. Uchino, H. Sato, M. Zakir, K. Kushiro, M. Imagawa, Y. Ogawa, S. Ono, H. Meng, X. Zhang, M. Katsuta, N. Isu & V. J. Wilson; "Commissural effects in the otolith system"; Experimental Brain Research **137**, pp. 421–430 (2001). ISSN 00144819. 22, 65, 66

[96] H. A. Burgess, S. L. Johnson & M. Granato; "Unidirectional startle responses and disrupted left–right co-ordination of motor behaviors in robo3 mutant zebrafish"; Genes, Brain and Behavior **8**, pp. 500–511 (2009). ISSN 1601-183X. https://onlinelibrary.wiley.com/doi/full/10.1111/j.1601-183X.2009.00499.xhttps://onlinelibrary.wiley.com/doi/abs/10.1111/j.1601-183X.2009.00499.xhttps://onlinelibrary.wiley.com/doi/10.1111/j.1601-183X.2009.00499.x. 25

[97] D. E. Ehrlich & D. Schoppik; "A primal role for the vestibular sense in the development of coordinated locomotion"; eLife **8** (2019). ISSN 2050084X. 25, 63

[98] S. J. Moorman, R. Cordova & S. A. Davies; "A critical period for functional vestibular development in zebrafish"; Developmental dynamics: an official publication of the American Association of Anatomists **223**, pp. 285–291 (2002). 25

[99] L. H. Ma, C. L. Grove & R. Baker; "Development of oculomotor circuitry independent of hox3 genes"; Nature Communications **5**, pp. 1–12 (2014). ISSN 20411723. http://dx.doi.org/10.1038/ncomms5221. 25

[100] M. J. Zimmermann, N. E. Nevala, T. Yoshimatsu, D. Osorio, D. E. Nilsson, P. Berens & T. Baden; "Zebrafish Differentially Process Color

across Visual Space to Match Natural Scenes"; Current Biology **28**, pp. 2018–2032.e5 (2018). ISSN 09609822. https://doi.org/10.1016/j.cub.2018.04.075. 26

[101] H. Trentesaux; *Microscope à nappe laser deux photons rotatif pour l'étude de l'intégration multisensorielle chez la larve de poisson zèbre*; Phd thesis; Sorbonne Université (2021). 28

[102] H. S. Young, L. G. Herbette & V. Skita; "α-Bungarotoxin binding to acetylcholine receptor membranes studied by low angle x-ray diffraction"; Biophysical Journal **85**, pp. 943–953 (2003). ISSN 00063495. 33

[103] K. E. Cullen; "The vestibular system: Multimodal integration and encoding of self-motion for motor control"; Trends in Neurosciences **35**, pp. 185–196 (2012). ISSN 01662236. http://dx.doi.org/10.1016/j.tins.2011.12.001. 33, 43

[104] K. E. Severi, R. Portugues, J. C. Marques, D. M. O'Malley, M. B. Orger & F. Engert; "Neural Control and Modulation of Swimming Speed in the Larval Zebrafish"; Neuron **83**, pp. 692–707 (2014). ISSN 10974199. 36

[105] R. Portugues & F. Engert; "Adaptive locomotor behavior in larval zebrafsh"; Frontiers in Systems Neuroscience (2011). ISSN 16625137. www.frontiersin.org. 36

[106] J. C. Liao & J. R. Fetcho; "Shared versus specialized glycinergic spinal interneurons in axial motor circuits of larval zebrafish"; Journal of Neuroscience **28**, pp. 12982–12992 (2008). ISSN 02706474. 36

[107] R. L. de Nó; "The regulation of eye positions and movements induced by the labyrinth: Chapter I. Tonic labyrinth reflexes on the eye"; The Laryngoscope **42** (1932). 45

[108] R. L. de Nó; "VESTIBULO-OCULAR REFLEX ARC"; Archives of Neurology Psychiatry **30**, pp. 245–291 (1933). ISSN 0096-6754. https://doi.org/10.1001/archneurpsyc.1933.02240140009001. 45

[109] S. Lac, J. L. Raymond, T. J. Sejnowski & S. G. Lisberger; "Learning and Memory in the Vestibulo-Ocular Reflex"; Annual Review of Neuroscience **18**, pp. 409–441 (1995). ISSN 0147-006X. https://doi.org/10.1146/annurev.ne.18.030195.002205. 45

[110] M. B. Orger, A. R. Kampff, K. E. Severi, J. H. Bollmann & F. Engert; "Control of visually guided behavior by distinct populations of spinal projection neurons"; Nature Neuroscience **11**, pp. 327–333 (2008). ISSN 10976256. 46

[111] N. Vladimirov, Y. Mu, T. Kawashima, D. V. Bennett, C.-T. Yang, L. L. Looger, P. J. Keller, J. Freeman & M. B. Ahrens; "Light-sheet functional imaging in fictively behaving zebrafish." Nature methods **11**, pp. 883 – 884 (2014). 47

[112] R. W. Köster & S. E. Fraser; "Tracing transgene expression in living zebrafish embryos"; Developmental Biology **233**, pp. 329–346 (2001). ISSN 00121606. 47

[113] G. D. Marquart, K. M. Tabor, M. Brown, J. L. Strykowski, G. K. Varshney, M. C. LaFave, T. Mueller, S. M. Burgess, S. I. Higashijima & H. A. Burgess; "A 3D searchable database of transgenic zebrafish gal4 and cre lines for functional neuroanatomy studies"; Frontiers in Neural Circuits **9**, pp. 1–17 (2015). ISSN 16625110. 47, 52, 59

[114] J. R. Sternberg, K. E. Severi, K. Fidelin, J. Gomez, H. Ihara, Y. Alcheikh, J. M. Hubbard, K. Kawakami, M. Suster & C. Wyart; "Optimization of a Neurotoxin to Investigate the Contribution of Excitatory Interneurons to Speed Modulation In Vivo"; Current Biology **26**, pp. 2319–2328 (2016). ISSN 09609822. http://www.cell.com/article/S0960982216306765/fulltexthttp://www.cell.com/article/S0960982216306765/abstracthttps://www.cell.com/current-biology/abstract/S0960-9822(16)30676-5. 47

[115] A. Eschstruth, S. Schneider-Maunoury & F. Giudicelli; "Creation of zebrafish knock-in reporter lines in the nefma gene by Cas9-mediated homologous recombination"; genesis **58**, p. e23340 (2020). ISSN 1526-954X. https://doi.org/10.1002/dvg.23340. 47

[116] O. Sand; "Effects of different ionic environments on the mechano-sensitivity of lateral line organs in the mudpuppy"; Journal of comparative physiology **102**, pp. 27–42 (1975). ISSN 1432-1351. https://doi.org/10.1007/BF00657483. 49

[117] A. C. Crawford, M. G. Evans & R. Fettiplace; "The actions of calcium on the mechano-electrical transducer current of turtle hair cells." The Journal of Physiology **434**, pp. 369–398 (1991). ISSN 0022-3751. https://doi.org/10.1113/jphysiol.1991.sp018475. 49

[118] J. A. Assad, G. M. Shepherd & D. P. Corey; "Tip-link integrity and mechanical transduction in vertebrate hair cells"; Neuron **7**, pp. 985–994 (1991). ISSN 08966273. 49, 59

[119] O. Randlett, C. L. Wee, E. A. Naumann, O. Nnaemeka, D. Schoppik, J. E. Fitzgerald, R. Portugues, A. M. Lacoste, C. Riegler, F. Engert & A. F. Schier; "Whole-brain activity mapping onto a zebrafish brain atlas"; Nature Methods 2015 12:11 **12**, pp. 1039–1046 (2015). ISSN 1548-7105. https://www.nature.com/articles/nmeth.3581. 52

[120] M. Baraban, I. Anselme, S. Schneider-Maunoury & F. Giudicelli; "Zebrafish Embryonic Neurons Transport Messenger RNA to Axons and Growth Cones In Vivo"; The Journal of Neuroscience **33**, pp. 15726 LP – 15734 (2013). http://www.jneurosci.org/content/33/40/15726.abstract. 52

[121] C. B. Kimmel; "Reticulospinal and Vestibulospinal Neurons in the Young Larva of a Teleost Fish, Brachydanio rerio"; Progress in Brain Research **57**, pp. 1–23 (1982). ISSN 18757855. 52, 53, 63

[122] W. K. Metcalfe, B. Mendelson & C. B. Kimmel; "Segmental homologies among reticulospinal neurons in the hindbrain of the zebrafish larva"; Journal of Comparative Neurology **251**, pp. 147–159 (1986). ISSN 10969861. 53

[123] S. J. B. Timerick, D. H. Paul & B. L. Roberts; "Dynamic characteristics of vestibular-driven compensatory fin movements of the dogfish"; Technical report (1990). 63

[124] N. Siomava & R. Diogo; "Comparative anatomy of zebrafish paired and median fin muscles: basis for functional, developmental, and macroevolutionary studies"; Journal of Anatomy **232**, pp. 186–199 (2018). ISSN 1469-7580. https://onlinelibrary.wiley.com/doi/full/10.1111/joa.12728https://onlinelibrary.wiley.com/doi/abs/10.1111/joa.12728https://onlinelibrary.wiley.com/doi/10.1111/joa.12728. 63

[125] R. H. Schor & A. D. Miller; "Vestibular reflexes in neck and forelimb muscles evoked by roll tilt." Journal of Neurophysiology **46**, pp. 167–178 (1981). ISSN 0022-3077. https://doi.org/10.1152/jn.1981.46.1.167. 63

[126] C. Chen-Huang, R. A. McCrea & J. M. Goldberg; "Contributions of regularly and irregularly discharging vestibular-nerve inputs to the discharge of central vestibular neurons in the alert squirrel monkey"; Experimental Brain Research **114**, pp. 405–422 (1997). ISSN 1432-1106. https://doi.org/10.1007/PL00005650. 65

[127] H. Baier & E. K. Scott; "Genetic and optical targeting of neural circuits and behavior–zebrafish in the spotlight"; Current opinion in neurobiology **19**, pp. 553–560 (2009). ISSN 1873-6882. https://pubmed.ncbi.nlm.nih.gov/19781935/. 71

[128] D. Schoppik, I. H. Bianco, D. A. Prober, A. D. Douglass, D. N. Robson, J. M. Li, J. S. Greenwood, E. Soucy, F. Engert & A. F. Schier; "Gaze-stabilizing central vestibular neurons project asymmetrically to extraocular motoneuron pools"; Journal of Neuroscience **37**, pp. 11353–11365 (2017). ISSN 15292401. 103